Insights into Metal–Organic Frameworks by High Performance Liquid Chromatography: Synthesis, Equilibrium & Mass Transfer Kinetics

Zur Erlangung des akademischen Grades eines
DOKTORS DER INGENIEURWISSENSCHAFTEN (Dr.-Ing.)

der Fakultät für Chemieingenieurwesen und Verfahrenstechnik des
Karlsruher Instituts für Technologie (KIT)
Vorgelegte

genehmigte
DISSERTATION

von
M.Eng. Weiwei Qin
aus Weifang, China

Referent: Prof. Dr.-Ing. Matthias Franzreb
Korreferent: Prof. Dr.-Ing. Jürgen Hubbuch
Tag der mündlichen Prüfung: 19.02.2016

AFFIRMATION

I declare that this thesis, submitted in fulfilment of the requirements for the award of Doctor of Engineering, in the Institute of Functional Interfaces (IFG), Karlsruhe Institute of Technology (KIT), is wholly my own work unless otherwise referenced or acknowledged. The thesis was completed under the supervision of Prof. Dr.-Ing. Matthias Franzreb and has not been submitted for qualification at any other academic institution.

Karlsruhe, 07 October, 2015

Weiwei Qin

Acknowledgments

First of all, I would like to express my deepest appreciation to my Ph.D supervisor, Prof. Dr.-Ing. Matthias Franzreb, for his wisdom, patient guidance, expert advice and constant support through my research and thesis. I feel very fortunate to be his Ph.D. student. Moreover, I would like to extent my sincere gratitude to Prof. Dr.-Ing. Jürgen Hubbuch for taking his precious time to be the co-referee of my thesis.

My special gratitude to Prof. Dr.-Ing Yonghui Song for his kind helps, sound advice and encouragement.

I particularly thank Dr.-Ing. Martín Eduardo Silvestre for teaching me the experiment details and skills. Thanks to Jonas Hübner for his contribution to translating the abstract of this thesis from English to German. I'm really missing all those joyful days we spent together. I am very thankful to Dr. Peter Weilder, Moritz Ebeler and Frank Kirschhöfer for experimental measurements and troubleshooting. I am also grateful to Mike Füßler for constructions of equipment and helping me out with tools. Thanks to Pierre Tremouilhac for the proof-reading of my manuscripts.

Thanks to all staff members of the Institute of Functional Interfaces (IFG), especially my coworkers, for contributing to such an inspiring and enjoyable working atmosphere full of solidarity, collaboration and warmth. Special thanks go to my colleagues Benedikt Ketterer, Ellen Biegert, Jonas Hübner, Regina Brakowski, Franziska Kazenwadel, Dr.-Ing. Christian Morhardt, Dr.-Ing. Ingo Fisher and Dr.-Ing. Anja Sarah Paulus for their invaluable suggestions and kind helps during my daily life in Germany. I am very thankful to membrane group member Dr. Yongli Li and the MOF group members Dr. Jinxuan Liu, Dr. Zhengbang Wang, Dr. Zhigang Gu, Dr. Manuel Tsotsalas, Sophia Schmitt, Wencai Zhou, Wei Guo, Jianxi Liu and Chengwu Yang for the help, discussion, advice, cooperation and thesis revision during the research activities.

Sincere thanks to all my friends for their constant support and deep friendship.

Finally, I would like to acknowledge my family for their boundless love, encouragement and supports throughout the years.

Karlsruhe, Germany, 14 September, 2015

Weiwei Qin

Abstract

This thesis focuses on the investigation of kinetics and adsorption equilibria in a new class of stationary phases for high performance liquid chromatography (HPLC), known as metal-organic frameworks (MOFs). The studies include: (i) the fabrication of core-shell MOF magnetic particles (MPs) with the desired shell thickness and particle properties for packing into HPLC columns, (ii) the practical evaluation of the column performance by pulse and breakthrough experiments, and (iii) the detailed modeling of the sorption processes revealing a fundamental understanding of the interaction between MOF based adsorbents and dissolved organic molecules. The procedure described above was realized via three different MOFs (UiO-67, HKUST-1, and MIL-100(Fe)) representing widely different chemical compositions, crystalline structures and pore sizes.

The recently introduced liquid-phase epitaxy (LPE) process can yield uniform MOFs with controlled orientation and thickness on the surface of functionalized substrates (SURMOFs). The three investigated MOFs were homogenously coated onto the outer surface of MPs with the LPE method in a layer-by-layer (LBL) fashion. The resulting core-shell MOF MPs were characterized by XRD and SEM to ensure their successful synthesis and acquire their structure data. With regard to UiO-67, HKUST-1, and MIL-100(Fe), approximately 0.4, 0.28 and 0.65 µm MOF shells were deposited on the MPs after 55, 60, and 55 deposition layers, respectively.

A combination of experimental data and simulations with a powerful chromatography modeling software, ChromX, recently developed at the KIT, was employed to study the column performance and gain insight into the interaction mechanism between solute molecules and MOF thin films. It was found that the intraparticle diffusion played a dominant role in the uptake kinetics while axial dispersion and film diffusion showed no significant influence. Regarding sorption equilibria, it showed that for the same MOF the affinities of different tested solutes are strongly different, while their maximum capacities remain almost constant.

In particular, baseline separation of three dissolved phenol derivatives (2,6-dimethylphenol (DMP), benzene-1,3-diol (BZD), and 2,6-dichlorophenol (DCP)) was achieved on the UiO-67 based stationary phase when gradient elution was applied using acetonitrile/water as mobile phase, due to hydrophobic and/or π-π interactions. Remarkable separations in pyridine and 4,4′-bipyridine due to size exclusion and in three chloroaniline (CLA) isomers due to polarity effects were achieved, using a HKUST-1 based stationary phase and applying methanol or acetonitrile as mobile phase. The MIL-100(Fe) based stationary phase shows good separation efficiency for two groups of mixed aromatic hydrocarbons (toluene, styrene and p-xylene; acetanilide, 2-nitroaniline and 1-naphthylamine) using methanol/water as mobile phase.

The pore diffusivities (D_p) of the solute molecules in UiO-67, HKUST-1 and MIL-100(Fe) were determined to be around 1.3×10^{-13}, 2.3×10^{-15}, and 5×10^{-12} m^2 s^{-1}, respectively. This order corresponds at least qualitatively with the pore diameter of the respective crystalline MOF structures being 1.2, 0.5 and 2.5 nm, respectively. Especially in case of the well-known MOF HKUST-1 the small size of its pores and the even smaller windows between them seem to result in a very small intraparticle mass transfer of solute molecules, limiting the usefulness of HKUST-1 for liquid chromatography. In contrast MIL-100(Fe) has pores of 2 to 3 nm diameter, resulting in pore diffusion coefficients comparable to commercial chromatographic media. Among the three investigated MOFs, MIL-100(Fe) exhibited also the highest maximum capacity (q^*_{MOFmax} = 3.5 mol L^{-1}) towards the solutes toluene, styrene and p-xylene, as well as (q^*_{MOFmax} = 3.1 mol L^{-1}) towards different anilines. These maximum capacities translate into a high number of solute molecules fitting into a single unit cell of the MIL-100(Fe) crystalline structure (approx. 840 for toluene, styrene and p-xylene, approx. 740 for aniline derivatives).

Combining these high capacities and good intraparticle kinetics of certain MOFs with the well-defined pore structure and enormous chemical variety of this new class of materials, it becomes obvious that MOFs possess a huge potential as chromatography material.

Zusammenfassung

Im Rahmen dieser Arbeit wurde eine neue Klasse chemischer Verbindungen, sogenannte metall-organische Gerüstverbindungen (engl. *metal-organic frameworks*, MOFs), als stationäre Phase in der Hochleistungsflüssigkeitschromatographie (engl. *high performance liquid chromatography*, HPLC) untersucht. Die Studie, in der insbesondere kinetische Experimente und Versuche zum Adsorptionsgleichgewicht an drei MOF Typen (UiO-67, HKUST-1 und MIL-100 (Fe)) mit unterschiedlichen Eigenschaften hinsichtlich ihrer chemischen Zusammensetzung, Kristallstruktur und Porengröße durchgeführt wurden, umfasst:

(i) Synthese von Kern-Hülle-MOF Sorbentien mit magnetischen Partikeln (engl. *magnetic particles*, MPs) als Kern und definierten MOF Schichtdicken als Schale. Packen analytischer HPLC-Säulen mit diesem Material.

(ii) Charakterisierung des chromatografischen Verhaltens der mit MOF-MP gepackten HPLC Säulen mittels Puls- und Durchbruchs-Experimenten

(iii) Detaillierte Modellierung und Identifikation der prozessbestimmenden Parameter bei der Sorption verschiedener organischer Moleküle an MOF-basierte Adsorbentien.

Bei der vor kurzem vorgestellten Flüssigphasenepitaxie (engl. *liquid phase epitaxy*, LPE) handelt es sich um eine Synthesemethode, mit der MOFs in definierter Orientierung und in gewünschter Schichtdicke auf die Oberfläche funktionalisierter Substrate gebunden werden können (engl. *surface mopunted MOFs*, SURMOFs). Die drei in dieser Arbeit untersuchten MOFs wurden zunächst mit Hilfe der LPE im Substratschichtungsverfahren (engl. *layer-by-layer*, LBL) homogen auf die Außenfläche von Magnetpartikeln gebunden. Zur Verifizierung der Kern-Hülle-MOF Synthese sowie zur Strukturaufklärung und allgemeinen Charakterisierung wurden Röntgenbeugungsanalysen und zusätzliche rasterelektronenmikroskopische Untersuchungen eingesetzt. Es zeigte sich, dass die MOFs UiO-67, HKUST-1 und MIL-100 (Fe) nach 55, 60 bzw. 55 Substratschichtungen eine Schichtdicke von etwa 0,4, 0,28 bzw. 0,65 µm aufwiesen.

ChromX, eine kürzlich am KIT entwickelte Software zur Versuchsplanung und Modellierung von flüssigchromatographischen Prozessen, verbindet die Verarbeitung experimenteller Daten mit Methoden der klassischen Modellsimulation. In dieser Arbeit wurde ChromX eingesetzt, um die Leistungsfähigkeit SURMOF basierterSäulen zu evaluieren sowie die Wechselwirkungen zwischen funktioneller MOF Schicht und Adsorptiv zu untersuchen. Die Modellierungen konnten zeigen, dass die intrapartikuläre Diffusion den dominierenden Faktor hinsichtlich der Sorptionskinetik darstellt, während der Einfluss der axialen Dispersion sowie der Filmdiffusion vernachlässigt werden kann.

Bezüglich des Sorptionsgleichgewichtes zeigten sich für alle untersuchten MOF-Typen hohe Affinitätsunterschiede bei nahezu konstanten maximalen Kapazitäten für verschiedene

untersuchte Adsorptive. An auf UiO-67 basierenden stationären Phasen konnte, insbesondere aufgrund hydrophober und/oder π-π-Wechselwirkungen, die Basislinientrennung dreier gelöster Phenolderivate (2,6-Dimethylphenol (DMP), Benzol-1,3-diol (BZD) und 2,6-Dichlorphenol (DCP)) bei Anwendung einer Gradientenelution mit einem Acetonitril/Wasser-Gemisch als mobile Phase erreicht werden.

Eine auf dem MOF-Typ HKUST-1 basierende stationäre Phase erreichte durch Größenausschluss eine gute Trennung von Pyridin und 4,4'-Bipyridin. Zudem konnte an HKUST-1 gezeigt werden, dass sich drei Chloranilin Isomere vor allem aufgrund von Polaritätseffekten und unter Anwendung von Methanol als mobile Phase voneinander separieren lassen.

Stationäre Phasen, die auf Basis von MIL-100 (Fe) synthetisiert wurden, zeigten unter Verwendung eines Methanol/Wasser-Gemisches als mobile Phase eine gute Trenneffizienz für zwei Gruppen von gemischten aromatischen Kohlenwasserstoffen (Toluol, Styrol und p-Xylol sowie Acetanilid, 2-Nirtoaniline und 1-Naphthylamin.

Analysen der Porendiffusionskoeffizienten verschiedener organischer Moleküle innerhalb der MOF Typen UiO-67, HKUST-1 und MIL-100 (Fe) ergaben Werte im Bereich $1{,}3 \times 10^{-13}$, $2{,}3 \times 10^{-15}$ und 5×10^{-12} m^2 s^{-1}, wobei sich eine qualitative Korrelation mit dem Porendurchmesser der jeweiligen kristallinen MOF Struktur (1,2, 0,5 und 2,5 nm) zeigte. Im Falle des gut beschriebenen MOF HKUST-1 scheint die geringe Porengröße und die noch kleineren Fenster dazwischen zu einem stark reduzierten intrapartikulären Massentransfer zu führen, was die Eignung von HKUST-1 für die Flüssigchromatographie limitiert. Im Gegensatz dazu verfügt MIL-100 (Fe) über Poren mit einem Durchmesser von 2-3 nm und einen Porendiffusionskoeffizienten, der vergleichbar mit kommerziellen Chromatographiemedien ist. Von den drei untersuchten MOF-Typen zeigte MIL-100 (Fe) sowohl gegenüber Toluol, Styrol und p-Xylol (q^*_{MOFmax} = 3,5 Mol L^{-1}), als auch gegenüber verschiedenen untersuchten Anilinen (q^*_{MOFmax} = 3,1 Mol L^{-1}) die höchsten Maximalkapazitäten. Diese maximalen Kapazitäten korrespondieren mit einer großen Anzahl gespeicherter Analytmoleküle pro Einheitszelle der MIL-100 (Fe) Kristallstruktur (ca. 840 für Toluol, Styrol und p-Xylol, ca. 740 für Anilinderivate.).

Diese Kombination aus einer hohen Adsorptionskapazität, guten kinetischen Eigenschaften, einer definierten Porenstruktur und einer hohen chemischen Variabilität machen MOFs zu einer Klasse von Materialien mit einem enormen Potenzial für den Einsatz als stationäre Phase in der Chromatographie.

Table of Contents

AFFIRMATION ..... **I**

Acknowledgments ..... **III**

Abstract ..... **V**

Zusammenfassung ..... **VII**

Table of Contents ..... **IX**

1. Introduction and Objectives **1**

1.1. Introduction 1

1.2. Objectives of This Work 2

References 3

2. Background **4**

2.1. High−Performance Liquid Chromatography (HPLC) 4

2.1.1. Development of Liquid Chromatography 4

2.1.2. Fundamentals of Liquid Chromatography 5

2.1.3. Stationary Phases in Liquid Chromatography 13

2.1.4. Adsorption Equilibrium Thermodynamics 20

2.2. Metal−Organic Frameworks (MOFs) 23

2.2.1. Design of MOFs 24

2.2.2. Synthetic Routes to MOFs 28

2.2.3. Properties and Applications of MOFs 29

2.2.4. Surface−Mounted Metal−Organic Frameworks (SURMOFs) 33

2.2.5. Introduction of MOFs Investigated in This Study 41

References 42

3. Publications and Manuscripts **53**

4. Insights into the Separation Performance of MOFs by High−Performance Liquid Chromatography and In-depth Modelling **55**

4.1. Introduction 56

4.2. Experimental 57

4.2.1. Materials and Reagents 57
4.2.2. Preparation of $Zr_6(OH)_4O_4(OMc)_{12}(PrOH)\cdot 3McOH$ 58
4.2.3. Synthesis of UiO-67 MPs Core–Shell Composites 58
4.2.4. Characterization Techniques 58
4.2.5. Preparation of the HPLC Column and Conducted HPLC Experiments 59
4.2.6. Simulation of Chromatographic Runs Using the Software ChromX 59
4.3.1. Characterization of UiO-67 Magnetic Microparticles Core-Shell Composites 61
4.3.2. Determination of Column Characteristics 63
4.3.3. Chromatographic Separation of Phenol Derivatives 64
4.3.4. Single Component Chromatography Runs with Isocratic Elution 65
4.3.5. Affinity Modulation through Mobile Phase Variation 70
4.3.6. Multicomponent Isocratic Pulse Experiments 70
4.4. Conclusions 73
Acknowledgements 73
References 74
4.5. Support Information 76
5. Insights into Chromatographic Separation Using Core–Shell Metal–Organic Frameworks: Size Exclusion and Polarity Effects 78
5.1. Introduction 79
5.2. Experimental 81
5.2.1. Materials and Chemicals 81
5.2.2. Preparation of COOH-terminated MPs 82
5.2.3. Fabrication of HKUST-1 on MPs 82
5.2.4. Material Characterization 83
5.2.5. Preparation of the HPLC Column and HPLC Experiments 83
5.2.6. Simulation of Chromatographic Runs by the Software ChromX 83
5.3. Results and Discussion 84
5.3.1. XRD and SEM Data 84
5.3.2. Determination of Column Characteristics 85

5.3.3. Separation of Pyridine and 4,4′-bipyridine Using a HKUST-1 MPs Packed Column 86

5.3.4. Separation of Chloroaniline Isomers Using a HKUST-1 MPs Packed Column 88

5.3.5. Theoretical Capacity of HKUST-1 90

5.4. Conclusions 91

References **91**

5.5 Support Information 93

6. High Performance Liquid Chromatography of Substituted Aromatics with the Metal-Organic Framework MIL-100(Fe): Mechanism Analysis and Model-based Prediction 96

6.1. Introduction 97

6.2. Materials and Methods 98

6.2.1. Chemicals and Reagents 98

6.2.2. Fabrication and Activation of MIL-100(Fe) Magnetic Microparticles 99

6.2.3. Characterization Techniques 100

6.2.4. Preparation of the HPLC Column and Conducted HPLC Experiments 100

6.2.5. Simulation of Chromatographic Runs Using the Software ChromX 101

6.3. Results and Discussion 101

6.3.1. Characterization of Synthesized MIL-100(Fe) MPs 101

6.3.2. Determination of Column Characteristics 103

6.3.3. Determination of Equilibrium Parameters 104

6.3.4. Mixture Separation on MIL-100(Fe) MPs Column with Isocratic and Stepwise Elution 107

6.3.5. Capacity of MIL-100(Fe) 108

6.4. Conclusions 110

References 110

6.5. Supporting Information 113

7. Magnetic Microparticles@UiO-67 Core–Shell Composites as a Novel Stationary Phase for High Performance Liquid Chromatography 114

7.1. Introduction 115

7.2. Experimental 115

7.2.1. Chemicals and Reagents 115

7.2.2. Instrumentation 116

7.2.3. Synthesis of Magnetic Microparticles@UiO-67 Core−shell Composites 116

7.2.4. Preparation of the HPLC Column 116

7.3. Results and Discussion 117

7.3.1. Characterization of the Synthesized UiO-67 117

7.3.2. HPLC Separation of Dissolved Phenol Derivatives on Microparticles@UiO-67 Core−Shell Composites 118

7.4 Conclusions 119

References 119

8 Conclusions & Outlook 120

1. Introduction and Objectives

1.1. Introduction

High performance liquid chromatography (HPLC) is one of the most popular techniques in separation and purification. It spans nearly all analytical fields in pharmaceutical and chemical industries due to the availability of diverse mobile and stationary phases. Nevertheless, new challenges in separation technologies require continuously novel porous materials suitable as stationary phases in HPLC. The corresponding design and development of novel materials is time-consuming and easily frustrating, mainly because of the complicated structure function relationship of porous adsorbents, combined with still restricted capabilities to model their interaction with varying analytes.

Metal–organic frameworks (MOFs), self-assembled by metal nodes and functional organic linkers, turned up in the field of adsorbents as an emerging type of porous crystalline materials two decades ago [1, 2]. Since then, MOFs have attracted considerable attention due to their flexible structure, tunable pore size, and promising applications in gas storage, separation, catalysis, sensing and luminescence, to name a few [3]. To tailor MOFs for certain applications, their properties, such as polarities, pores sizes and functional groups, can be modified by using different metals or linkers. The wide structural choices of MOFs, along with their salient features such as low density, high uptake capacity, and absence of dead volume, make MOFs attractive candidates for stationary phases in HPLC [4, 5].

In recent years, an increasing number of studies have reported the potential of MOFs as a new class of chromatographic materials. In 2007, Alaerts and co-workers [6] first reported the use of the MOF materials MIL-47(V) and MIL-53(Al) as liquid chromatography stationary phases and they showed different column performances for the separation of xylene isomers and ethylbenzene with hexane as the mobile phase. Yan and co-workers [7] made great contribution to the use of MOFs for HPLC separations. They found that columns packed with the MOF MIL-53(Al) provided high-resolution separations of a broad range of analytes using acetonitrile/water as the mobile phase.

Up to now, MOFs are mainly synthesized in the form of large and irregular crystals, resulting e.g. from sol-gel processes in bulk solutions. However, the bulky MOF crystals are not favorable for their application in HPLC because the diffusion of molecules is much slower in liquids and thus, the penetration of analyte molecules into the MOF pores is a rather slow process. One way to overcome this problem is to reduce the particle size into the micro- or nano-meter range, but the small particles will result in high pressure drops of the respective packed beds [8].

Besides, the irregular shapes and wide size distributions of MOFs also cause other drawbacks such as suboptimal column packing, and low column efficiency [9]. Compared to completely porous microparticles, larger core-shell particles with a thin active shell can increase column

performance while showing relatively low backpressure [10, 11]. Therefore, an ideal solution would be to synthesize uniform MOF particles having a core-shell structure. The recently introduced liquid phase epitaxy (LPE) process, applying a layer-by-layer (LBL) approach to add metal nodes and linkers, can produce homogenous MOFs with controllable thickness and growth direction on functionalized surfaces (SURMOFs) [12-16]. Therefore, applying LPE SURMOF shells can be successfully synthesized onto the outer surface of a functionalized magnetic core, which is suitable for handling by magnetic separations [17].

Most importantly, although remarkable progress in the field of MOF based HPLC columns has been made, the development of MOFs for HPLC applications has been hindered by the lack of fundamental understanding of the interactions between the MOF solid phases and the guest molecules. Especially, knowledge of the adsorption kinetics and mass transfer behavior, which would allow for an essential understanding of the performance of MOFs based stationary phases, remains undetermined. Furthermore, this fundamental information is a prerequisite for tailoring the functionality of MOF based stationary phase for challenging separation tasks by a rational design of chemistry, pore structure and shell-core particle dimensions.

1.2. Objectives of This Work

This thesis deals with the development and characterization of magnetic MOF hybrid materials as new adsorbents for separation tasks. Besides a thorough physico-chemical characterization, detailed investigations of their performances and interactions with various solutes by means of HPLC were conducted. The main objectives and tasks of the thesis can be summarized as follows:

(1) Target setting: Identification of organic substances representing challenging separation tasks and selection of applicable MOFs specifically tailored for the determined analytes.

(2) Synthesis and characterization of magnetic MOFs particles: Well-defined core-shell structures with a MOF layer grown evenly on uniform magnetic microparticles (MPs) by the LPE process have to be synthesized and the as-synthesized composites characterized by XRD, FT-IR and SEM.

(3) Column packing and characterization: The as-synthesized core-shell structured MOF MPs should be packed into HPLC columns and the column characteristics have to be determined in order to demonstrate the effect of MOF specific properties onto chromatographic performance.

(4) Mechanisms study: The transport mechanisms and interactions between the MOF core-shell solid phase and the target analytes should be elucidated on a more fundamental level by means of comparison between experimental and simulated HPLC runs.

In this thesis, three different types of MOFs with different physical and chemical properties are selected. Based on their chromatographic performance as well as extracted equilibrium and kinetic data of these MOFs and different analytes, the influence of the MOF properties (e.g., structure, pore size, water-stability, and selectivity) on the suitability as chromatographic material will be evaluated.

References

[1] J.L.C. Rowsell, O.M. Yaghi, Metal-organic frameworks: A new class of porous materials, Micropor. Mesopor. Mater. 73 (2004) 3-14.

[2] S. Kitagawa, R. Kitaura, S. Noro, Functional porous coordination polymers, Ind. Eng. Chem. Res. 43 (2004) 2334-2375.

[3] H. Furukawa, K.E. Cordova, M. O'Keeffe, O.M. Yaghi, The chemistry and applications of metal−organic frameworks, Science 341 (2013) 974.

[4] K. Yusuf, A. Aqel, Z. ALOthman, Metal−organic frameworks in chromatography, J. Chromatogr. A 1348 (2014) 1-16.

[5] Y.B. Yu, Y.Q. Ren, W. Shen, H.M. Deng, Z.Q. Gao, Applications of metal−organic frameworks as stationary phases in chromatography, TrAC-Trends. Anal. Chem. 50 (2013) 33-41.

[6] L. Alaerts, C.E.A. Kirschhock, M. Maes, M.A. van der Veen, V. Finsy, A. Depla, J.A. Martens, G.V. Baron, P.A. Jacobs, J.E.M. Denayer, D.E. De Vos, Selective adsorption and separation of xylene isomers and ethylbenzene with the microporous vanadium(IV) terephthalate MIL-47, Ind. Eng. Chem. Res. 46 (2007) 4293-4297.

[7] S.S. Liu, C.X. Yang, S.W. Wang, X.P. Yan, Metal−organic frameworks for reverse-phase high-performance liquid chromatography, Analyst 137 (2012) 816-818.

[8] N. Wu, A.M. Clausen, Fundamental and practical aspects of ultrahigh pressure liquid chromatography for fast separations, J. Sep. Sci. 30 (2007) 1167-1182.

[9] A. Ahmed, M. Forster, R. Clowes, D. Bradshaw, P. Myers, H. Zhang, Silica SOS@HKUST-1 composite microspheres as easily packed stationary phases for fast separation, J. Mater. Chem. B 1 (2013) 3276.

[10] J.M. Cunliffe, T.D. Maloney, Fused-core particle technology as an alternative to sub-2-µm particles to achieve high separation efficiency with low backpressure, J. Sep. Sci. 30 (2007) 3104-3109.

[11] J.J. DeStefano, T.J. Langlois, J.J. Kirkland, Characteristics of superficially-porous silica particles for fast HPLC: Some performance comparisons with sub-2-µm particles, J. Chromatogr. Sci. , 46 (2008) 254-260.

[12] H. Gliemann, C. Wöll, Epitaxially grown metal-organic frameworks, Mater. Today 15 (2012) 110-116.

[13] O. Shekhah, J. Liu, R.A. Fischer, C. Wöll, MOF thin films: existing and future applications, Chem. Soc. Rev. 40 (2011) 1081-1106.

[14] B. Liu, R.A. Fischer, Liquid-phase epitaxy of metal organic framework thin films, Science China-Chemistry 54 (2011) 1851-1866.

[15] O. Shekhah, Layer-by-layer method for the synthesis and growth of surface mounted metal-organic frameworks (SURMOFs), Materials 3 (2010) 1302-1315.

[16] O. Shekhah, H. Wang, S. Kowarik, F. Schreiber, M. Paulus, M. Tolan, C. Sternemann, F. Evers, D. Zacher, R.A. Fischer, C. Wöll, Step-by-step route for the synthesis of metal-organic frameworks, J. Am. Chem. Soc. 129 (2007) 15118-15119.

[17] M.E. Silvestre, M. Franzreb, P.G. Weidler, O. Shekhah, C. Wöll, Magnetic cores with porous coatings: growth of metal-organic frameworks on particles using liquid phase epitaxy, Adv. Funct. Mater. 23 (2013) 1210-1213.

2. Background

2.1. High−Performance Liquid Chromatography (HPLC)

2.1.1. Development of Liquid Chromatography

Chromatography is defined as a terminology to describe various separation techniques of sample mixtures between two phases, the stationary phase and the mobile phase. In most cases the stationary phase is a fixed-bed, which may be either a sheet of paper (paper chromatography), a thin layer of porous materials coated on the surface of a planar material such as paper, metallic or glass plates (thin layer chromatography, TLC), a tube filled with small-particles (column chromatography) or a layer in a capillary tube (capillary chromatography). The mobile phase can be a gas, liquid or supercritical fluid, where the process is known as gas chromatography (GC), liquid chromatography (LC), and supercritical fluid chromatography (SFC), respectively. The mobile phase carries the dissolved mixture moving along the stationary phase and individual analytes are separated in time over the length of the fixed-bed column as a result of differential retention.

The first type of chromatography was liquid-solid chromatography, which was discovered by the Russian scientist Tswett in the 1890s [1]. He separated and isolated different kinds of plant pigments using liquid chromatography. Willstätter and Stoll [2] repeated Tswett's experiment using an aggressive adsorbent in 1913, with the chlorophylls being accordingly decomposed. In the late 1930s and early 1940s, Martin and Synge isolated acetyl amino acids on silica gel [3]. They proposed a gas rather than a liquid mobile phase to accelerate the movement between the mobile and stationary phases. Additionally, they suggested that applying high pressures and small packing particles in liquid chromatography can lead to a better separation. That was the start of the development of high−performance liquid chromatography, also called high pressure liquid chromatography (HPLC).

Chromatography is the most important separation technique for analytical purposes, and within the field of chromatography HPLC is the most commonly used method [4]. The main advantages of HPLC over other techniques are its high selectivity, reliability, sensitivity, versatility and accuracy. In particular, (1) high selectivity can be achieved due to the large amount of various stationary and mobile phase combinations available; (2) it can separate components from very complex mixtures containing e.g. sugars, proteins, enantiomers, drugs, fine chemicals, flavorings, etc.; (3) separated components can be collected individually; (4) only small amounts of samples are needed for analysis; (5) analysis can be highly accurate and reproducible. However, chromatography also has disadvantages compared to simpler separation techniques, like e.g. precipitation. The main disadvantages are: (1) the equipment and supplies (columns, fittings, etc.) are costly; (2) well-trained person is required because of the complex chemistry and equipment; (3) the processes within the column are often complex and advanced simulation tools are required for prediction.

Today, chromatography has become a very versatile technique used to identify the presence or to quantify certain components in a mixture (analytical chromatography), as well as to separate individual components from a mixture for purification (preparative chromatography). Table 2.1 explains the analytical and preparative chromatography from the perspective of scales.

Table 2.1 Scales of chromatography.

Types	Amount of components	ID column [mm]
Analytical	µg – mg	4 – 10
Preparative (Laboratory scale)	mg – g	up to 25
Preparative (Pilot scale)	g – kg	up to 80
Preparative (Production)	kg – t	up to 1500

2.1.2. Fundamentals of Liquid Chromatography

2.1.2.1. The HPLC process

A typical HPLC instrument consists of pumps, sample injection system, column, detector and data acquisition system (Figure 2.1). HPLC features the sample of interest being dissolved in the mobile phase, before being brought into the column by the injection system. Within the column the components of the sample undergo a series of interactions (e.g. partitioning or adsorption) at the mobile phase-stationary phase boundary as they move through the HPLC system. The pumps deliver the desired flow and, in case of gradient elution, also composition of the mobile phase. The detector generates a signal proportional to the amount of sample component emerging from the column, hence allowing for quantitative analysis of the sample components. A digital microprocessor and user software control the HPLC instrument and provide data analysis. Some models of mechanical pumps in a HPLC instrument can mix multiple solvents together in ratios changing over time, generating a composition gradient in the mobile phase. Various detectors are in common use for both qualitative and quantitative analysis, such as UV/Vis, photodiode array (PDA) or mass spectrometry (MS). Most HPLC instruments also have a column oven that allows for adjusting the temperature.

The fundamental principle of choosing the phases is that the components of the sample have different affinities towards the stationary phase. A component having a high affinity towards the stationary phase will take longer to travel through the column than a component having a higher affinity towards the mobile phase rather than towards the stationary phase. The sample mixture will be separated while travelling through the column due to these different mobilities of the components in the two phases [5].

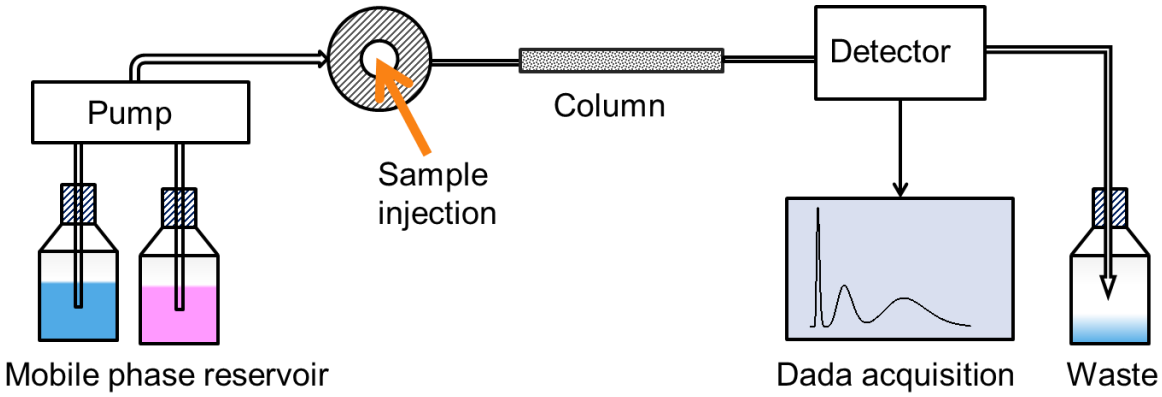

Figure 2.1. Schematic diagram of HPLC.

The graphical representation of the separation process is detailed as follows [6]:

(a) A mixture of two components A and B, represented by circles and triangles, respectively, is forced through the stationary phase (Figure 2.2a).

(b) The component B has higher affinity towards the stationary phase while component A has higher affinity towards the mobile phase. Hence, the mean time taken by component B to get through the stationary phase is longer than that for component A (Figure 2.2b).

(c) When fresh mobile phase comes in, a new equilibrium will be created afterwards: molecules of sample in the mobile phase are partly adsorbed by the unloaded stationary phase surface, in conformity to the distribution coefficients, while the molecules previously adsorbed by the stationary phase surface desorb again into the mobile phase (Figure 2.2c).

(d) After repeating this process many times, components A and B are eventually isolated. Component B which tends to stick to the stationary phase will migrate more slowly than component A (Figure 2.2d).

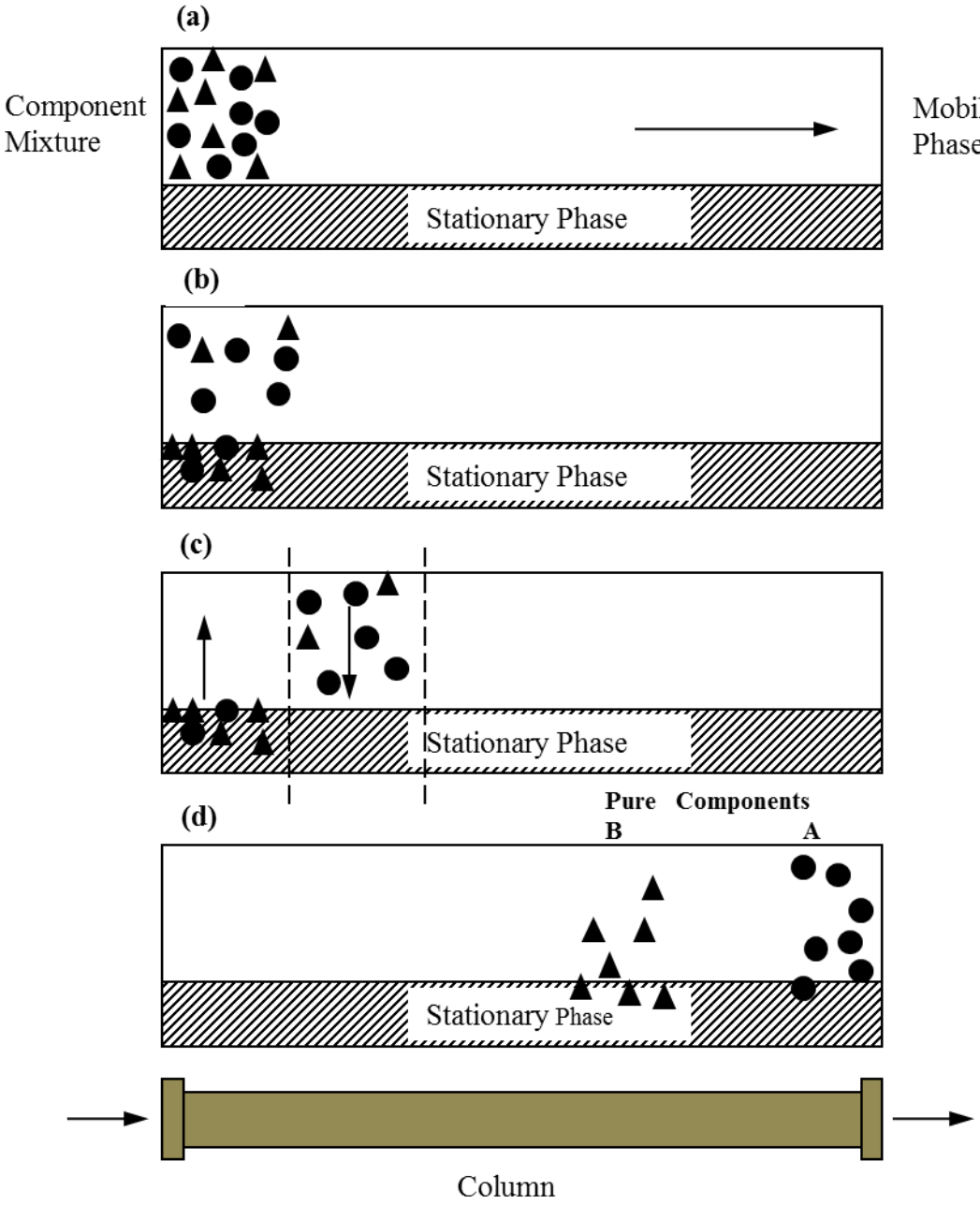

Figure 2.2. Representation of a chromatographic separation. (Figure modified after ref. [6])

2.1.2.2 Elution modes

Isocratic elution and gradient elution are two basic elution methods of liquid chromatography [7]. In an isocratic elution, the composition of the mobile phase keeps constant during the separation process. Isocratic elution is the simplest and preferred mode while developing a method for analytical chromatography. On the other hand, gradient elution refers to an operation mode in which the mobile phase composition is changed during the separation process.

In a gradient elution, applying the two components “A” and “B” of the mobile phase, A is the “weak” solvent which elutes the solute from the column slowly, whereas B is the “strong” solvent which allows the solute to elute rapidly. Gradient elution reduces the retention time of the later-eluting components to make them elute faster, shortening the analysis time, giving narrow peaks and improving the detection limit [4]. For the separation of complex mixtures containing many compounds with widely differing affinities, isocratic elution is often unsuitable because of the unacceptably long analysis time and broad peaks. In such cases a well-designed gradient program is very useful to achieve an optimum separation in minimum time.

2.1.2.3. Chromatographic mechanisms

During a chromatographic separation process one or multiple types of interactions may happen between the stationary phase and the analytes. Based on the dominating interactions HPLC separation modes can be classified as normal phase chromatography (NPC), reverse phase chromatography (RPC), ion-exchange chromatography (IEX), hydrophilic interaction chromatography (HILIC), hydrophobic interaction chromatography (HIC), size exclusion chromatography (SEC), and partition chromatography, etc. They are briefly introduced as follows.

(1) Normal phase chromatography (NPC)

The earliest liquid chromatography was conducted using polar stationary phases in combination with nonpolar liquids in which the sample is dissolved [8]. This method is now referred to as “normal phase chromatography”. In NPC, the stationary phase is more polar (hydrophilic), typically silica or alumina, than the mobile phase [9-11]. Therefore, the polar molecules in the mobile phase tend to adsorb to the stationary phase and migrate slowly through the column, while the nonpolar (hydrophobic) molecules elute first. Figure 2.3 schematically shows a part of a porous silica particle with silanol groups (Si-OH) residing at the particle surface and inside its pores. One major disadvantage of normal phase chromatography is that the polar surfaces can be easily contaminated by sample components.

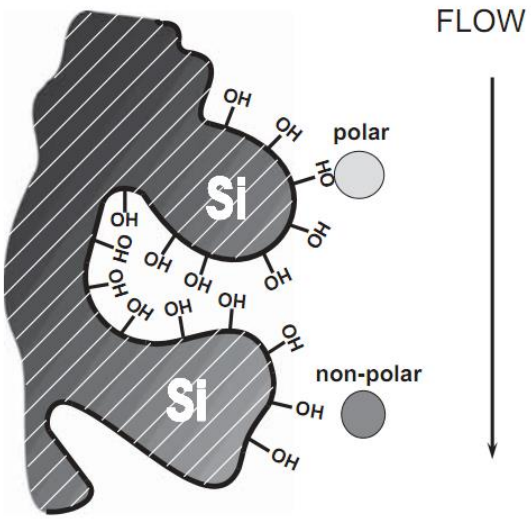

Figure 2.3 Schematic sketch depicting the surface chemistry and interactions of a stationary phase for normal-phase chromatography. (Figure cited from ref. [8])

NPC could be applied for the separation of organic isomers, especially if the analytes are insoluble or not stable in water, or if the analytes being too hydrophilic for reverse phase separation.

(2) Reverse phase chromatography (RPC)

In contrast to NPC, RPC refers to liquid chromatography which uses a hydrophobic (non-polar) stationary phase and a polar mobile phase. Figure 2.4 shows a scheme of reversed phase chromatography. In RPC, polar molecules in the mobile phase are eluted first while nonpolar molecules tend to bind to the column due to the strong interactions with the stationary phase. Hydrophobic molecules can pass through the column by reducing the polarity of the mobile phase using a nonpolar solvent, decreasing hydrophobic interactions. The mechanism of separation is primarily based on hydrophobic interaction. RPC is the most popular HPLC mode with more than 70% of all HPLC analyses using this method [8]. Reverse phase chromatography is useful in the analysis of polar (water-soluble), medium-polar, and some nonpolar analytes [12].

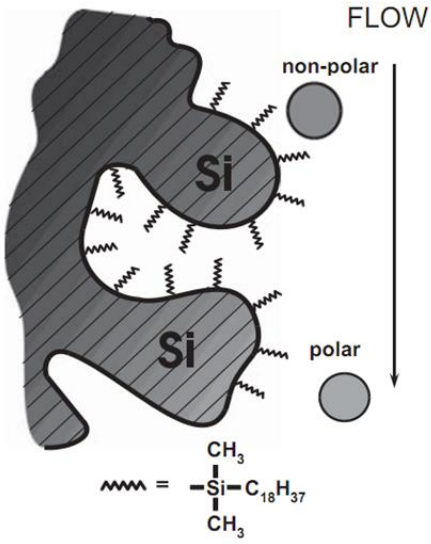

Figure 2.4 Schematic diagram depicting the surface chemistry and interactions of a stationary phase for reversed-phase chromatography (Figure cited from ref [3]).

(3) Ion-exchange chromatography (IEX)

Ion-exchange chromatography (or ion chromatography) is based on differences in ion exchange affinities of charged solutes towards the ionic groups attached to the solid support. It is often applied in the separation of ionic or ionizable compounds. Figure 2.5 shows a scheme of the interaction mechanism of ion-exchange chromatography. This method has been in use for a long time. Nowadays, reversed-phase chromatography dominates analytical use of HPLC while ion-exchange chromatography is mainly used for preparative and industrial use. However, ion-exchange chromatography is commonly used in the analysis of inorganic ions and biological components such as proteins/peptides, amino acids, and polynucleotides [8, 13].

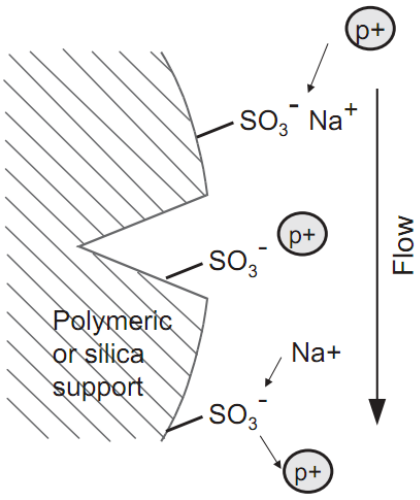

Figure 2.5 Scheme of the interaction mechanism of ion-exchange chromatography (IEC), presenting the exchange of analyte ions p+ with sodium counter ions of the functional sulfonate groups attached to the surface (Figure taken from ref [8]).

(4) Hydrophilic interaction chromatography (HILIC)

HILIC is based mainly on differences in the hydrophilicity of the sample components. The separations are carried out with a polar stationary phase such as silica or ion-exchange materials and a less polar mobile phase. HILIC is a variant of NPC and their major difference lies in the different types of mobile phase used, organic solvents without water for NPC and with some water for HILIC, leading to a difference in chromatographic mechanism. Hydrophilic interaction chromatography plays some role in analytical separations, whereas nowadays NPC is rarely used. Analogous to NPC, HILIC favors retention of a more polar substance [14]. Hence, substances elute in order of increasing polarity or decreasing hydrophobicity. HILIC is most commonly applied in isolating polar analytes and hydrophilic peptides [15].

(5) Hydrophobic interaction chromatography (HIC)

HIC is based mainly on differences in the hydrophobicity of the sample components. Columns used for HIC are analogous to RPC, except that the stationary phase is less hydrophobic due to: (a) hydrophilic groups that are incorporated into short alkyl ligands, and (b) a less dense coverage of the surface with ligands [14]. The mobile phase is usually an aqueous solution with low organic solvent content and high salt concentrations [8, 14]. HIC has been used to separate proteins [16], viruses [17], and (less often) nucleic acids [18].

(6) Size exclusion chromatography

Size exclusion chromatography, previously also known as gel permeation chromatography and gel filtration chromatography, is a chromatographic method which separates the molecules of a sample by their ability to penetrate the pores of the stationary phase rather than interact with the surface of the stationary phase (Figure 2.6**)** [13]. The separation is based on exclusion effects resulting from differences in molecular size and/or shape and charge. Molecules of different sizes will migrate down the column at different rates, leading to their separation. Smaller molecules can penetrate into the pores and elute late, while large molecules are excluded from the pores and elute quickly [8].

This method is usually used for large molecules or macromolecular complexes such as proteins and industrial polymers. Also, size exclusion chromatography is a widely used polymer characterization method due to its capacity of providing good molar mass distribution results for polymers.

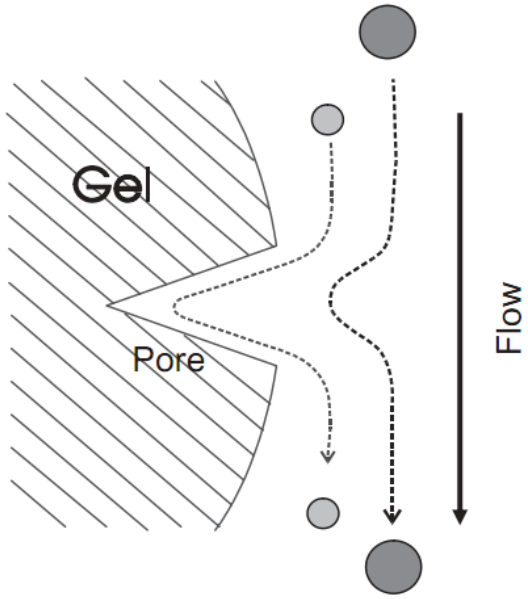

Figure 2.6 Schematic diagram of the mechanism of size-exclusion chromatography (SEC), presenting the faster migration of large molecules. (Figure taken from ref [8])

(7) Partition chromatography

In case of partition chromatography the stationary phase is a liquid, which is immiscible with the mobile phase and held as thin layer (or film) on the surface of an inert solid. Separation is based mainly on the different partitioning coefficients (solubilities) of the solutes between the mobile phase and the stationary phase. When the compounds travel through the column, the ones having lower solubilities within the stationary phase travel faster and arrive at the end of the column first. A schematic diagram of partition chromatography is illustrated in Figure 2.7.

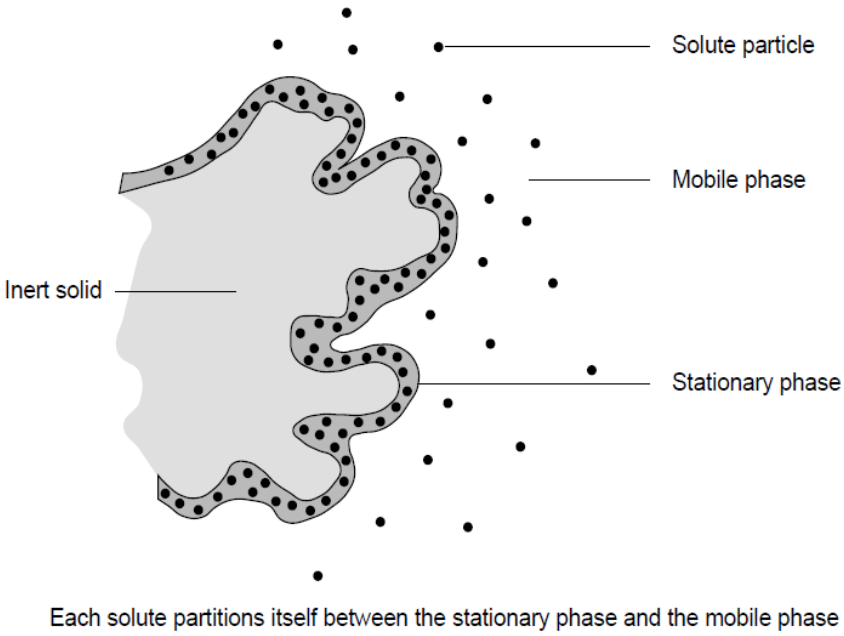

Figure 2.7 Schematic diagram of the solute interaction during partition chromatography.

2.1.3. Stationary Phases in Liquid Chromatography

2.1.3.1. State-of-the-art in HPLC stationary phases

Once the chromatographic material is packed into the column and interacts with the mobile phase, it becomes the stationary phase. There is no omnipotent HPLC column for all kinds of purposes, meaning usually columns are only for specific applications. For example, enantiomer columns are designed for enantiomer separations. Therefore, continuous research of suitable materials for HPLC columns is ongoing for various types of samples such as chiral chemicals or pharmaceuticals. Monolithic columns and packed columns are the two types of stationary phases for routine HPLC.

Frequently used materials for monolithic columns are porous silica and cross-linked polymers. Due to the highly interconnected porosity, monolithic columns develop high permeability and subsequent low back pressure even when the flow rate is high [19]. However, the main disadvantages of applying monolithic columns are the reproducibility of the pore structures and the difficulty of fitting the monolith into a column, which affects the analysis performance of monolithic columns. Consequently, monolithic columns may deliver variations in the analysis results from batch to batch. In addition, monolithic columns generally feature weak mechanical stability. In addition, another issue with polymer monoliths is their potential swelling problems in the presence of solvents.

For packed columns, although numerous organic polymer and ceramic microspheres have been used as packing materials, silica microspheres are the most modern and widely used stationary phase today [4, 9], due to their versatile sizes and varying degree of porosity. Polymeric layers could be bonded to the surface of the silica, hence extending the application of the silica particles [9]. Spherical particles can be packed more tightly and uniformly than irregular ones, hence they are generally the best choice for HPLC. The used particles can be either porous (like most silica gels) or nonporous (like glass beads). The porous ones are preferred as they have larger specific surface areas. The larger the specific surface area of a packing, the more sites for sorption of the analytes are available. For liquid phase separation, a pore size of above 7 nm is recommended for sufficient mass transport. In the case of large biomolecules separation, larger pores sizes of up to 100 nm may be required for efficient separation [20].

Common challenges in HPLC are highly efficient and fast separation for a wide range of samples from analytical to preparative scale [21]. HPLC prefers packings of small porous particles. However, a decrease of the particle diameter increases the efficiency as well as the pressure requirements ($\Delta P \propto 1/d^2$, where ΔP is the column pressure drop; d is the average particle diameter [20]). This leads to the smallest particle sizes in routine use being around 3 µm. In order to further decrease the diffusion length within the stationary phases, they can be realized in the form of thin layers of a crosslinked polymer bonded to the inner wall of a capillary [4]. Alternatively, stationary phases with very short diffusion length can be achieved

by coating a thin layer of porous solid on a nonporous core. In the early days of HPLC, pellicular supports were widely used. The materials in use today are microporous solids being created by bonding nanometer-thick layers of porous silica onto solid particles with diameters of 3 to 5 µm. In comparison to microporous solids, pellicular solids are less stable, are more expensive, and have smaller capacities, despite that they are easier to pack.

Recent years have seen an increased use of core-shell silica particles, also known as solid core and porous shell or superficially porous particles, in HPLC applications due to their relatively low back pressure allowing fast flow rates [22]. The advantage of core-shell particles as packing material is that the small shell thickness decreases the diffusion path length within the stationary phase and therefore peak broadening because of intraparticle diffusion [19].

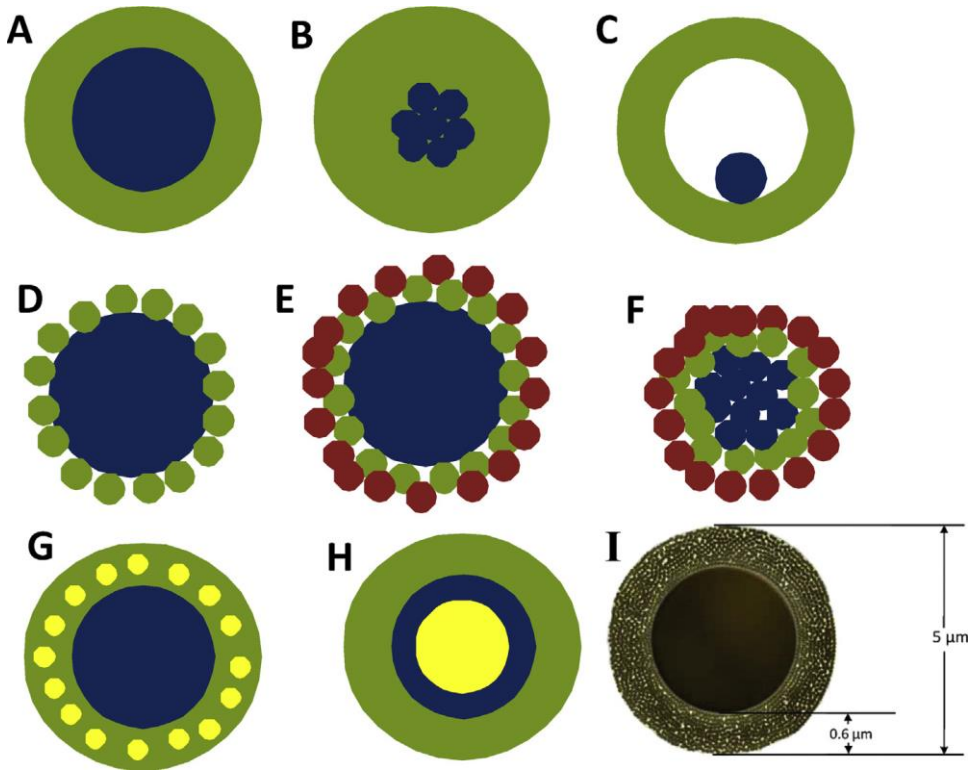

Figure 2.8 Different types of core-shell particles. (Figure adapted from ref. [19])

Core-shell particles are made of a core and a shell which can be different materials or the same material having different structures. Different types of core/shell particles represented by different colors are schematically shown in Figure 2.8. The core can be a single sphere as shown in Figure. 2.8A, an aggregate of several small spheres (Figure 2.8B), or a rattle-like or yolk-shell structure [23] having a hollow shell and a small sphere inside (Figure 2.8C). The shell structure of particles in Figure 2.8A-C can be a continuous layer. The shell of Figure 2.8D-E is made of smaller spheres on the surface of a big core and Figure 2.8F shows a variant usage of small spheres to build the core as well as the shell [24]. It is possible to have

a core-shell structure being made by embedding smaller spheres into the shell as shown in Figure 2.8G [25] or the particle has more than one shell as shown in Figure 2.8H [26]. In chromatography, the core-shell structures are usually made of the same material but with the core being solid and the shell being porous Figure 2.8I [27].

2.1.3.2. Characterization of column performance

(1) Chromatograms and valuation criteria

A chromatogram is the basic and direct expression of a chromatographic separation process. It is a graph that monitors the detector signal (concentration of analyte) over time. Figure 2.9 shows a typical chromatogram of two different components with analytical amounts of injection.

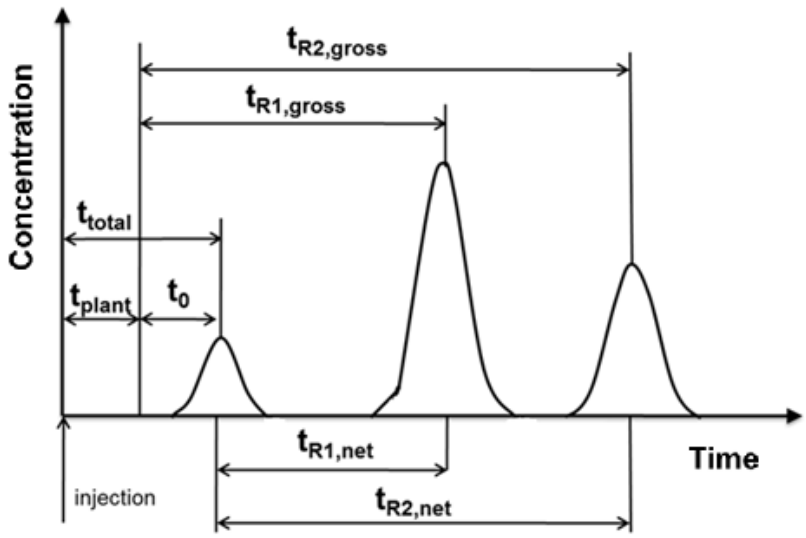

Figure 2.9 A typical HPLC chromatogram of one nonretained and two retained components. (Figure adapted from ref. [28])

Retention time $t_{R,i}$ indicates the time for each component to elute out of the column, taken at the maximum of the peak indicating the specific component in the sample. The total dead time t_{total} is the time of an unretained substance spent from the point of injection to the point of detection. t_{plant} represents the dead time of the chromatographic system without column. Hence, the dead time t_0 of a column can be determined by Equation 2.1. Retention time $t_{Ri,gross}$ represents the time a substance i needs to elute the column[1]. The net retention time $t_{Ri,net}$ is the time that the substance is adsorbed onto the surface of the stationary phase, which

[1] If not done automatically by the HPLC system used, t_{plant} has to be substracted from the measured retention time in order to determine $t_{Ri,gross}$

is determined by subtraction of t_0 from $t_{Ri,gross}$ (Equation 2.2). The dead time is typically determined by tracer molecules, which are not retained on the solid phase.

$$t_0 = t_{total} - t_{plant} \tag{2.1}$$

$$t_{Ri,net} = t_{Ri,gross} - t_0 \tag{2.2}$$

The retention time depends not only upon the specific structure of the analyte, but also on the parameters of the column, as well as the nature and flowrate of the mobile phase. The retention factor (capacity factor) k' is defined as the ratio of the time a component stays on the stationary phase to the time it remains in the mobile phase. The retention factor is an important dimensionless parameter for analytical applications of chromatography, because it is independent of the column geometry and the flow rate of the fluid phase. It can be written as follows:

$$k_i' = \frac{t_{Ri,gross} - t_0}{t_0} = \frac{t_{Ri,net}}{t_0} \tag{2.3}$$

The separation factor α, also called selectivity, is another common and useful parameter for the evaluation of a LC sepration process. The value of α reflects the affinity difference of two substances towards the used stationary phase. It is defined as the ratio of the retention factors of two chromatographic peaks:

$$\alpha = \frac{k_2'}{k_1'} = \frac{t_{R2,gross} - t_0}{t_{R1,gross} - t_0} \tag{2.4}$$

The selectivity α is influenced by the analyte, the nature of the mobile phase and the stationary phase. A larger value for α indicates the potential for a better separation. An efficient separation typically needs $\alpha > 1.2$, which is also a frequent basis for the selection of a suitable chromatographic column.

Due to dispersion and diffusion effects the rectangular injection pulse transfers into a bell shaped peak, which in the ideal case of strictly linear isotherm behavior can be fully described by a Gaussian curve (Figure 2.10). In a Gaussian curve, the width can be defined in diferent ways, including the width at half peak height (W_h), the width at the inflection point (W_i), and the baseline width (W_b). For the ideal Gaussian peak, the peak-widths are a fixed function of the standard deviation (σ), which reflects the extent of peak broadening:

$$W_h = 2(2\,ln\,2)^{0.5}\sigma = 2.355\sigma \tag{2.5}$$

$$W_b = 4\sigma = 1.7W_h \tag{2.6}$$

$$W_i = 2\sigma \tag{2.7}$$

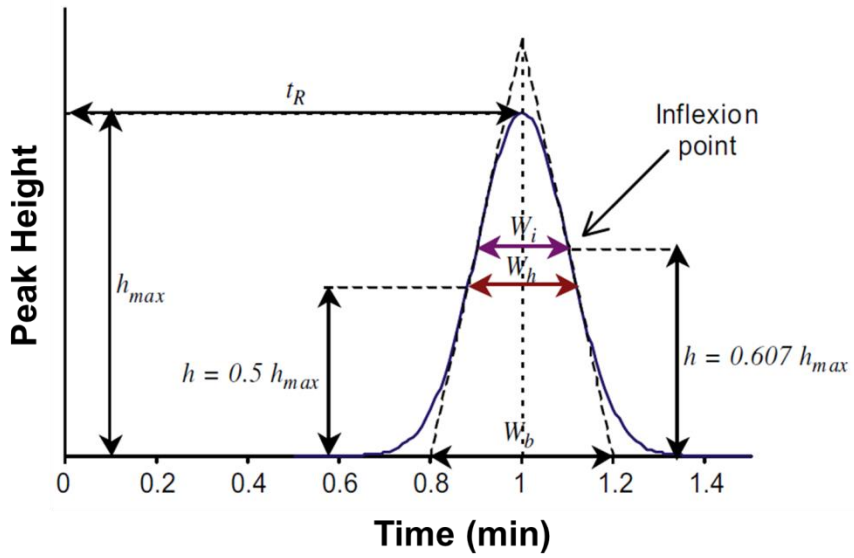

Figure 2.10 Measurement of peak brodening W_i, W_h and W_b for a typical Gaussian peak. (Figure adapted from ref. [29])

Column performance is typically described by the height equivalent H of a theoretical plate (HETP), as well as the corresponding theoretical plate number N. N is related to the peak broadending. The ideal behavior is H → 0 or N → ∞. That is, the smaller the plate height or the larger the plate number of a column, the higher is the efficiency, the narrower the peak width and shape. The relationship of H and N is shown below:

$$N = L_c\ /\ H \tag{2.8}$$

where L_c is the column length.

Assuming a Gaussian peak for a uniformaly packed column, H can also be calculated from:

$$H = (\sigma')^2/L_c \quad with\ \sigma' = \sigma \cdot u \tag{2.9}$$

σ' corresponds to the standard deviation of the peak measured in meters, which can be easily derived from σ by multiplication with the average flow velocity u within the column.

Accordingly, N can be expressed by:

$$N = {L_c}^2/(\sigma')^2 \tag{2.10}$$

In practice, chromatograms of tracer substances are measured over time with the retention time t_R and the peak width w_b. Hence, plate number can be calculated from:

$$N = (\frac{t_R}{\sigma})^2 = 16(\frac{t_R}{W_b})^2 = 5.545(\frac{t_R}{W_h})^2 \tag{2.11}$$

Instead of the theoretical plate number N, the effective plate number N_{eff} determined by using $t_{R,net}$ can also characterize the efficiency of a column. Usually, N_{eff} is 10 to 30% smaller than N. N_{eff} is simply named “efficiency”:

$$N_{eff} = (\frac{t_{R,net}}{\sigma})^2 = 16(\frac{t_{R,net}}{W_b})^2 = 5.545(\frac{t_{R,net}}{W_h})^2 \tag{2.12}$$

As mentioned before, selectivity α is an important measuremnet criteria of column performance. However, α itself cannot describe the separation quality of two components even if it has a large value. That is, although the distance of the two peaks may be far, the peaks may be very broad, resulting in a poor separation. Here another papameter features the peak separation, named resolution R_s. R_s is defined as:

$$R_s = \frac{2(t_{R2,net}-t_{R1,net})}{W_{b1}+W_{b2}} = \frac{1.177(t_{R2,net}-t_{R1,net})}{W_{h1}+W_{h2}} = \frac{\alpha-1}{\alpha}\frac{2t_{R2,net}}{W_{b1}+W_{b2}} = \frac{1}{4}\frac{\alpha-1}{\alpha}\left(\frac{k'}{1+k'}\right)N^{\frac{1}{2}} \tag{2.13}$$

As can be seen from the above Equation 2.13, R_s is dependent on three parameters: α (selectivity), k' (retention factor), and N (column efficiency). The two peaks are separated at the baseline when $R_s > 1.5$. In reality, $R_s > 1$ is enough for most purposes, indicating nearly 98% separation [6].

(2) Void fraction and porosity

The fluid flow through the packing of the stationary phase and the solute transport within the particles greatly impact on the design and performance of the chromatographic process (Figure 2.11). In this context three porosities have to be considered: (i) the column porosity ε_b (extra-particle porosity, void fraction of column, bed porosity), (ii) the intra-particle prostiy ε_p, and (iii) the total column porosity ε_t (total void fraction).

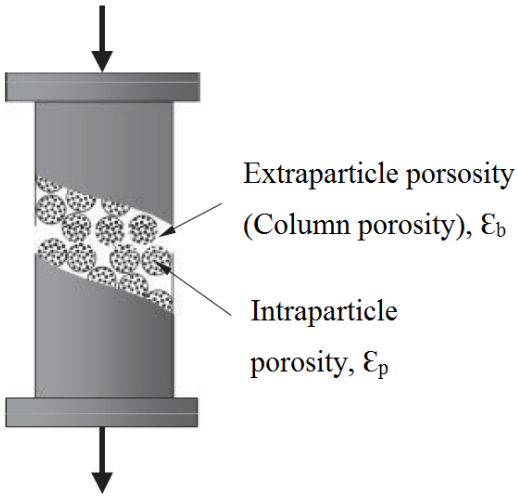

Figure 2.11 Column porosity and intraparticle porosity in a packed chromatographic column (Figure adapted from ref. [30]).

The total column volume (V_c) consists of the interstitial volume of the fluid phase (V_{int}) and the volume of the stationary phase ($V_{partile}$):

$$V_c = \frac{\pi d_c^2 L_c}{4} = V_{int} + V_{particle} \tag{2.14}$$

In addition, the volume of the stationary phase (V_{sta}) includes the volume of the solid matrix (V_{matrix}) and the volume of the pores of the particle (V_{pore}):

$$V_{particle} = V_{matrix} + V_{pore} \tag{2.15}$$

The three porosities can be derived from above volumes:

Cloumn porosity: $\varepsilon_b = \frac{V_{int}}{V_c} = \frac{V_c - V_{particle}}{V_c}$ (2.16)

Particle porosity: $\varepsilon_p = \frac{V_{pore}}{V_{particle}}$ (2.17)

Total column porosity: $\varepsilon_t = \frac{V_{int}+V_{pore}}{V_c} = \varepsilon_b + (1-\varepsilon_b)\varepsilon_p$ (2.18)

The accurate determination of these three porosities is very important for quantification and simulation of chromatographic processes. Generally, large tracer substances with a high molecular weight (e.g. blue dextran) which cannot penetrate the solid pores are used to determine the column prosity ε_b (Equation 2.19), while small tracer substances (e.g. acetone, toluene) which are able to penetrate into the pores of the solid particle are used to calculate the total porosity ε_t (Equation 2.20). Subsequently, the particle porosity can be determined by Equation 2.18.

$$\varepsilon_b = \frac{Q \cdot t_{R,large\ tracer}}{V_c} \quad (2.19)$$

$$\varepsilon_t = \frac{Q \cdot t_{R,small\ tracer}}{V_c} \quad (2.20)$$

where Q represents the volumetric flow rate of the moblie phase.

For columns randomly packed with spherical or irregular particles, bed voidage ε_b lies theoretically in a relatively narrow range (0.3 – 0.5 is typical) and mean values of 0.4 can be applied [28, 31]. The value of particle porosities ε_p vary broadly from near zero for pellicular particles without intra-particle pores, to 0.90 or even higher for low-density gels (e.g. agarose or cross-linked dextran). In general, the total porosity ε_t varies over a range of 0.65 – 0.80. For monilithic columns, ε_t will be up to 0.80 – 0.90.

2.1.4. Adsorption Equilibrium Thermodynamics

Adsorption isotherms are of great importance for the prediction of chromatographic processes and further for the process design. An adsorption isotherm is a plot of the loading of a substance within a solid adsorbent as a function of its concentration in the mobile phase. Although more sophisticated isotherms have been developed, the Langmuir isotherm is still the most frequently used adsorption model in chromatography.

2.1.4.1. Single component Langmuir isotherms

In practice, the parameters of multi-component isotherms are commonly determined by a series of single component experiments of the respective substances. Figure 2.12 shows a single component Langmuir isotherm. Only at the very beginning when the concentration of the solute in the mobile phase (c_i) is low, there is a linear relationship with a steep slope between the solute concentration (c_i) and the loading of the solid phase (q_i). Within this initial region the retention time will remain unchanged with the injected amounts and concentrations of the solute. Therefore, operation conditions within this linear range are used for quantitative analysis in analytical chromatography. In contrast, for preparative and industrial chromatography in most cases the relationship between c_i and q_i becomes non-linear and the loading q_i reaches a saturation level with increasing concentration c_i.

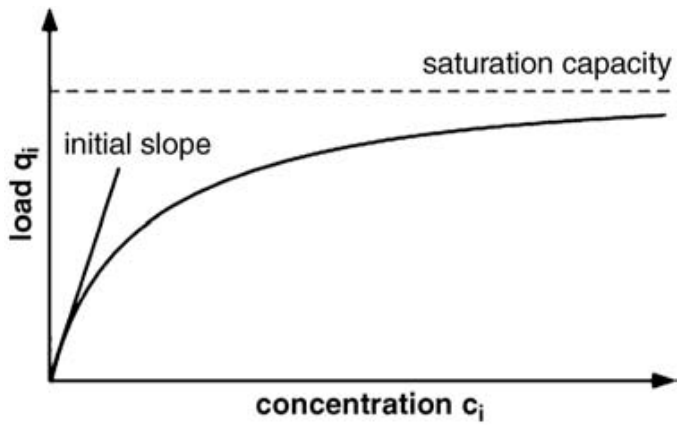

Figure 2.12. Single-component Langmuir isotherm. (Figure cited from ref. [28])

The linear range applies to Henry's Law, that is, the stationary phase concentration (q_i) is proportional to the mobile phase concentration (c_i):

$$q_i = H_i c_i \tag{2.21}$$

The Henry coefficient H_i is determined by the dead time of column (t_0), the retention time of substance i ($t_{Ri,gross}$), and the total porosity (ε_t):

$$H_i = \left(\frac{t_{Ri,gross}}{t_0} - 1\right)\frac{\varepsilon_t}{1-\varepsilon_t} \tag{2.22}$$

The Langmuir adsorption isotherm model is described by:

$$q_i = q_{max,i} \frac{K_{L,i} c_i}{1+K_{L,i} c_i} \tag{2.23}$$

In the above equation q_{max} is the maximum adsorption capacity and K_L is the Langmuir equilibrium constant (affinity coefficient). As can be seen for the case $c_i \rightarrow 0$, $q_{max} \cdot K_L$ is equal to the Henry coefficient H.

2.1.4.2. Multi-component Langmuir isotherms

Multi-component isotherms can be derived from their single component counterparts. In case of the Langmuir isotherm, the multicomponent version can be written as:

$$q_i = q_{max} \frac{K_{L,i} c_i}{1+\sum_j K_{L,j} C_i} \tag{2.24}$$

In the above Equation the maximum adsorption capacity q_{max} is assumed to be equal for all components.

In case of different binding capacities for the individual components due to their different sizes, here assuming component 1 is larger than component 2 for a bi-component system, a modified multi-component Langmuir isotherm is defined [20]:

$$q_1 = \frac{K_1 C_1 [(1+K_2 c_2) q_{max,1} - \Theta_{1,2} K_2 c_2 q_{max,2}]}{1+K_1 c_1 + K_2 c_2 + (1-\Theta_{1,2}) K_1 K_2 c_1 c_2} \tag{2.25}$$

$$q_2 = \frac{K_2 C_2 [(1+K_1 c_1) q_{max,2} - K_1 c_1 q_{max,1}]}{1+K_1 c_1 + K_2 c_2 + (1-\Theta_{1,2}) K_1 K_2 c_1 c_2} \tag{2.26}$$

$$\Theta_{1,2} = \frac{q_{max,1}}{q_{max,2}} < 1 \tag{2.27}$$

where $\Theta_{1,2}$ is the ratio of maximum adsorption capacities.

2.2. Metal−Organic Frameworks (MOFs)

Synthetic nanoporous solids have emerged as an own research field since about 1980s [32]. Emerging more or less from curiosity, they have drawn significant attention in both scientific and industrial community due to their capability to store and separate other molecules. Since more than a decade, the number of papers is strongly increasing, leading to a burst of papers in recent years [33-36]. In general, nanoporous solids can be grouped into two major categories: amorphous solids and crystalline solids. Amorphous solids are composed of subunits with random size and arrangement in three dimensions [37], such as gels, polymers, carbons, glasses, and metal foam. Amorphous solids have two unique properties: (1) cleft or breakage of them will lead to irregular fragments, normally with curved surfaces; (2) they cannot be defined by X-ray radiation due to the irregular arrangement of their components (e.g., atoms, ions or molecules). As a consequence of the disorderly structures, classic amorphous solids show the drawbacks of wide pore size distribution, poor mechanical stability, limited surface area to volume ratio, as well as difficulties in characterization and prediction of topologies. In contrast, crystalline solids are built of regular and repetitive three-dimensional structural subunits (named “crystal lattice”), leading to defined geometrical shapes, relatively sharp and well-defined melting or boiling points and rigid structures. A well-known example is zeolites with their regular pore sizes in the nanometer range. Hence, new classes of crystalline solids have been extensively developed and intensively studied due to their advantages of simple characterization, reproducible topologies and dimensions, and remarkable mechanical and thermal stabilities [38, 39].

Metal−organic frameworks (MOFs), also called porous coordination polymers (PCPs) [40-42], are a new class of highly ordered and usually crystalline porous solids discovered about two decades ago [43]. MOFs are built from inorganic metal ions or clusters interconnected by functional organic linkers through strong coordination bonds to form infinite one-dimensional (1D) chains or ladders, two-dimensional (2D) grids, or three-dimensional (3D) frameworks [44-51], as shown in Figure 2.13. The first MOF material was reported by Kinoshita in 1959 [52], but it did not receive much attention until Yaghi, Zaworotko, Kitagawa, and other scientists discovered the enormous potential provided by MOF materials in recent years [46,53]. In particular, Yaghi [54] first proposed the term of MOFs in 1995 for the fabrication of the highly crystalline framework [Cu(4,4′-bipyridyl)$_{1.5}$ · $NO_3(H_2O)_{1.25}$]. Since then, a growing number of research has been conducted on MOFs materials with a wide range of applications from separation [55], to gas storage [56,57], catalysis [58-60], sensing [61,62], magnetism [63], and so on.

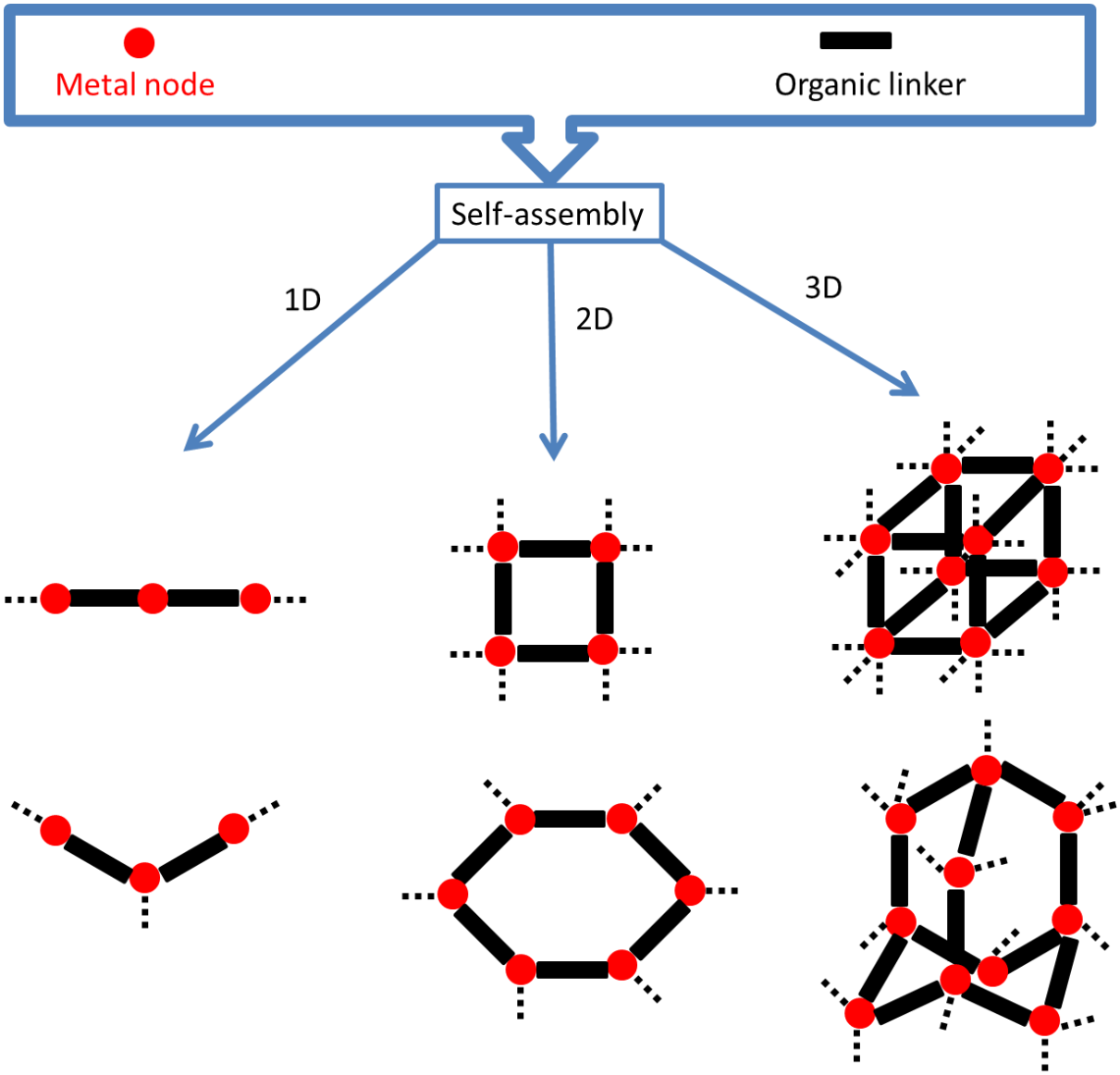

Figure 2.13 Self-assembly of metal modes and organic linkers into 1-3D MOFs structures.

2.2.1. Design of MOFs

Inorganic metal-containing nodes and organic linkers are the two building units of MOFs. In principle, rational design of MOFs with unique functional properties can be incorporated into the framework, based on the wide range of structural, adsorption, electrical, catalysis and sensing properties of the inorganic metal nodes and organic ligands.

2.2.1.1. Secondary building units (SBUs)

The construction of MOF architectures depends on the primary building blocks and one generally accepted concept for depicting MOF self-assembling is called secondary building units (SBUs) [64]. SBUs are known as the basic geometric figures (generally referred to inorganic clusters or coordination spheres) connected by the organic ligands for the assembling of MOF frameworks. The metal atoms are regarded as vertices and the organic

ligands as linkers or edges. The information of a SBU is important for the prediction of MOF topologies, although they are commonly not introduced individually. A review focused on SBUs for MOFs has been published by Yaghi and 131 SBUs geometries were introduced [65]. Different transition metal ions are coordinated with the organic ligands, which can give rise to different SBUs geometries, such as tetrahedral, octahedral, tetragonal paddlewheel, trigonal, square planar, and so on. Figure 2.14 shows several examples of commonly occurring SBUs in MOFs.

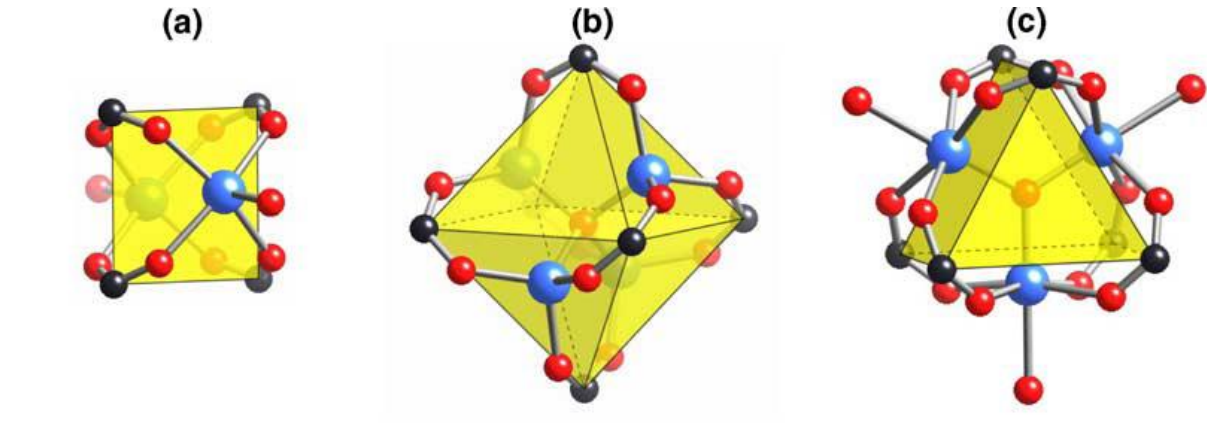

Figure 2.14 Structural representations of several common SBUs of MOFs, including (a) the square paddlewheel, (b) the octahedral paddlewheel, and (c) the trigonal planar. (Figure taken from ref. [43])

2.2.1.2. Metal nodes

Transition metal ions play a significant role as the connector node, leading to diverse coordination numbers and binding orientations (coordination geometries) in the construction of MOFs. In general, the metal elements from group 3 to 12 in the periodic table (Figure 2.15 marked in the blue frame) are mostly chosen to comprise the SBUs in MOF structures. The characteristic of these transition metal elements is that their d-orbitals are partially filled, and therefore the lone electron pairs can be filled into these orbitals. Furthermore, the metal ions will provide the required charge balance for MOFs if anions are introduced. The neutral skeleton of MOFs is favorable for the stability of the structures.

During the construction of MOFs, the metal atoms are usually centered in the SBUs and encircled by the organic linkers to form the coordinative bond. Even if the same metal and its oxidation state are used, it can form various coordination numbers (usually 2 to 7) which will lead to versatile geometries. For example, Cu^{II} ions with d^9 configuration prefer square-planar and tetrahedral geometries. However, other coordination numbers and geometries can be realized by varying the reaction conditions, such as solvents and ligands [66]. In addition, lanthanide ions can generate fresh and uncommon geometries because of their large coordination numbers from 7 to 10 [67-69]. Moreover, removing coordinated solvent molecules sometimes can be used for the generation of useful vacant sites (i.e., coordinately unsaturated lanthanide ion centers), which can be applied in gas adsorption, sensors, and catalysis [70, 71].

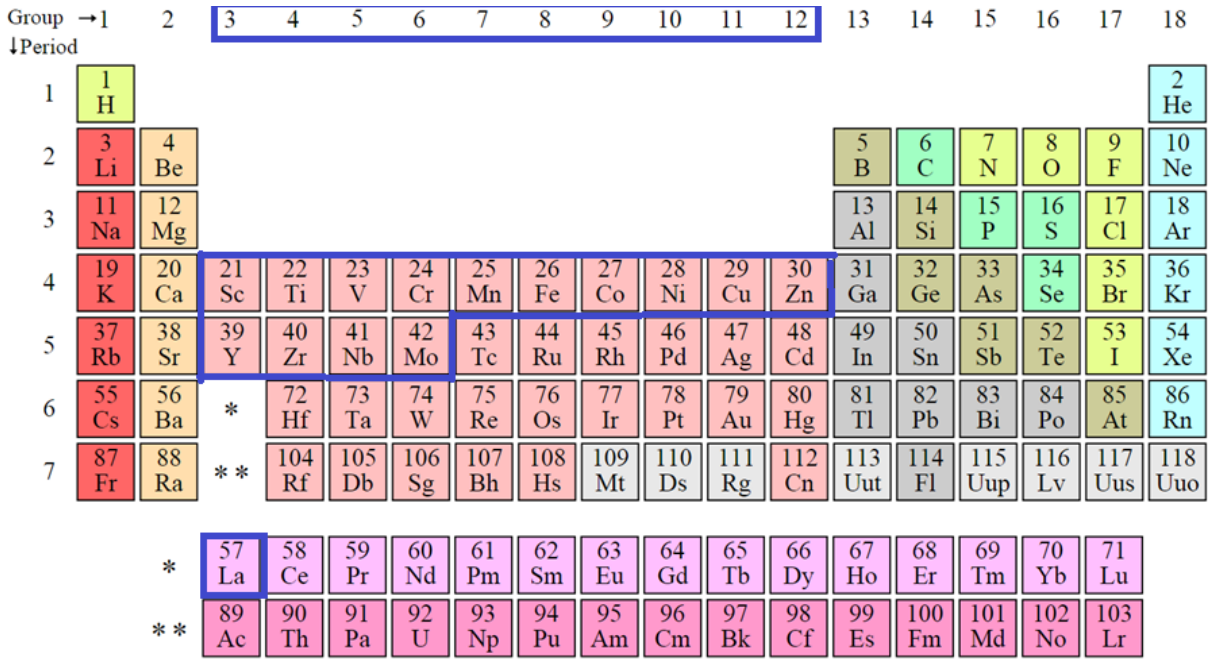

Figure 2.15 The extended metal elements (marked in the blue frame) used to form the SBUs in MOFs.

Obviously, different transition metal centers may generate the same MOF structures, but have considerable impact on the functionality of MOFs, and further dominate their application. For instance, M-MOF-74 (also known as M/DOBDC, $DOBDC^{4-}$ = 2,5-dioxido-1,4-benzenedicarboxylate), are a group of isostructural MOF crystals with diverse open $metal^{II}$ ions, where M can be Zn [72], Fe [73], Mn [74], Ni [75], Mg [76], and Co [77]. Yaghi et al. [78] demonstrated that different metal sites of MOF-74 provide quite different behaviour with respect to gas adsorption.

2.2.1.3. Organic linkers

The organic linkers or ligands, as the lone electron pair donors (also denoted as Lewis base), play a prominent role in the flexibility and directionality of MOF structures, indicating a tunable functionality and topology of engineered MOFs.

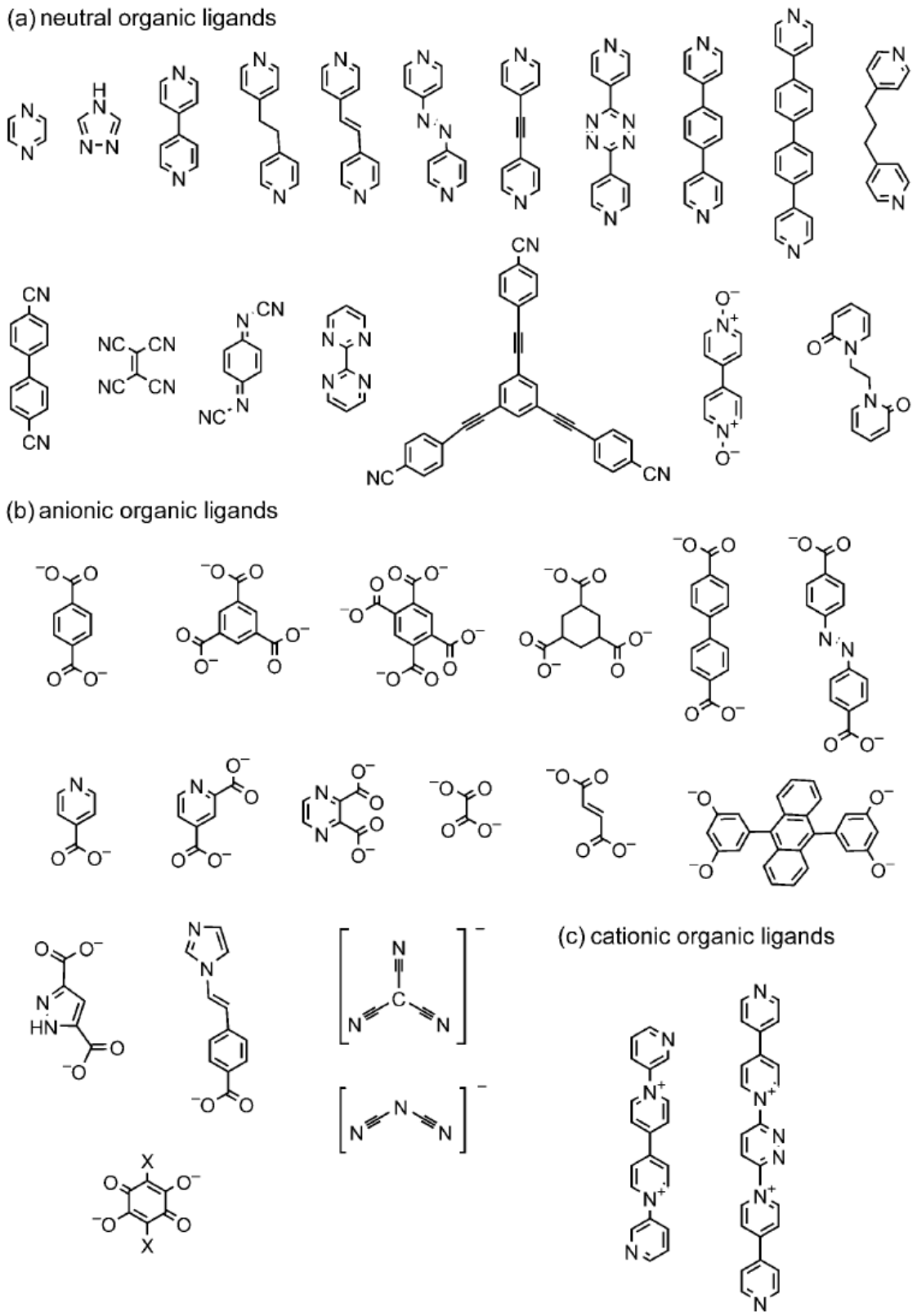

Figure 2.16 Some examples of organic linkers used in MOFs. (Figure taken from ref. [42])

Furthermore, the linkers can be simple halides (F, Cl, Br, and I) [79] and CN^{-1} ions [80, 81], or neutral, anionic and cationic organic molecules [82-85] (Figure 2.16). The pyrazine [86]

and 4,4′-bipyridine [87, 88] are the two most commonly used neutral organic linkers to form 3D MOFs. Additionally, carboxylic acid based molecules are the most popular anionic linkers due to their capacity of aggregating metal ions into clusters and giving rise to more stable and robust MOF networks [89-92]. Cationic organic linkers are rarely utilized, because they have very low affinities for cationic metal ions [93, 94]. In brief, linkers with rigid backbones are frequently chosen due to their rigidity allowing for a prediction of the MOF geometry before its synthesis, and also for their ability to preserve the open-pore structure after the included solvent is removed.

The design of organic linkers determines the shape, pore size, open space and interpenetration of the MOF networks, which guides the application of MOFs. For example, size and/or shape exclusion, also known as steric separation, is one of the most frequent applications of MOFs. Appropriate pore size and/or geometry of MOFs can be achieved by using the organic linkers with different sizes or shapes [95]. Also, the desired functionalities of MOFs can be created through incorporating linkers with functional groups of particular interest into the frameworks during the MOF synthesis.

2.2.2. Synthetic Routes to MOFs

Numerous approaches for the preparation of MOFs have been developed, including hydro/solvothermal, microwave, electrochemical, mechanochemical, and sonochemical methods [96]. Based on the reaction conditions, these synthesis methods can be classified into two categories: solvent-free chemistry [97-99] and solvent-based chemistry [100]. The merit of the solvent-free method is the easiness of operation, such as e.g. in the case of the mechanochemical synthesis method [101]. However, often these methods have difficulties in separating and obtaining the required MOF crystals from the unconverted reactants. Therefore, the liquid-based chemistry method is more commonly used. The hydro/solvothermal method, adopted from zeolites synthesis [102], is the earliest and the most popular (about 70%) technique for the preparation of MOFs [103]. Typically, in a closed reactor, the metal nodes and the organic ligands are dissolved together in a solvent and the mixture is subjected to heating until the end of the reaction to crystallize the MOF products. Frequently-used solvents are water, dimethylformamide (DMF), ethanol (EtOH), methanol (MeOH), acetone, acetonitrile (ACN), diethylformamide, and so on. Mixed solvents are sometimes required to ensure that the various reactants with different solubilities can mix thoroughly. The crystallization reaction significantly varies with multiple parameters, such as temperature, pH, type of solvent, heating time, as well as concentrations and solubilities of reactants. The advantages of the hydro/solvothermal synthesis method include their large-size crystal products, easy accessibility and scale-up. However, with this method, it is challenging to produce nanocrystals, to control the size and orientation of the crystals, and to have a high yield. Therefore, persistent efforts have been made towards the development of new synthesis methods.

In the past two decades, MOFs have attracted extensive attentions and more than 20,000 different MOF structures have been reported [104], such as the typical IR-MOFs (isoreticular MOFs) [95, 105, 106], MIL-*n* series (Materials Institute Lavoisier) [107-110], and ZMOFs (zeolitic MOFs) [111,112].

2.2.3. Properties and Applications of MOFs

The advantages of MOFs over conventional zeolites are the multiple design aspects on the basis of the metal nodes and organic linkers [65, 113, 114]. The versatile SBUs provide MOFs with elastic structures, versatile framework functionalities, and tunable pore sizes. Generally, by controlling the length of the organic linkers, the pores of MOFs can be tuned from zero, to microsize (< 2 nm) and mesosize (2 nm < pore diameter < 50 nm) with open channels or cavities surrounded by microporous windows. The architecturally robust MOF structures give rise to ultrahigh porosity, mostly up to 90% free volume. MOFs have incredibly high surface areas typically ranging from 1000 to 10,000 m^2 g^{-1} [115, 116], which surpass the conventional porous materials (e.g. zeolites, carbons). Additionally, MOFs are characterized by permanent porosity, excellent thermal and chemical stability and versatile chemistry, allowing for easy postsynthetic modification. Such properties offer this class of materials numerous promising applications. Here, a few of the typical applications, including gas storage and adsorption, separation processes, catalysis, sensing and chromatography, are mentioned.

2.2.3.1. Gas storage and separation

With the growing global energy needs and the threat of climate change, the demand for new energy is expanding. Gases, such as hydrogen (H_2) and methane (CH_4), are of great importance for energy production. The global warming caused by greenhouse gases (e.g. carbon dioxide, CO_2) also becomes an urgent problem to be solved. Hence, questions about storage and separation of these gases are being paid intensive attention. MOF materials have shown good capabilities as host matrix for gas storage and separation (CH_4, H_2, CO_2, *etc.*) as a result of their large surface areas, tunable pore sizes and low crystal densities [117-119].

The exceptional specific surface area and high porosity of MOFs make them efficiently capture miscellaneous gas molecules. In brief, the gas can be either adsorbed by the MOFs via the strong interaction between the framework (mainly the metal nodes sites) [120] and the gas molecules, or be stored in the MOF cavities without gas-solid interaction [121]. Yaghi *et al.* [122] reported in 2010 that MOF-210 exhibited unprecedented uptake capacity of 2400 mg g^{-1} (298 K and 60 bar), 176 mg g^{-1} (77 K and 70 bar) and 264 mg g^{-1} (298 K and 80 bar) for CO_2, H_2 and CH_4, respectively. MOFs have also been explored for the adsorptive separation of hydrocarbons and hazardous gases (e.g. carbon monoxide, ammonia) [123]. Generally, the principal reasons behind the gas adsorption in MOF materials are the affinity towards the targeted gases and the size of the pores. For instance, amino-functionalized MIL-

53(Al) showed the successful separation of CO_2/CH_4 binary mixtures, due to the fact that the amino groups have a high sorption affinity for CO_2 but not for CH_4 [124].

2.2.3.2. Liquid adsorption and separation

Adsorptive separations play a significant role in chemical and pharmaceutical industry and represent a huge market demand for the sorbents. The adsorptive separation in liquid phase is much more complex than in gas phase, because both the solute and the solvent compete for the solid sorbents. Due to the tunable pore sizes and shapes, large surface areas, and readily accessible space, MOFs have achieved promising abilities in adsorptive removal of hazardous materials, and separation of complex mixtures through selectively adsorption or size exclusion effects. In many instances, MOFs exceed their counterparts, including zeolites, activated carbon, and metal oxides [125]. For example, MIL-101(Cr) outperforms activated carbon both kinetically and in efficiency in case of the adsorption of volatile organic compounds (VOCs) [126]. Besides, chiral MOFs are capable of enantioselective adsorption and separation of enantiomers [127].

Adsorbents can be used in different modes. The most economic manner is to prepare adsorbent-supported membranes [128, 129]. More commonly, MOF adsorbents are mixed with the liquid and separation is caused by different adsorption (diffusion) speed or adsorption affinity [130]. Generally, chromatography (including GC and LC) is an effective method to evaluate the separation performance of an adsorbent. The unique features of low density, absence of dead volume, good solvent stability, and high loading capacity for solutes make MOFs an attractive material for preparative chromatographic separation [131, 132].

Extensive studies have been carried out in gas chromatography (GC) since the bulk MOF-508 was first reported as stationary phases for GC to separate alkanes in 2006 by Chen et al. [133]. The separation resulted from different interactions between the pore walls of the framework and the alkane molecules. Besides the separation of light gases, MOF based GC has also been applied in selective adsorptions and separations of various liquid compounds in vapor phase. In 2010, Gu and Yan [134] reported the first MOF-coated capillary for high-resolution GC separation of a mixture of xylene isomers and ethylbenzene using MIL-101(Cr) as stationary phase.

In comparison to GC, LC separations using MOFs are less investigated. Although only a handful of MOFs have been investigated for HPLC, it was found that MOFs with good solvent stability used as stationary phases show high resolution, selectivity and reproducibility for LC separations. Therefore, since the last decade an increasing attention has been paid to the utility of MOFs for liquid-phase separation. The application of MOFs in HPLC not only opens a new possibility for superior stationary phases, but also offers new insights into the properties of MOFs, including pore sizes, shapes and surface functions.

HKUST-1 (HKUST: Hong Kong University of Science and Technology), MIL-47(V) and MIL-53(Al) (MIL: Materials Institute Lavoisier) were the first MOF-based columns to be

employed for adsorption and separation in LC by Alaerts et al. [135]. These materials displayed strong differences in the order of selectivity regarding xylene isomers and ethylbenzene in a normal phase mode using hexane as the mobile phase, where MIL-47 performed the best and HKUST-1 the worst. The separation performance heavily depends on the nature of analytes and MOFs. Further research from the same group reported the adsorption separation of alkylaromatics with different alkyl groups on MIL-47 and MIL-53 [136]. It was found that MIL-47 showed stronger affinity for n-propylbenzene than cumene as a result of a preferential adsorption enthalpy owing to the presence of a branched isopropyl group. Moreover, the adsorption enthalpy increased with alkyl chain length of n-alkylbenzenes. Both MOFs showed a more favorable adsorption of xylenes than EB. However, the competitive adsorption on MIL-47 was dominated by entropic effects, in contrast to the enthalpic effects on MIL-53.

In 2010, Xu et al. [137] prepared three Cd-MOF isomers with continuously tunable pore sizes (non-, micro- and meso-porous) with 4,4′-bipyridine and 2-amino-1,4-benzenedicarboxylic acid as linkers by simply decreasing reactant concentrations and reaction time. The meso-porous Cd-MOF with a pore dimension of 1.7×2 nm^2 exhibited size-exclusion dominated LC separations for dyes, where the smaller dye Rhodamine 6G (1.3×1.6 nm^2) was allowed for the incorporation, whereas the larger dye Brilliant Blue R-250 (1.8×2.2 nm^2) was size-excluded. However, the micro-porous Cd-MOF isomer (0.8×1.5 nm^2) with smaller pores did not work in the separation of the two dyes.

Yan and co-workers made significant progress on the development of applications of MOFs in chromatography. Using a binary mobile phase of hexane/dichloromethane or dichloromethane/methanol, high-resolution separations of ethylbenzene and xylene isomers, dichlorobenzene, chlorotoluene, and nitrophenol isomers were achieved on a MIL-53(Al) based column [138]. It was found that the mobile phase composition plays an important role on the retention, resolution, and selectivity. In addition, in 2012 this group reported the first application of MOF materials in reverse-phase HPLC [139]. A MIL-53(Al) packed column in combination with a CH_3CN/H_2O mobile phase was investigated to separate a wide range of mixtures, from non-polar to polar and acidic to basic substances with high selectivity, resolution and reproducibility. The mechanisms underlying the separation were related to size-exclusion, shape selectivity and hydrophobicity [139]. In 2013, Yan's group reported the feasibility of MIL-100(Fe) for both normal phase separation of chloroanilines and toluidine isomers, and reverse phase separation of neutral and basic analytes due to the π-π, hydrogen bond and coordination interactions [140]. Recently, a fast and effective HPLC separation of four tocopherols was reached on a post-synthetic modification of MIL-101(Cr) with grafted-pyridine and the separation performance was found to be better than the commercial amino-bonded silica column [141]. This successful application of post-modified MOFs is of great significance for its expansion in separation sciences.

Nevertheless, often HPLC columns packed with bulk MOF particles suffer from problems of low resolution, high backpressure and undesirable peak shapes resulting from the irregular shapes and wide size distribution of pure MOFs. Uniform spherical MOF composites were explored to overcome these problems. To date, only few studies of core-shell MOF composites for HPLC separation have been reported. Tanaka et al. [142] demonstrated the enantioselective separation of chiral sulfoxides using a homochiral MOF-silica composite by simply mixing the MOFs and silica particles. Ameloot et al. [143] synthesized HKUST-1-silica composite spheres by depositing nano-sized HKUST-1 particles inside the meso-pores of silica for chromatographic separation of styrene and ethylbenzene. It was found that this HKUST-1-silica packed column shows high resolution, whereas the mass-transfer efficiency was low, resulting in peak broadening. In another approach, a zeolitic imidazolate framework 8 (ZIF-8) shell was fabricated onto the surface of carboxyl-terminated silica spheres [144]. Due to surface interactions between the analytes and ZIF-8, the obtained ZIF-8@SiO_2 core-shell microspheres showed fast and high-resolution separations of two groups of mixtures (endocrine disrupting chemicals and pesticides) with low column backpressure [144]. In the past two years, the MOF UiO-66 has been paid great attention for the application as HPLC stationary phase, owing to its permanent porosity and high stability in water. Zhang and coworkers [145] prepared a silica-UiO-66 composite via a hydrothermal synthesis and the packed column showed efficient HPLC separation for a series of substituted aromatics, such as chlorobenzene compounds, polycyclic aromatic hydrocarbons (PAHs) and positional isomers. Ding and coworkers [146] reported a one-pot synthesis of UiO-66@SiO_2 shell-core microspheres as HPLC stationary phase for the separation of xylenes and ethylbenzene.

2.2.3.3. Heterogeneous catalysis

Heterogeneous catalysis is one of the most promising applications of MOFs. As solid catalysts, they are easily separated. Furthermore, the tailoring of structures and pore sizes enables them to be of shape- and size-selectivity. Moreover, the high crystalline structure offers a homogeneous distribution of the active sites. Active sites within MOFs can result from three sources: (a) the frameworks themselves, either metal nodes [147] or functional ligands [148]; (b) postsynthetic modification of MOFs by introducing functional centers [149, 150]; (c) encapsulation of dispersed metal nanoparticles into the MOF structure [151]. Although much effort has been made and exciting progress has been gained, there is still a long way left for MOFs serving as catalysts. This is mainly because MOFs are lacking the required stability during their repeated and long time use in practice.

2.2.3.4. Sensing

The sensitive detection of a target compound and the sharp differentiation from other compounds are essential in environment and industrial fields. The structural versatility and predictability of MOFs offer them another important application as luminescent sensors to detect the vapor-, liquid- or solution-phase target analyte. Fluorescence and phosphorescence are the two most common types of luminescence in case of MOF-based sensors. In general,

luminescence either comes from the MOF building components: metal ions or clusters and/or organic linkers, or from the emission of the adsorbed guest molecules. Photoluminescence arises from photo-excitation. Incorporation of lanthanide metal ions (particularly Eu and Tb) into MOF structures is widely employed to make luminescent MOFs, owing to their charge transfer from *d* to *f* shells, accompanied by a strongly visible luminescence in the red and green regions, respectively [152, 153]. Organic linkers with aromatic groups or large conjugated π systems are usually chosen to synthesize luminescent MOFs, such as stilbene, naphthalene, perylene, anthracene, to name a few [154, 155]. Contributing greatly to the π electrons in such linkers, the luminescence of transition-metal MOFs are initiated by various charge transfer processes: (a) ligand-to-ligand charge transfer (LLCT); (b) the metal-to-ligand charge transfer (MLCT); and (c) the ligand-to-metal charge transfer (LMCT) [156-159]. So far, MOF-based luminescence has been successfully applied in different fields, including the detection of target species [160], biosensing and imaging [161], luminescent thermometers [162], and so forth.

2.2.4. Surface−Mounted Metal−Organic Frameworks (SURMOFs)

Metal−organic framework (MOF) thin films, which are adhesive to solid substrates and ranging from nanometers to micrometers in thickness, are especially important in some applications, as for example optical coatings [163, 164], gas separation or sensor applications [128, 165, 166]. So far, there have been several innovative approaches developed for the synthesis of MOF thin films, like Langmuir-Blodgett [167], mother solution [168], seeded growth [169], spin-coating [170], electrochemical methods [171], assembly of preformed MOF nanocrystals [172, 173], stepwise dosing of reagents [174] and liquid-phase epitaxy [175, 176]. Among these methods, the liquid-phase epitaxy (LPE), also referred as layer-by-layer (LBL) method, relying on the stepwise, layer-by-layer adsorption of MOF components from the liquid or gas phase to a surface plays an important role in the fabrication of highly orientated MOF coatings with controlled thickness. The resulting MOF thin films are referred to as surface-mounted metal-organic frameworks (SURMOFs).

2.4.1.1. Surface functionalization

Different from the conventional one-pot reaction of bulk MOFs, SURMOFs are prepared on the surface of a solid substrate in a layer-by-layer fashion, in which the substrate is alternatively immersed in the metal solution and then in the organic linker solution. Therefore, based on the LPE method, the substrate surfaces must be chemically modified with different groups, like carboxyl (-COOH), hydroxyl (-OH) or pyridyl, to provide active sites to bind the metal ions in the first step [168,177].

The first functionalized surfaces employed for the growth of SURMOFs were self-assembled monolayers (SAMs) on Au substrate [168]. SAMs, exposing an organic surface, become an attractive interface for the MOF growth because of their easy preparation, spontaneous

assembly and diverse functional groups. In particular, under controlled synthesis conditions, organic thiols attached -SH groups, such as 16-mercaptohexadecanoic acid (MHDA) [178], (4-(4-pyridyl)phenyl)-methanethiol (PP1) [179] or 11-mercapto-1-undecanol (MUD) [180], could form a monolayer terminated with the desired functional group on suitable substrates for SURMOFs growth.

Apart from SAMs, SURMOFs can also be prepared on other nonmetallic substrates, ranging from polymer surfaces and conductive substrates (Indium tin oxide and Fluorine-doped tin oxide) over quartz glass to metal-oxide membranes. In addition all sorts of shaped surfaces, like magnetic particles [181], soft materials (papers or textiles) [182], or even previously prepared multilayered SURMOF thin films [183] can be used. Generally, chemical modifications of the nonmetallic substrates to obtain the suitable functionalized group on the surfaces are required [181, 184, 185].

2.4.1.2. Preparation of SURMOFs

The most common and effective method to prepare SURMOFs is the liquid-phase epitaxy (LPE) or layer-by-layer procedure, which was originally proposed to fabricate multilayer organic Langmuir Blodgett (LB) films [186]. After several decades, Decher and Hong employed the LPE method to fabricate coatings of oppositely charged polymers by immersing substrates alternatingly in a polyanion and polycation solution [187, 188]. The LPE method was soon used to fabricate lamellar Hofmann clathrate films by coordination polymers and metal complexes [189].

In 2007, the LPE method was demonstrated to grow MOF films on surfaces by Fisher and Wöll [175]. The first example is the growth of HKUST-1 ($[Cu_3(BTC)_2]$) on functionalized substrates (MHDA SAMs on Au). The inorganic ($Cu(OAc)_2$) and organic (BTC) precursors were dissolved in ethanol in separate containers. The functionalized substrate was sequentially immersed into the two solutions and washing steps with ethanol were performed following each immersion to remove unreacted metal or organic molecules. The repetition of these processes was performed to obtain MOF thin films. During this procedure, the paddle-wheel-like $Cu(OAc)_2$ compound chemically binds to the SAM and then the BTC-linker molecules bind to the $Cu(OAc)_2$, resulting in a periodic and interconnected crystalline structure.

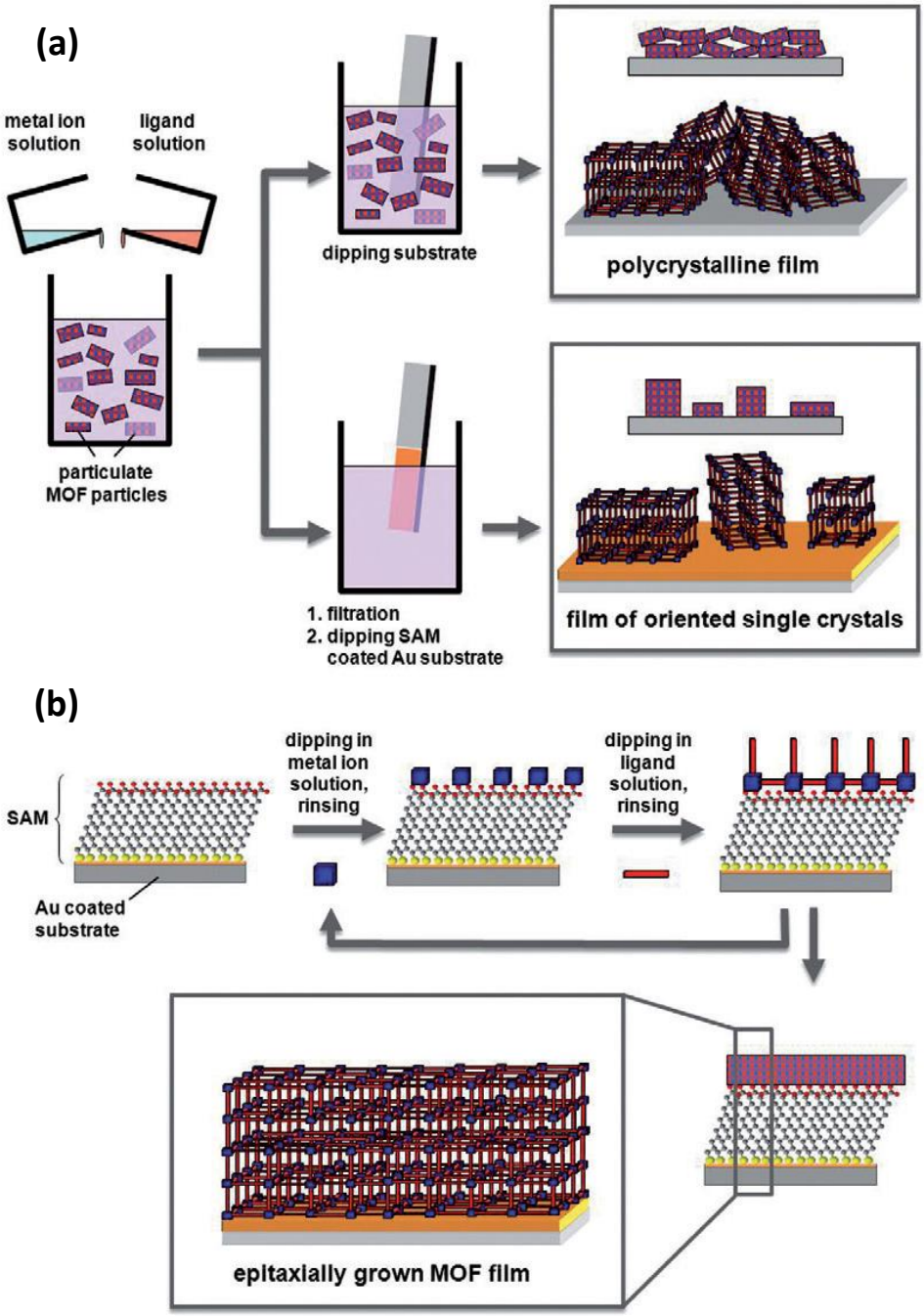

Figure 2.17 Schematic representation of the preparation of SURMOFs. (a) The coating of a substrate with freshly prepared particulate MOF (above), and the growth of MOF crystals directly on a SAM-terminated gold surface immersed in a mix with metal nodes and linkers (below). (b) Deposition of SURMOFs by a LPE process starting from a functionalized SAM attached to a gold coated substrate. The thickness of the SURMOF depends on the number of deposition cycles. (Figure taken from ref. [190])

The LPE method has a huge advantage with respect to its ability to control thickness and orientation of the MOF thin films on the surface. The thickness is controlled by adjusting the numbers of growth cycles and the orientation is tuned by the functional groups exposed on the surface [190]. Figure 2.17 illustrates the difference between the conventional way to

produce MOF films by immersing a substrate into a fresh mixture of the precursors (Figure 2.17a) and the LPE method (Figure 2.17b). Figure 2.17a shows two techniques for conventional SURMOF growth: either (1) a coating of MOF particles is attached to an arbitrary substrate by simply mixing the metal ion-containing solution and the linker solution, followed by the immersion of the substrate directly into the freshly prepared particulate MOF suspension [165, 168]; or (2) a substrate functionalized with a SAM is immersed in the mixture after suspended MOF particles have been filtered out in advance [177]. These techniques always result in heterogeneous MOF coatings. Such MOF films consist of individual particles with often arbitrary directions and sizes, even not specifically bounded to the substrate, leading to numerous major drawbacks in many applications. Obliviously, the LPE method has overcome these defects and provides well-defined homogenous and uniform MOF thin films (Figure 2.17b).

Due to the superiority of the generated SURMOFs, over the last years several techniques have been developed for their preparation using different LPE methods.

(1) Dipping method.

A hand-dipping procedure was the initial method to prepare SURMOFs by LPE. The procedure uses three containers for the three different solutions (metal ion precursor, linker solution and pure solvent) [175]. The scheme is shown in Figure 2.18 and an exemplary process of preparing HKSUT-1 is as follows:

- The functionalized substrate is firstly dipped in the $Cu(OAc)_2$ EtOH solution for 30 min.
- Then the substrate is taken out and immersed in pure EtOH in order to remove the unreacted metal ions.
- Then the substrate is dipped into the BTC EtOH solution for 60 min.
- The substrate is taken out and immersed in pure EtOH in order to remove the excess BTC.
- By subsequently repeating the above steps using the same substrate, thicker HKUST-1 MOF films are prepared.

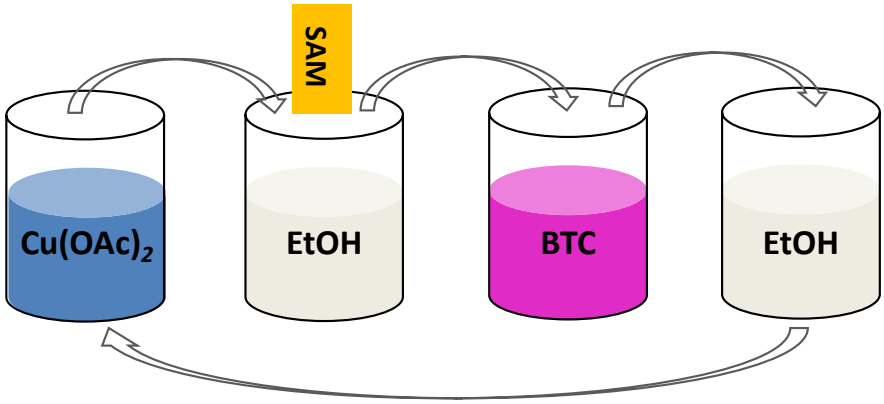

Figure 2.18 Schematic representation of the steps of the "dipping by hand" method for SURMOFs preparation. (Figure taken from ref. [191])

Since the hand-dipping method is very time-consuming, a robot dipping machine was developed, which is automatic and computer controlled. The setup is shown in Figure 2.19. The procedure follows the same steps as the 'dipping by hand' method. After each step, there is an EtOH shower for rinsing in the center of the setup. Compared to the hand-dipping, there are more containers and the rinsing container can be in an ultrasonic bath in order to improve the rinsing efficiency.

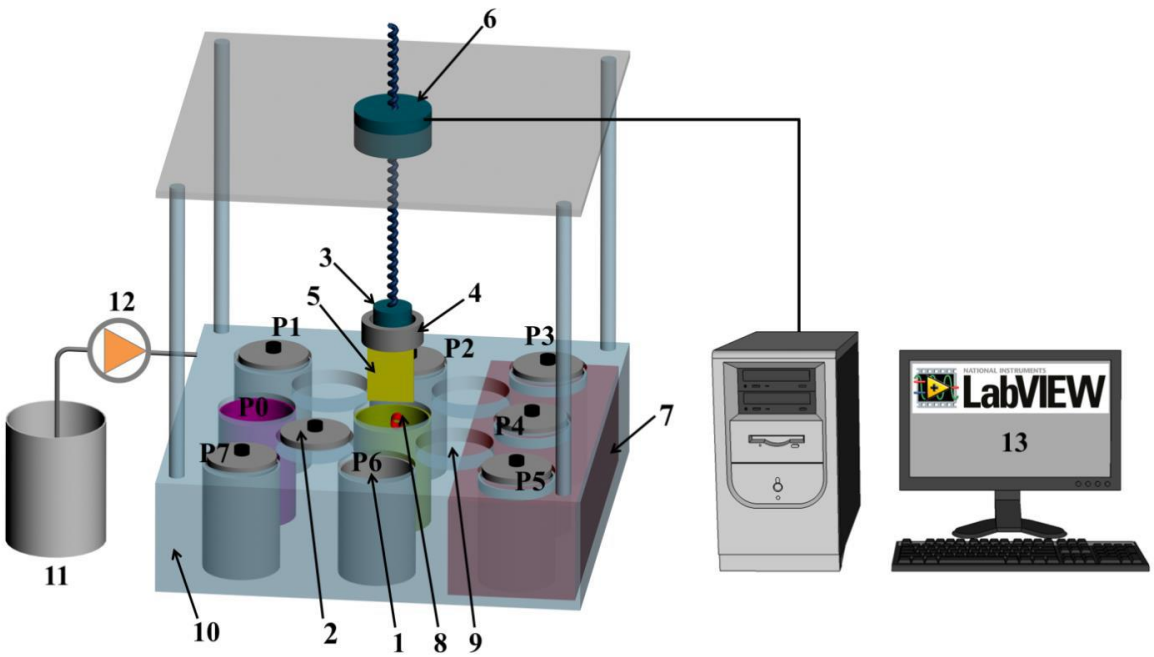

Figure 2.19 The setup of a dipping robot system: (1) containers for immersion solutions or placement for sample (P1~P7); (2) container lid; (3) magnetic connector; (4) sample holder; (5) sample; (6) position controller; (7) ultrasonic bath; (8) shower; (9) parking position of container lid; (10) Teflon working table; (11) solution bottle for showering; (12) pump; (13) PC. (Figure taken from ref. [191])

(2) Spray method.

The spray method, a high-throughput technique, can reduce the time needed to prepare SURMOFs by more than two orders of magnitude [185]. It is based on a nozzle system, and the scheme is displayed in Figure 2.20. During the spraying an aerosol of the metal ion and organic linker solution is produced. The metal and organic linker reactants are sprayed on the substrates alternatively in a fashion similar to that occurring during the LPE process. When the droplets within the aerosol impinge on the substrate, the reactants will be deposited on the surface, resulting in the surface coated with a thin film of the reactant. Between the spraying steps with the MOF compounds, rinsing with ethanol has been shown to be a crucial step to remove unreacted materials.

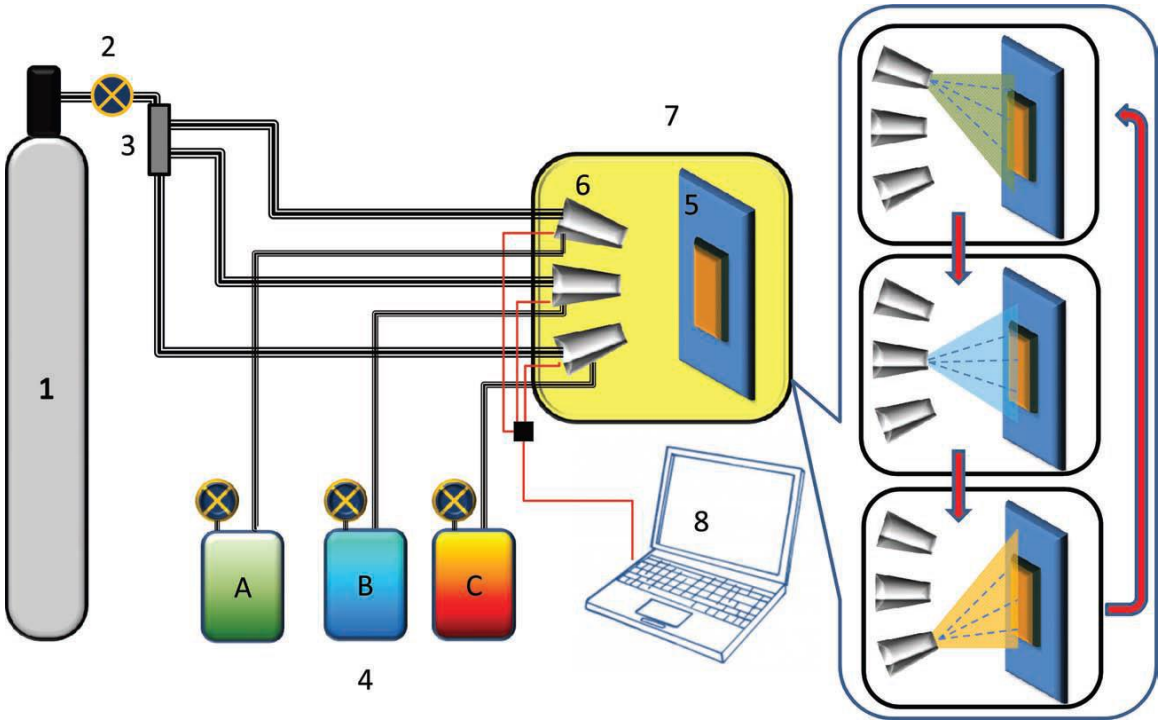

Figure 2.20 Sketch of the spray system for layer-by-layer growth of SURMOFs (1) Gas supply, (2) gas flow controller, (3) three-way valve gas distributor, (4) (A, B, C) solutions storage containers, (5) sample holder, (6) dosing valves, (7) spray chamber, (8) PC. (Figure reproduced from ref. [185])

There are two kinds of spraying machines in operation at the IFG: hand-spray and automatic-spray. For the hand spray method, there are two nozzles for spraying the reactant solutions and the solvent used for rinsing is kept in a squeeze bottle. All the procedures are performed manually. For the automatic spray method, there are three nozzles, two of which are for spraying the reactant solutions (metal ion source, organic linkers) and the third is for the rinsing solvent. All the steps are executed automatically by a computer.

Using again the exemplary preparation of HKUST-1, the detailed procedure of the automatic spray method is as follows:

- $Cu(OAc)_2$, BTC ethanolic solution and pure ethanol are kept in three separate containers sealed with lids.
- The parameters (i.e. spray pressure or time) of the automatic system are set, and the functionalized substrate is fixed on the sample holder.
- The functionalized substrate is first sprayed with $Cu(OAc)_2$ EtOH solution for 15 s.
- After waiting for 30 s, the substrate is rinsed with pure EtOH for 5 s to remove unreacted metal ions.
- Then the substrate is subsequently sprayed with the BTC EtOH solution for 30 s.
- After waiting for 30 s, the substrate is rinsed again with pure EtOH for 5 s to remove unreacted organic ligands.

Repetition of the above steps using the same substrate until the desired number of cycles is reached results in a HKUST-1 thin film of the desired thickness.

(3) Pump method.

The pump method was developed to control the temperature during the growth of MOFs [192] within a range of -20 ~ 150 °C (i.e. 20 ~ 70 °C for ethanol as solvent). A scheme of the pump system setup is shown in Figure 2.21. The procedure used by the pump method is similar to the one of the spray method based on the layer-by-layer fabrication concept. There are four pumps, three of which are used to deliver the solutions (metal ion solution, linker solution and pure solvent) into the container where the substrate is placed, and the forth is responsible to discharge the solutions from the container. The temperature of the container is controlled by a heating/cooling circulation system. Compared to the spray method, the pump method requires much longer time to reach the same thickness of the SURMOF films. Exemplarily, a detailed procedure of HKUST-1 synthesis by the pump method is given below:

- A substrate is placed within the container and the temperature is set at 50 °C.
- The freshly prepared substrate is immersed in a 1 mmol L^{-1} solution of the metal precursor ($Cu(OAc)_2$) EtOH for 15 min.
- The substrate is rinsed with EtOH solution for 2 min.
- The substrate is immersed in a 0.2 mmol L^{-1} solution of BTC EtOH for 30 min.
- The substrate is rinsed with EtOH solution for 2 min.
- The steps 2 to 5 are repeated in order to grow thicker layers.

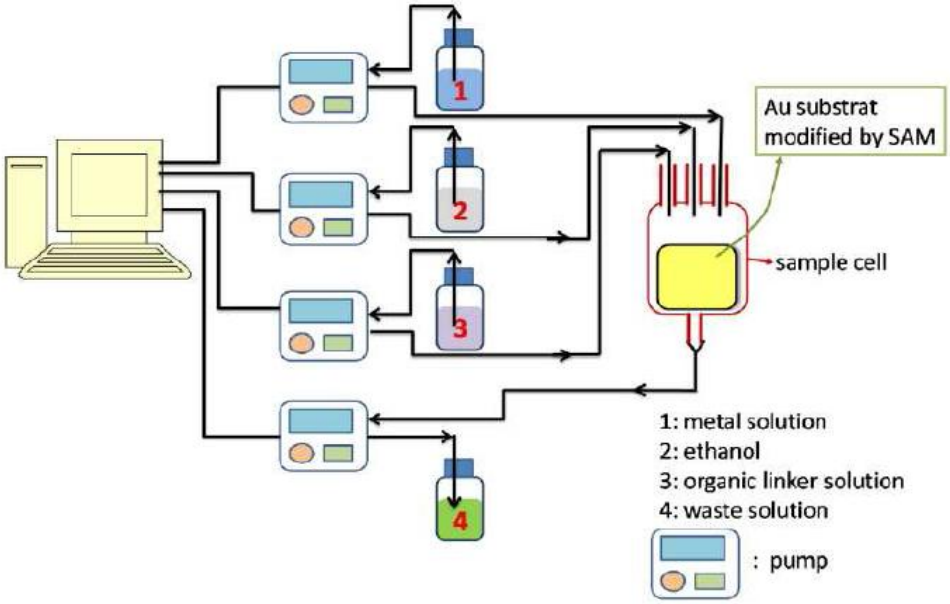

Figure 2.21 Schematic diagram for the automated LBL growth of MOF thin films applying a multi-pump system. (Figure taken from the supporting information of ref. [192])

(4) Synthesis in a quartz crystal microbalance (QCM) cell.

A QCM is an instrument on the basis of piezoelectricity to monitor very small mass changes. The growth of SURMOFs can be conducted by *in-situ* synthesis in a QCM cell, while the system monitors the changes of the resonance frequency of the quartz sensor as a function of the deposition and removal of material [180]. Connecting a QCM cell to a pump system as described in (3), the growth of MOF thin films by LPE can be followed step by step.

2.4.1.3. Properties and applications of SURMOFs

Except for possessing the advantages of MOFs, oriented SURMOFs offer a series of unique properties due to their defined structures: (i) precisely controlled thickness and growth orientation, (ii) smooth and homogenous surface coating.

Apart from the common properties, SURMOFs may also diverge in a controlled matter their metal nodes or linkers between different layers. E.g., the copper precursor can be replaced by a zinc precursor during the epitaxial growth process [193]. Liu et al. [194] employed porphyrin ligands to obtain light-harvesting SURMOFs because of the intrinsic property of the organic linkers. The prepared SURMOF thin films also can be functionalized by post-synthetic modification (PSM) [195]. This chemical variety of the connecting nodes and linkers provides versatile SURMOFs.

Taking into account the advantages of controlled thickness and orientation, versatile chemistry, as well as the choice of diverse substrates, such as metals, oxides, polymers, conductive substrates and textiles, SURMOFs have a wide range of applications, such as gas separation [196], sensing [197], electronic applications [194] and several more [198-200].

2.2.5. Introduction of MOFs Investigated in This Study

Screened from the series of MOFs, three different micro- or meso-MOFs, i.e. UiO-67, HKUST-1, and MIL-100(Fe), are applied in this work. All three MOFs are named after the location where they were originally synthesized, namely the Hong Kong University of Science and Technology (HKUST), Materials Institute Lavoisier (MIL), and University of Oslo (UiO). The properties of the investigated MOFs are shown in Table 2.2.

Table 2.2 Investigated MOFs synthesized by LPE method and their properties.

MOF material	Surface area Langmuir (m^2 g^{-1})	Window diameter/Pore opening (Å)	Pore/Channel diameter (Å)	Thermal stability (°C)	Water stability	Volume per unit cell ($Å^3$)	Ref.
UiO-67, Zr-BPDC	1800–3000	8	11.5; 16	300	yes	19889	[201, 202]
HKUST-1, Cu-BTC	1500–2200	4.6; 9	6; 11.1	280	no	18280	[203, 204]
MIL-100(Fe), Fe-BTC	2500–4500	4.7–5.5; 8.6	25; 29	270	yes	2198805	[205]

References

[1] M.S. Tswett, On a new category of adsorption phenomena and their application to biochemical analysis, Tr. Protok. Varshav. Obshch. Estestvoispyt. Otd. Biol. 14 (1903) 20-39.

[2] R. Willstätter, A. Stoll, Untersuchungen über Chlorophyll: Methoden und Ergebnisse, 1_{st} ed. Julius Springer-Verlag, Berlin, 1913.

[3] A.J.P. Martin, R.L.M. Synge, A new form of chromatogram employing two liquid phases, Biochem. J. 35 (1941) 1358-1368.

[4] J.M. Miller, Chromatography: Concepts and Contrasts, 2_{nd} ed. Wiley-Interscience, New Jersey, 2005.

[5] A. Seidel-Morgenstern, M. Schulte, A. Epping, Preparative Chromatography, (2_{nd}), Wiley-VCH Verlag GmbH & Co. KGaA, 2012.

[6] V.R. Meyer, Practical High-Performance Liquid Chromatography, 5_{th} ed. Wiley, Switzerland, 2010.

[7] G. Guiochon, A. Felinger, D.G. Shirazi, A.M. Katti, Fundamentals of Preparative and Nonlinear Chromatography, 2_{nd} ed. Elsevier, Amsterdam, 2006.

[8] M.W. Dong, Modern HPLC for Practicing Scientists, 1_{st} edition ed. John Wiley & Sons, Inc., New Jersey, 2006.

[9] L.R. Snyder, J.J. Kirkland, Introduction to Modern Liquid Chromatography, 2_{nd} ed. John Wiley&Sons, New York, 1979.

[10] L.R. Snyder, J.J. Kirkland, J.L. Glajch, Practical HPLC Method Development, 2_{nd} ed. Wiley-Interscience, New York, 1997.

[11] V.R. Meyer, Practical High-Performance Liquid Chromatography, 4_{th} ed. John Wiley & Sons, New York, 2004.

[12] S. Fekete, J.L. Veuthey, D. Guillarme, New trends in reversed-phase liquid chromatographic separations of therapeutic peptides and proteins: Theory and applications, J. Pharm. Biomed. Anal. 69 (2012) 9-27.

[13] U.D. Neue, HPLC Columns Theory Technology practice. John Wiley&Sons,Inc., New York, 1997.

[14] T. Takeuchi, Lloyd R. Snyder and John W. Dolan: High-performance gradient elution. The practical application of the linear-solvent-strength model, Anal. Bioanal. Chem. 389 (2007) 1659-1660.

[15] A.J. Alpert, Hydrophilic-interaction chromatography for the separation of peptides, nucleic-acids and other polar compounds, J. Chromatogr. 499 (1990) 177-196.

[16] J.A. Queiroz, C.T. Tomaz, J.M.S. Cabral, Hydrophobic interaction chromatography of proteins, J. Biotechnol. 87 (2001) 143-159.

[17] E. Boschetti, Antibody separation by hydrophobic charge induction chromatography, Trends Biotechnol. 20 (2002) 333-337.

[18] M.M. Diogo, J.A. Queiroz, D.M.F. Prazeres, Studies on the retention of plasmid DNA and Escherichia coli nucleic acids by hydrophobic interaction chromatography, Bioseparation 10 (2001) 211-220.

[19] R. Hayes, A. Ahmed, T. Edge, H. Zhang, Core–shell particles: Preparation, fundamentals and applications in high performance liquid chromatography, J. Chromatogr. A 1357 (2014) 36-52.

[20] T. Gu, G.J. Tsai, G.T. Tsao, Multicomponent adsorption and chromatography with uneven saturation capacities, AlChE J. 37 (1991) 1333-1340.

[21] S. Fekete, E. Oláh, J. Fekete, Fast liquid chromatography: The domination of core–shell and very fine particles, J. Chromatogr. A 1228 (2012) 57-71.

[22] G. Guiochon, F. Gritti, Shell particles, trials, tribulations and triumphs, J. Chromatogr. A 1218 (2011) 1915-1938.

[23] J. Liu, S.Z. Qiao, J.S. Chen, X.W. Lou, X. Xing, G.Q. Lu, Yolk/shell nanoparticles: new platforms for nanoreactors, drug delivery and lithium-ion batteries, Chem. Commun. 47 (2011) 12578-12591.

[24] X. Zhang, H. Niu, W. Li, Y. Shi, Y. Cai, A core-shell magnetic mesoporous silica sorbent for organic targets with high extraction performance and anti-interference ability, Chem. Commun. 47 (2011) 4454-4456.

[25] N. Insin, J.B. Tracy, H. Lee, J.P. Zimmer, R.M. Westervelt, M.G. Bawendl, Incorporation of iron oxide nanoparticles and quantum dots into silica microspheres, ACS Nano 2 (2008) 197.

[26] X. Lai, J. Li, B.A. Korgel, Z. Dong, Z. Li, F. Su, J. Du, D. Wang, General synthesis and gas-sensing properties of multiple-shell metal oxide hollow microspheres, Angew. Chem. Int. Ed. 50 (2011) 2738-2741.

[27] J.J. DeStefano, S.A. Schuster, J.M. Lawhorn, J.J. Kirkland, Performance characteristics of new superficially porous particles., J. Chromatogr. A 1258 (2012) 76.

[28] H. Schmidt-Traub, M. Schulte, A. Seidel-Morgenstern, Preparative Chromatography. Wiley-VCH, Weinheim, 2012.

[29] S.C. Moldoveanu, V. David, Essentials in Modern HPLC Separations, 1_{st} ed. Elsevier, 2012.

[30] G. Carta, A. Jungbauer, Protein Chromatography: Process Development and Scale-Up, 1_{st} ed. Wiley-VCH, Weinheim, 2010.

[31] M.N. Gupta, Methods for Affinity-Based Separations of Enzymes and Proteins, 1_{st} ed. Birkhäuser Basel, 2002.

[32] B.F. Hoskins, R. Robson, Infinite Polymeric Frameworks Consisting of 3 Dimensionally Linked Rod-Like Segments, J. Am. Chem. Soc. 111 (1989) 5962-5964.

[33] E.J. Anglin, L.Y. Cheng, W.R. Freeman, M.J. Sailor, Porous silicon in drug delivery devices and materials, Adv. Drug Delivery Rev. 60 (2008) 1266-1277.

[34] M.V. Wolkin, J. Jorne, P.M. Fauchet, G. Allan, C. Delerue, Electronic states and luminescence in porous silicon quantum dots: The role of oxygen, Phys. Rev. Lett. 82 (1999) 197-200.

[35] F. Priolo, T. Gregorkiewicz, M. Galli, T.F. Krauss, Silicon nanostructures for photonics and photovoltaics, Nat. Nanotechnol. 9 (2014) 19-32.

[36] V. Torres-Costa, R.J. Martin-Palma, Application of nanostructured porous silicon in the field of optics. A review, Journal of Materials Science 45 (2010) 2823-2838.

[37] L.R. Hilden, K.R. Morris, Physics of amorphous solids, J. Pharm. Sci. 93 (2004) 3-12.

[38] M.L.K. Hoa, M.H. Lu, Y. Zhang, Preparation of porous materials with ordered hole structure, Adv. Colloid Interface Sci. 121 (2006) 9-23.

[39] M.E. Davis, Ordered porous materials for emerging applications, Nature 417 (2002) 813-821.

[40] K. Uemura, R. Matsuda, S. Kitagawa, Flexible microporous coordination polymers, J. Solid State Chem. 178 (2005) 2420-2429.

[41] Z. Huang, H.B. Song, M. Du, S.T. Chen, X.H. Bu, J. Ribas, Coordination polymers assembled from angular dipyridyl ligands and Cu-II, Cd-II, Co-II salts: Crystal structures and properties, Inorg. Chem. 43 (2004) 931-944.

[42] S. Kitagawa, R. Kitaura, S. Noro, Functional porous coordination polymers, Ind. Eng. Chem. Res. 43 (2004) 2334-2375.

[43] J.L.C. Rowsell, O.M. Yaghi, Metal-organic frameworks: a new class of porous materials, Micropor. Mesopor. Mater. 73 (2004) 3-14.

[44] S.L. James, Metal-organic frameworks, Chem. Soc. Rev. 32 (2003) 276-288.

[45] M.D. Allendorf, C.A. Bauer, R.K. Bhakta, R.J.T. Houk, Luminescent metal-organic frameworks, Chem. Soc. Rev. 38 (2009) 1330-1352.

[46] J.R. Long, O.M. Yaghi, The pervasive chemistry of metal-organic frameworks, Chem. Soc. Rev. 38 (2009) 1213-1214.

[47] M. Guo, H.L. Cai, R.G. Xiong, Ferroelectric metal organic framework (MOF), Inorg. Chem. Commun. 13 (2010) 1590-1598.

[48] S.T. Meek, J.A. Greathouse, M.D. Allendorf, Metal-organic frameworks: A rapidly growing class of versatile nanoporous materials, Adv. Mater. 23 (2011) 249-267.

[49] H.C. Zhou, J.R. Long, O.M. Yaghi, Introduction to metal-organic frameworks, Chem. Rev. 112 (2012) 673-674.

[50] X.L. Tong, H.L. Lin, J.H. Xin, F. Liu, M. Li, X.P. Zhu, Recent advances as materials of functional metal-organic frameworks, J. Nanomater. (2013).

[51] Q.L. Zhu, Q. Xu, Metal−organic framework composites, Chem. Soc. Rev. 43 (2014) 5468-5512.

[52] Y. Kinoshita, I. Matsubara, Y. Saito, The crystal structure of bis(succinonitrilo)copper(i) nitrate, Bull. Chem. Soc. Jpn. 32 (1959) 741-747.

[53] G. Ferey, Hybrid porous solids: past, present, future, Chem. Soc. Rev. 37 (2008) 191-214.

[54] O.M. Yaghi, H.L. Li, Hydrothermal synthesis of a metal−organic framework containing large rectangular channels, J. Am. Chem. Soc. 117 (1995) 10401-10402.

[55] D. Banerjee, A.J. Cairns, J. Liu, R.K. Motkuri, S.K. Nune, C.A. Fernandez, R. Krishna, D.M. Strachan, P.K. Thallapally, Potential of metal-organic frameworks for separation of xenon and krypton, Acc. Chem. Res. 48 (2015) 211-219.

[56] J.L.C. Rowsell, O.M. Yaghi, Strategies for hydrogen storage in metal-organic frameworks, Ind. Eng. Chem. Res. 44 (2005) 4670-4679.

[57] K. Konstas, T. Osl, Y.X. Yang, M. Batten, N. Burke, A.J. Hill, M.R. Hill, Methane storage in metal organic frameworks, J. Mater. Chem. 22 (2012) 16698-16708.

[58] J. Lee, O.K. Farha, J. Roberts, K.A. Scheidt, S.T. Nguyen, J.T. Hupp, Metal−organic framework materials as catalysts, Chem. Soc. Rev. 38 (2009) 1450-1459.

[59] A. Dhakshinamoorthy, H. Garcia, Cascade reactions catalyzed by metal organic frameworks, ChemSusChem 7 (2014) 2392-2410.

[60] S. Abedi, A. Morsali, Ordered mesoporous metal organic frameworks incorporated with amorphous tio_2 as photocatalyst for selective aerobic oxidation in sunlight irradiation, ACS Catal. 4 (2014) 1398-1403.

[61] Z.C. Hu, B.J. Deibert, J. Li, Luminescent metal-organic frameworks for chemical sensing and explosive detection, Chem. Soc. Rev. 43 (2014) 5815-5840.

[62] Y.J. Cui, B.L. Chen, G.D. Qian, Lanthanide metal-organic frameworks for luminescent sensing and light-emitting applications, Coord. Chem. Rev. 273 (2014) 76-86.

[63] M. Kurmoo, Magnetic metal-organic frameworks, Chem. Soc. Rev. 38 (2009) 1353-1379.

[64] J. Kim, B.L. Chen, T.M. Reineke, H.L. Li, M. Eddaoudi, D.B. Moler, M. O'Keeffe, O.M. Yaghi, Assembly of metal-organic frameworks from large organic and inorganic secondary building units: New examples and simplifying principles for complex structures, J. Am. Chem. Soc. 123 (2001) 8239-8247.

[65] D.J. Tranchemontagne, J.L. Mendoza-Cortes, M. O'Keeffe, O.M. Yaghi, Secondary building units, nets and bonding in the chemistry of metal-organic frameworks, Chem. Soc. Rev. 38 (2009) 1257-1283.

[66] M. Wriedt, H.C. Zhou, Systematic investigations on magneto-structural correlations of copper(II) coordination polymers based on organic ligands with mixed carboxylic and nitrogen-based moieties, Dalton Trans. 41 (2012) 4207-4216.

[67] X.D. Guo, G.S. Zhu, F.X. Sun, Z.Y. Li, X.J. Zhao, X.T. Li, H.C. Wang, S.L. Qiu, Synthesis, structure, and luminescent properties of microporous lanthanide metal-organic frameworks with inorganic rod-shaped building units, Inorg. Chem. 45 (2006) 2581-2587.

[68] M. Gustafsson, A. Bartoszewicz, B. Martin-Matute, J.L. Sun, J. Grins, T. Zhao, Z.Y. Li, G.S. Zhu, X.D. Zou, A family of highly stable lanthanide metal-organic frameworks: Structural evolution and catalytic activity, Chem. Mater. 22 (2010) 3316-3322.

[69] Q.F. Yang, X.B. Cui, Y. Chen, Z. Wang, J.H. Yu, J.Q. Xu, T.G. Wang, Two new 3D lanthanide metal-organic frameworks constructed from nitrilotriacetate and oxalate ligands, Inorg. Chem. Commun. 14 (2011) 320-323.

[70] L. Pan, K.M. Adams, H.E. Hernandez, X.T. Wang, C. Zheng, Y. Hattori, K. Kaneko, Porous lanthanide-organic frameworks: Synthesis, characterization, and unprecedented gas adsorption properties, J. Am. Chem. Soc. 125 (2003) 3062-3067.

[71] T.M. Reineke, M. Eddaoudi, M. Fehr, D. Kelley, O.M. Yaghi, From condensed lanthanide coordination solids to microporous frameworks having accessible metal sites, J. Am. Chem. Soc. 121 (1999) 1651-1657.

[72] N.L. Rosi, J. Kim, M. Eddaoudi, B.L. Chen, M. O'Keeffe, O.M. Yaghi, Rod packings and metal-organic frameworks constructed from rod-shaped secondary building units, J. Am. Chem. Soc. 127 (2005) 1504-1518.

[73] E.D. Bloch, L.J. Murray, W.L. Queen, S. Chavan, S.N. Maximoff, J.P. Bigi, R. Krishna, V.K. Peterson, F. Grandjean, G.J. Long, B. Smit, S. Bordiga, C.M. Brown, J.R. Long, Selective binding of O_2 over N_2 in a redox-active metal−organic framework with open iron(II) coordination sites, J. Am. Chem. Soc. 133 (2011) 14814-14822.

[74] W. Zhou, H. Wu, T. Yildirim, Enhanced H_2 adsorption in isostructural metal-organic frameworks with open metal sites: Strong dependence of the binding strength on metal ions, J. Am. Chem. Soc. 130 (2008) 15268.

[75] P.D.C. Dietzel, B. Panella, M. Hirscher, R. Blom, H. Fjellvag, Hydrogen adsorption in a nickel based coordination polymer with open metal sites in the cylindrical cavities of the desolvated framework, Chem. Commun. (2006) 959-961.

[76] P.D.C. Dietzel, R. Blom, H. Fjellvag, Base-induced formation of two magnesium metal−organic framework compounds with a bifunctional tetratopic ligand, Eur. J. Inorg. Chem. (2008) 3624-3632.

[77] P.D.C. Dietzel, Y. Morita, R. Blom, H. Fjellvag, An in situ high-temperature single-crystal investigation of a dehydrated metal−organic framework compound and field-induced magnetization of one-dimensional metaloxygen chains, Ind. Eng. Chem. Res. 44 (2005) 6354-6358.

[78] T.G. Glover, G.W. Peterson, B.J. Schindler, D. Britt, O. Yaghi, MOF-74 building unit has a direct impact on toxic gas adsorption, Chem. Eng. Sci. 66 (2011) 163-170.

[79] H. Okamoto, M. Yamashita, Solitons, polarons, and excitons in quasi-one-dimensional halogen-bridged transition metal compounds, Bull. Chem. Soc. Jpn. 71 (1998) 2023-2039.

[80] A.M.A. Ibrahim, E. Siebel, R.D. Fischer, [CuCN·Me_3SnCN·0.5bpy] (bpy = 4,4'-bipyridine): A novel supramolecular assembly involving the no longer unusual {$Cu_2(\mu\text{-}CN)_2(CN)_2$} motif, Inorg. Chem. 37 (1998) 3521-3525.

[81] D.J. Chesnut, D. Plewak, J. Zubieta, Solid state coordination chemistry of the copper(I)-cyano-organodiimine system. Two- and three-dimensional copper cyanide phases incorporating linear dipodal ligands, J. Chem. Soc., Dalton Trans. (2001) 2567-2580.

[82] J. Lu, T. Paliwala, S.C. Lim, C. Yu, T.Y. Niu, A.J. Jacobson, Coordination polymers of $Co(NCS)_2$ with pyrazine and 4,4'-bipyridine: Syntheses and structures, Inorg. Chem. 36 (1997) 923-929.

[83] S. Banfi, L. Carlucci, E. Caruso, G. Ciani, D.M. Proserpio, Using long bis(4-pyridyl) ligands designed for the self-assembly of coordination frameworks and architectures, J. Chem. Soc., Dalton Trans. (2002) 2714-2721.

[84] G.J.E. Davidson, S.J. Loeb, Channels and cavities lined with interlocked components: Metal-based polyrotaxanes that utilize pyridinimn axles and crown ether wheels as ligands, Ind. Eng. Chem. Res. 42 (2003) 74-77.

[85] J. Zhang, M.M. Matsushita, X.X. Kong, J. Abe, T. Iyoda, Photoresponsive coordination assembly with a versatile logs-stacking channel structure based on redox-active ligand and cupric ion, J. Am. Chem. Soc. 123 (2001) 12105-12106.

[86] P. Kar, Y. Ida, T. Ishida, A. Ghosh, Formation of two drastically different MOFs based on Mn(ii)-benzoate and pyrazine with a change in seasonal temperature: structural analysis and magnetic study, CrystEngComm 15 (2013) 400-410.

[87] P. Pachfule, T. Panda, C. Dey, R. Banerjee, Structural diversity in a series of metal-organic frameworks (MOFs) composed of divalent transition metals, 4,4'-bipyridine and a flexible carboxylic acid, CrystEngComm 12 (2010) 2381-2389.

[88] P. Song, B. Liu, Y.Q. Li, J.Z. Yang, Z.M. Wang, X.G. Li, Two pillared-layer metal-organic frameworks constructed with Co(II), 1,2,4,5-benzenetetracarboxylate, and 4,4'-bipyridine: Syntheses, crystal structures, and gas adsorption properties, CrystEngComm 14 (2012) 2296-2301.

[89] S.O.H. Gutschke, D.J. Price, A.K. Powell, P.T. Wood, Hydrothermal synthesis, structure, and magnetism of $[Co_2(OH)\{1,2,3\text{-}(O_2C)_3C_6H_3\}(H_2O)]\cdot H_2O$ and $[Co_2(OH)\{1,2,3\text{-}(O_2C)_3C_6H_3\}]$: magnetic Δ-chains with mixed cobalt geometries, Angew. Chem. Int. Ed. 40 (2001) 1920-1923.

[90] M. Eddaoudi, D.B. Moler, H. Li, B. Chen, T.M. Reineke, M. O'Keeffe, O.M. Yaghi, Modular chemistry: secondary building units as a basis for the design of highly porous and robust metal−organic carboxylate frameworks, Acc. Chem. Res. 34 (2001) 319-330.

[91] O.M. Yaghi, H. Li, T.L. Groy, Construction of porous solids from hydrogen-bonded metal complexes of 1,3,5-benzenetricarboxylic acid, J. Am. Chem. Soc. 118 (1996) 9096-9101.

[92] M.E. Kosal, J.H. Chou, S.R. Wilson, K.S. Suslick, A functional zeolite analogue assembled from metalloporphyrins, Nat. Mater. 1 (2002) 118-121.

[93] G.J.E. Davidson, S.J. Loeb, Channels and cavities lined with interlocked components: metal-based polyrotaxanes that utilize pyridinium axles and crown ether wheels as ligands, Angew. Chem. Int. Ed. 42 (2003) 74-77.

[94] E. Lee, J. Heo, K. Kim, A three-dimensional polyrotaxane network, Angew. Chem. Int. Ed. 39 (2000) 2699-2701.

[95] M. Eddaoudi, J. Kim, N. Rosi, D. Vodak, J. Wachter, M. O'Keeffe, O.M. Yaghi, Systematic design of pore size and functionality in isoreticular MOFs and their application in methane storage, Science 295 (2002) 469-472.

[96] Y.R. Lee, J. Kim, W.S. Ahn, Synthesis of metal-organic frameworks: A mini review, Korean J. Chem. Eng. 30 (2013) 1667-1680.

[97] W. Yuan, T. Friščić, D. Apperley, S.L. James, High reactivity of metal–organic frameworks under grinding conditions: Parallels with organic molecular materials, Angew. Chem. Int. Ed. 49 (2010) 3916-3919.

[98] T. Friščić, D.G. Reid, I. Halasz, R.S. Stein, R.E. Dinnebier, M.J. Duer, Ion- and liquid-assisted grinding: Improved mechanochemical synthesis of metal–organic frameworks reveals salt inclusion and anion templating, Angew. Chem. Int. Ed. 49 (2010) 712-715.

[99] A. Pichon, S.L. James, An array-based study of reactivity under solvent-free mechanochemical conditions-insights and trends, CrystEngComm 10 (2008) 1839-1847.

[100] Y.K. Seo, J.W. Yoon, J.S. Lee, U.H. Lee, Y.K. Hwang, C.H. Jun, P. Horcajada, C. Serre, J.S. Chang, Large scale fluorine-free synthesis of hierarchically porous iron(III) trimesate MIL-100(Fe) with a zeolite MTN topology, Microporous Mesoporous Mater. 157 (2012) 137-145.

[101] A. Pichon, A. Lazuen-Garay, S.L. James, Solvent-free synthesis of a microporous metal-organic framework, CrystEngComm 8 (2006) 211-214.

[102] C.S. Cundy, P.A. Cox, The hydrothermal synthesis of zeolites: History and development from the earliest days to the present time, Chem. Rev. 103 (2003) 663-702.

[103] M. Alhamami, H. Doan, C.H. Cheng, A review on breathing behaviors of metal-organic-frameworks (mofs) for gas adsorption, Materials 7 (2014) 3198-3250.

[104] M. Zhang, M. Bosch, T. Gentle III, H.C. Zhou, Rational design of metal-organic frameworks with anticipated porosities and functionalities, CrystEngComm 16 (2014) 4069-4083.

[105] H. Li, M. Eddaoudi, M. O'Keeffe, O.M. Yaghi, Design and synthesis of an exceptionally stable and highly porous metal-organic framework, Nature 402 (1999) 276-279.

[106] H.X. Deng, S. Grunder, K.E. Cordova, C. Valente, H. Furukawa, M. Hmadeh, F. Gandara, A.C. Whalley, Z. Liu, S. Asahina, H. Kazumori, M. O'Keeffe, O. Terasaki, J.F. Stoddart, O.M. Yaghi, Large-pore apertures in a series of metal-organic frameworks, Science 336 (2012) 1018-1023.

[107] C. Serre, F. Millange, C. Thouvenot, M. Nogues, G. Marsolier, D. Louer, G. Ferey, Very large breathing effect in the first nanoporous chromium(III)-based solids: MIL-53 or Cr-III(OH)·{O_2C-C_6H_4-CO_2}·{HO_2C-C_6H_4-CO_2H}$_x$·H_2O_y, J. Am. Chem. Soc. 124 (2002) 13519-13526.

[108] P. Horcajada, S. Surble, C. Serre, D.Y. Hong, Y.K. Seo, J.S. Chang, J.M. Greneche, I. Margiolaki, G. Ferey, Synthesis and catalytic properties of MIL-100(Fe), an iron(III) carboxylate with large pores, Chem. Commun. (2007) 2820-2822.

[109] C. Serre, C. Mellot-Draznieks, S. Surble, N. Audebrand, Y. Filinchuk, G. Ferey, Role of solvent-host interactions that lead to very large swelling of hybrid frameworks, Science 315 (2007) 1828-1831.

[110] G. Ferey, C. Mellot-Draznieks, C. Serre, F. Millange, J. Dutour, S. Surble, I. Margiolaki, A chromium terephthalate-based solid with unusually large pore volumes and surface area, Science 309 (2005) 2040-2042.

[111] M. Eddaoudi, D.F. Sava, J.F. Eubank, K. Adil, V. Guillerm, Zeolite-like metal-organic frameworks (ZMOFs): design, synthesis, and properties, Chem. Soc. Rev. 44 (2015) 228-249.

[112] B.L. Chen, Z.X. Yang, Y.Q. Zhu, Y.D. Xia, Zeolitic imidazolate framework materials: recent progress in synthesis and applications, J. Mater. Chem. B 2 (2014) 16811-16831.

[113] M. O'Keeffe, Design of MOFs and intellectual content in reticular chemistry: a personal view, Chem. Soc. Rev. 38 (2009) 1215-1217.

[114] J.J. Perry Iv, J.A. Perman, M.J. Zaworotko, Design and synthesis of metal-organic frameworks using metal-organic polyhedra as supermolecular building blocks, Chem. Soc. Rev. 38 (2009) 1400-1417.

[115] O.K. Farha, I. Eryazici, N.C. Jeong, B.G. Hauser, C.E. Wilmer, A.A. Sarjeant, R.Q. Snurr, S.T. Nguyen, A.Ö. Yazaydın, J.T. Hupp, Metal–organic framework materials with ultrahigh surface areas: Is the sky the limit?, J. Am. Chem. Soc. 134 (2012) 15016-15021.

[116] H. Furukawa, K.E. Cordova, M. O'Keeffe, O.M. Yaghi, The chemistry and applications of metal-organic frameworks, Science 341 (2013) 974.

[117] R. Babarao, Z. Hu, J. Jiang, S. Chempath, S.I. Sandler, Storage and separation of CO_2 and CH_4 in silicalite, C_{168} schwarzite, and IRMOF-1: A comparative study from monte carlo simulation, Langmuir 23 (2007) 659-666.

[118] Z. Chang, D.S. Zhang, Q. Chen, X.H. Bu, Microporous organic polymers for gas storage and separation applications, Phys. Chem. Chem. Phys. 15 (2013) 5430-5442.

[119] S. Ma, H.C. Zhou, Gas storage in porous metal-organic frameworks for clean energy applications, Chem. Commun. 46 (2010) 44-53.

[120] D. Zhao, D. Yuan, H. C. Zhou, The current status of hydrogen storage in metal-organic frameworks, Energy Environ. Sci. 1 (2008) 222-235.

[121] W. Zhou, H. Wu, M.R. Hartman, T. Yildirim, Hydrogen and methane adsorption in metal−organic frameworks: A high-pressure volumetric study, J. Phys. Chem. C 111 (2007) 16131-16137.

[122] H. Furukawa, N. Ko, Y.B. Go, N. Aratani, S.B. Choi, E. Choi, A.Ö. Yazaydin, R.Q. Snurr, M. O'Keeffe, J. Kim, O.M. Yaghi, Ultrahigh porosity in metal-organic frameworks, Science 329 (2010) 424-428.

[123] J.B. DeCoste, G.W. Peterson, Metal-organic frameworks for air purification of toxic chemicals, Chem. Rev. 114 (2014) 5695-5727.

[124] S. Couck, J.F.M. Denayer, G.V. Baron, T. Rémy, J. Gascon, F. Kapteijn, An amine-functionalized MIL-53 metal−organic framework with large separation power for CO_2 and CH_4, J. Am. Chem. Soc. 131 (2009) 6326-6327.

[125] K.A. Cychosz, R. Ahmad, A.J. Matzger, Liquid phase separations by crystalline microporous coordination polymers, Chemical Science 1 (2010) 293-302.

[126] D.-Y. Hong, Y.K. Hwang, C. Serre, G. Férey, J.S. Chang, Porous chromium terephthalate MIL-101 with coordinatively unsaturated sites: surface functionalization, encapsulation, sorption and catalysis, Adv. Funct. Mater. 19 (2009) 1537-1552.

[127] Z.G. Gu, G. S., B. S., W. C., L. Heinke, Enantioselective adsorption in homochiral metal-organic frameworks: the pore size influence, Chem. Commun. (2015) 1-4.

[128] H. Guo, G. Zhu, I.J. Hewitt, S. Qiu, "Twin copper source" growth of metal−organic framework membrane: Cu_3BTC_2 with high permeability and selectivity for recycling H_2, J. Am. Chem. Soc. 131 (2009) 1646-1647.

[129] S.R. Venna, M.A. Carreon, Highly permeable zeolite imidazolate framework-8 membranes for CO_2/CH_4 separation, J. Am. Chem. Soc. 132 (2010) 76-78.

[130] K.H. Li, D.H. Olson, J. Seidel, T.J. Emge, H.W. Gong, H.P. Zeng, J. Li, Zeolitic imidazolate frameworks for kinetic separation of propane and propene, J. Am. Chem. Soc. 131 (2009) 10368-+.

[131] Y.B. Yu, Y.Q. Ren, W. Shen, H.M. Deng, Z.Q. Gao, Applications of metal-organic frameworks as stationary phases in chromatography, TrAC-Trends. Anal. Chem. 50 (2013) 33-41.

[132] Z.Y. Gu, C.X. Yang, N. Chang, X.P. Yan, Metal–organic frameworks for analytical chemistry: From sample collection to chromatographic separation, Acc. Chem. Res. 45 (2012) 734-745.

[133] B.L. Chen, C.D. Liang, J. Yang, D.S. Contreras, Y.L. Clancy, E.B. Lobkovsky, O.M. Yaghi, S. Dai, A microporous metal−organic framework for gas-chromatographic separation of alkanes, Ind. Eng. Chem. Res. 45 (2006) 1390-1393.

[134] Z.-Y. Gu, X.-P. Yan, Metal–organic framework MIL-101 for high-resolution gas-chromatographic separation of xylene isomers and ethylbenzene, Angew. Chem. Int. Ed. 49 (2010) 1477-1480.

[135] L. Alaerts, C.E.A. Kirschhock, M. Maes, M.A. van der Veen, V. Finsy, A. Depla, J.A. Martens, G.V. Baron, P.A. Jacobs, J.F.M. Denayer, D.E. De Vos, Selective adsorption and separation of xylene isomers and ethylbenzene with the microporous vanadium(IV) terephthalate MIL-47, Angew. Chem. Int. Ed. 46 (2007) 4293-4297.

[136] M. Maes, F. Vermoortele, M. Boulhout, T. Boudewijns, C. Kirschhock, R. Ameloot, I. Beurroies, R. Denoyel, D.E. De Vos, Enthalpic effects in the adsorption of alkylaromatics on the metal-organic frameworks MIL-47 and MIL-53, Microporous Mesoporous Mater. 157 (2012) 82-88.

[137] H.L. Jiang, Y. Tatsu, Z.H. Lu, Q. Xu, Non-, micro-, and mesoporous metal−organic framework isomers: Reversible transformation, fluorescence sensing, and large molecule separation, J. Am. Chem. Soc. 132 (2010) 5586-5587.

[138] C.X. Yang, S.S. Liu, H.F. Wang, S.W. Wang, X.P. Yan, High-performance liquid chromatographic separation of position isomers using metal−organic framework MIL-53(Al) as the stationary phase, Analyst 137 (2012) 133-139.

[139] S.S. Liu, C.X. Yang, S.W. Wang, X.P. Yan, Metal-organic frameworks for reverse-phase high-performance liquid chromatography, Analyst 137 (2012) 816-818.

[140] Y.Y. Fu, C.X. Yang, X.P. Yan, Metal−organic framework MIL-100(Fe) as the stationary phase for both normal-phase and reverse-phase high performance liquid chromatography, J. Chromatogr. A 1274 (2013) 137-144.

[141] F. Yang, C.X. Yang, X.P. Yan, Post-synthetic modification of MIL-101(Cr) with pyridine for high-performance liquid chromatographic separation of tocopherols, Talanta 137 (2015) 136-142.

[142] K. Tanaka, T. Muraoka, D. Hirayama, A. Ohnish, Highly efficient chromatographic resolution of sulfoxides using a new homochiral MOF-silica composite, Chem. Commun. 48 (2012) 8577-8579.

[143] R. Ameloot, A. Liekens, L. Alaerts, M. Maes, A. Galarneau, B. Coq, G. Desmet, B.F. Sels, J.F.M. Denayer, D.E. De Vos, Silica-MOF Composites as a Stationary Phase in Liquid Chromatography, Eur. J. Inorg. Chem. (2010) 3735-3738.

[144] Y.Y. Fu, C.X. Yang, X.P. Yan, Fabrication of ZIF-8@SiO_2 Core-Shell Microspheres as the Stationary Phase for High-Performance Liquid Chromatography, Chem. Eur. J. 19 (2013) 13484-13491.

[145] Z.M. Yan, J.N. Zheng, J.F. Chen, P. Tong, M.H. Lu, Z. Lin, L. Zhang, Preparation and evaluation of silica-UIO-66 composite as liquid chromatographic stationary phase for fast and efficient separation, J. Chromatogr. A 1366 (2014) 45-53.

[146] X.Q. Zhang, Q. Han, M.Y. Ding, One-pot synthesis of UiO-66@SiO_2 shell-core microspheres as stationary phase for high performance liquid chromatography, RSC Adv. 5 (2015) 1043-1050.

[147] U. Ravon, M.E. Domine, C. Gaudillere, A. Desmartin-Chomel, D. Farrusseng, MOFs as acid catalysts with shape selectivity properties, New J. Chem. 32 (2008) 937-940.

[148] S. Hasegawa, S. Horike, R. Matsuda, S. Furukawa, K. Mochizuki, Y. Kinoshita, S. Kitagawa, Three-dimensional porous coordination polymer functionalized with amide groups based on tridentate ligand: Selective sorption and catalysis, J. Am. Chem. Soc. 129 (2007) 2607-2614.

[149] Y.K. Hwang, D.Y. Hong, J.S. Chang, S.H. Jhung, Y.K. Seo, J. Kim, A. Vimont, M. Daturi, C. Serre, G. Férey, Amine grafting on coordinatively unsaturated metal centers of mofs: Consequences for catalysis and metal encapsulation, Angew. Chem. Int. Ed. 47 (2008) 4144-4148.

[150] M. Banerjee, S. Das, M. Yoon, H.J. Choi, M.H. Hyun, S.M. Park, G. Seo, K. Kim, Postsynthetic modification switches an achiral framework to catalytically active homochiral metal−organic porous materials, J. Am. Chem. Soc. 131 (2009) 7524-7525.

[151] A. Henschel, K. Gedrich, R. Kraehnert, S. Kaskel, Catalytic properties of MIL-101, Chem. Commun. (2008) 4192-4194.

[152] M.L.P. Reddy, S. Sivakumar, Lanthanide benzoates: A versatile building block for the construction of efficient light emitting materials, Dalton Trans. 42 (2013) 2663-2678.

[153] Y. Cui, H. Xu, Y. Yue, Z. Guo, J. Yu, Z. Chen, J. Gao, Y. Yang, G. Qian, B. Chen, A luminescent mixed-lanthanide metal–organic framework thermometer, J. Am. Chem. Soc. 134 (2012) 3979-3982.

[154] J. Rocha, L.D. Carlos, F.A.A. Paz, D. Ananias, Luminescent multifunctional lanthanides-based metal-organic frameworks, Chem. Soc. Rev. 40 (2011) 926-940.

[155] S.Z. Zhan, M. Li, S.W. Ng, D. Li, Luminescent metal–organic frameworks (mofs) as a chemopalette: tuning the thermochromic behavior of dual-emissive phosphorescence by adjusting the supramolecular microenvironments, Chem. Eur. J. 19 (2013) 10217-10225.

[156] N.B. Shustova, B.D. McCarthy, M. Dincă, Turn-on fluorescence in tetraphenylethylene-based metal–organic frameworks: An alternative to aggregation-induced emission, J. Am. Chem. Soc. 133 (2011) 20126-20129.

[157] J.C. Dai, X.T. Wu, Z.Y. Fu, S.M. Hu, W.X. Du, C.P. Cui, L.M. Wu, H.H. Zhang, R.Q. Sun, A novel ribbon-candy-like supramolecular architecture of cadmium(ii)-terephthalate polymer with giant rhombic channels: twofold interpenetration of the 3D 8210-a net, Chem. Commun. (2002) 12-13.

[158] W. Chen, J.Y. Wang, C. Chen, Q. Yue, H.M. Yuan, J.S. Chen, S.N. Wang, Photoluminescent metal−organic polymer constructed from trimetallic clusters and mixed carboxylates, Inorg. Chem. 42 (2003) 944-946.

[159] G.A. Senchyk, V.O. Bukhan'ko, A.B. Lysenko, H. Krautscheid, E.B. Rusanov, A.N. Chernega, M. Karbowiak, K.V. Domasevitch, Ag^{I}/V^{V} heterobimetallic frameworks generated from novel-type $\{Ag_2(VO_2F_2)_2(triazole)_4\}$ secondary building blocks: A new aspect in the design of SVOF hybrids, Inorg. Chem. 51 (2012) 8025-8033.

[160] S. Pramanik, Z. Hu, X. Zhang, C. Zheng, S. Kelly, J. Li, A systematic study of fluorescence-based detection of nitroexplosives and other aromatics in the vapor phase by microporous metal–organic frameworks, Chem. Eur. J. 19 (2013) 15964-15971.

[161] P. Wu, J. Wang, C. He, X. Zhang, Y. Wang, T. Liu, C. Duan, luminescent metal-organic frameworks for selectively sensing nitric oxide in an aqueous solution and in living cells, Adv. Funct. Mater. 22 (2012) 1698-1703.

[162] R.F. D'Vries, S. Alvarez-Garcia, N. Snejko, L.E. Bausa, E. Gutierrez-Puebla, A. de Andres, M.A. Monge, Multimetal rare earth MOFs for lighting and thermometry: Tailoring color and optimal temperature range through enhanced disulfobenzoic triplet phosphorescence, J. Mater. Chem. C 1 (2013) 6316-6324.

[163] A. Demessence, P. Horcajada, C. Serre, C. Boissiere, D. Grosso, C. Sanchez, G. Ferey, Elaboration and properties of hierarchically structured optical thin films of MIL-101(Cr), Chem. Commun. (2009) 7149-7151.

[164] P. Horcajada, C. Serre, D. Grosso, C. Boissière, S. Perruchas, C. Sanchez, G. Férey, Colloidal route for preparing optical thin films of nanoporous metal–organic frameworks, Adv. Mater. 21 (2009) 1931-1935.

[165] G. Lu, J.T. Hupp, Metal−organic frameworks as sensors: A ZIF-8 based fabry−pérot device as a selective sensor for chemical vapors and gases, J. Am. Chem. Soc. 132 (2010) 7832-7833.

[166] L.E. Kreno, J.T. Hupp, R.P. Van Duyne, Metal−organic framework thin film for enhanced localized surface plasmon resonance gas sensing, Anal. Chem. 82 (2010) 8042-8046.

[167] R. Makiura, S. Motoyama, Y. Umemura, H. Yamanaka, O. Sakata, H. Kitagawa, Surface nano-architecture of a metal–organic framework, Nat. Mater. 9 (2010) 565-571.

[168] S. Hermes, F. Schröder, R. Chelmowski, C. Wöll, R.A. Fischer, Selective nucleation and growth of metal−organic open framework thin films on patterned COOH/CF_3-terminated self-assembled monolayers on Au(111), J. Am. Chem. Soc. 127 (2005) 13744-13745.

[169] V.V. Guerrero, Y. Yoo, M.C. McCarthy, H.-K. Jeong, HKUST-1 membranes on porous supports using secondary growth, J. Mater. Chem. 20 (2010) 3938-3943.

[170] J.-L. Zhuang, D. Ceglarek, S. Pethuraj, A. Terfort, Rapid room-temperature synthesis of metal–organic framework HKUST-1 crystals in bulk and as oriented and patterned thin films, Adv. Funct. Mater. 21 (2011) 1442-1447.

[171] U. Mueller, M. Schubert, F. Teich, H. Puetter, K. Schierle-Arndt, J. Pastre, Metal-organic frameworks-prospective industrial applications, J. Mater. Chem. 16 (2006) 626-636.

[172] H. Bux, F. Liang, Y. Li, J. Cravillon, M. Wiebcke, J. Caro, Zeolitic Imidazolate Framework Membrane with Molecular Sieving Properties by Microwave-Assisted Solvothermal Synthesis, J. Am. Chem. Soc. 131 (2009) 16000-16001.

[173] A. Demessence, C. Boissiere, D. Grosso, P. Horcajada, C. Serre, G. Ferey, G.J.A.A. Soler-Illia, C. Sanchez, Adsorption properties in high optical quality nanoZIF-8 thin films with tunable thickness, J. Mater. Chem. 20 (2010) 7676-7681.

[174] A. Bétard, H. Bux, S. Henke, D. Zacher, J. Caro, R.A. Fischer, Fabrication of a CO_2-selective membrane by stepwise liquid-phase deposition of an alkylether functionalized pillared-layered metal−organic framework [Cu_2L_2P]n on a macroporous support, Micropor. Mesopor. Mat. 150 (2012) 76-82.

[175] O. Shekhah, H. Wang, S. Kowarik, F. Schreiber, M. Paulus, M. Tolan, C. Sternemann, F. Evers, D. Zacher, R.A. Fischer, C. Wöll, Step-by-step route for the synthesis of metal−organic frameworks, J. Am. Chem. Soc. 129 (2007) 15118-15119.

[176] O. Shekhah, H. Wang, M. Paradinas, C. Ocal, B. Schupbach, A. Terfort, D. Zacher, R.A. Fischer, C. Wöll, Controlling interpenetration in metal-organic frameworks by liquid-phase epitaxy, Nat. Mater. 8 (2009) 481-484.

[177] E. Biemmi, C. Scherb, T. Bein, Oriented growth of the metal organic framework $Cu_3(BTC)_2(H_2O)_3 \cdot xH_2O$ tunable with functionalized self-assembled monolayers, J. Am. Chem. Soc. 129 (2007) 8054-8055.

[178] R. Arnold, W. Azzam, A. Terfort, C. Wöll, Preparation, modification, and crystallinity of aliphatic and aromatic carboxylic acid terminated self-assembled monolayers, Langmuir 18 (2002) 3980-3992.

[179] J. Liu, B. Schupbach, A. Bashir, O. Shekhah, A. Nefedov, M. Kind, A. Terfort, C. Wöll, Structural characterization of self-assembled monolayers of pyridine-terminated thiolates on gold, Phys. Chem. Chem. Phys. 12 (2010) 4459-4472.

[180] O. Shekhah, H. Wang, D. Zacher, R.A. Fischer, C. Wöll, Growth mechanism of metal–organic frameworks: Insights into the nucleation by employing a step-by-step route, Angew. Chem. Int. Ed. 48 (2009) 5038-5041.

[181] M.E. Silvestre, M. Franzreb, P.G. Weidler, O. Shekhah, C. Wöll, Magnetic cores with porous coatings: Growth of metal-organic frameworks on particles using liquid phase epitaxy, Adv. Funct. Mater. 23 (2013) 1210-1213.

[182] J.L. Zhuang, D. Ar, X.J. Yu, J.X. Liu, A. Terfort, Patterned deposition of metal-organic frameworks onto plastic, paper, and textile substrates by inkjet printing of a precursor solution, Adv. Mater. 25 (2013) 4631-4635.

[183] Z. Wang, J. Liu, B. Lukose, Z. Gu, P.G. Weidler, H. Gliemann, T. Heine, C. Wöll, Nanoporous designer solids with huge lattice constant gradients: multiheteroepitaxy of metal–organic frameworks, Nano Lett. 14 (2014) 1526-1529.

[184] A. Velamakanni, J.R. Torres, K.J. Ganesh, P.J. Ferreira, J.S. Major, Controlled assembly of silane-based polymers: chemically robust thin-films, Langmuir 26 (2010) 15295-15301.

[185] H.K. Arslan, O. Shekhah, J. Wohlgemuth, M. Franzreb, R.A. Fischer, C. Wöll, High-throughput fabrication of uniform and homogenous mof coatings, Adv. Funct. Mater. 21 (2011) 4228-4231.

[186] K.B. Blodgett, I. Langmuir, Built-up films of barium stearate and their optical properties, Phys. Rev. 51 (1937) 964-982.

[187] G. Decher, J.D. Hong, Buildup of ultrathin multilayer films by a self-assembly process, 1 consecutive adsorption of anionic and cationic bipolar amphiphiles on charged surfaces, Makromolekulare Chemie. Macromolecular Symposia 46 (1991) 321-327.

[188] G. Decher, Fuzzy nanoassemblies: Toward layered polymeric multicomposites, Science 277 (1997) 1232-1237.

[189] C.M. Bell, M.F. Arendt, L. Gomez, R.H. Schmehl, T.E. Mallouk, Growth of lamellar Hofmann clathrate films by sequential ligand exchange reactions: Assembling a coordination solid one layer at a time, J. Am. Chem. Soc. 116 (1994) 8374-8375.

[190] H. Gliemann, C. Wöll, Epitaxially grown metal-organic frameworks, Mater. Today 15 (2012) 110-116.

[191] Z.G. Gu, Fakultät für Chemie und Biowissenschaften, Karlsruher Institut für Technologie, Karlsruhe, 2014, p. 97.

[192] H.K. Arslan, O. Shekhah, D.C.F. Wieland, M. Paulus, C. Sternemann, M.A. Schroer, S. Tiemeyer, M. Tolan, R.A. Fischer, C. Wöll, intercalation in layered metal–organic frameworks: reversible inclusion of an extended π-system, J. Am. Chem. Soc. 133 (2011) 8158-8161.

[193] O. Shekhah, K. Hirai, H. Wang, H. Uehara, M. Kondo, S. Diring, D. Zacher, R.A. Fischer, O. Sakata, S. Kitagawa, S. Furukawa, C. Wöll, MOF-on-MOF heteroepitaxy: Perfectly oriented $[Zn_2(ndc)_2(dabco)]_n$ grown on $[Cu_2(ndc)_2(dabco)]_n$ thin films, Dalton T. 40 (2011) 4954-4958.

[194] J. Liu, W. Zhou, J. Liu, I. Howard, G. Kilibarda, S. Schlabach, D. Coupry, M. Addicoat, S. Yoneda, Y. Tsutsui, T. Sakurai, S. Seki, Z. Wang, P. Lindemann, E. Redel, T. Heine, C. Wöll, Photoinduced charge-carrier generation in epitaxial MOF thin films: High efficiency as a result of an indirect electronic band gap?, Angew. Chem. Int. Ed. (2015) 7441-7445.

[195] Z. Wang, J. Liu, H.K. Arslan, S. Grosjean, T. Hagendorn, H. Gliemann, S. Bräse, C. Wöll, Post-synthetic modification of metal–organic framework thin films using click chemistry: the importance of strained C–C triple bonds, Langmuir 29 (2013) 15958-15964.

[196] B. Liu, O. Shekhah, H.K. Arslan, J. Liu, C. Wöll, R.A. Fischer, Enantiopure metal–organic framework thin films: Oriented SURMOF growth and enantioselective adsorption, Angew. Chem. Int. Ed. 51 (2012) 807-810.

[197] M.D. Allendorf, R.J.T. Houk, L. Andruszkiewicz, A.A. Talin, J. Pikarsky, A. Choudhury, K.A. Gall, P.J. Hesketh, Stress-induced chemical detection using flexible metal−organic frameworks, J. Am. Chem. Soc. 130 (2008) 14404-14405.

[198] O. Zybaylo, O. Shekhah, H. Wang, M. Tafipolsky, R. Schmid, D. Johannsmann, C. Wöll, A novel method to measure diffusion coefficients in porous metal-organic frameworks, Phys. Chem. Chem. Phys. 12 (2010) 8093-8098.

[199] L. Heinke, C. Wöll, Adsorption and diffusion in thin films of nanoporous metal−organic frameworks: Ferrocene in SURMOF $Cu_2(ndc)_2(dabco)$, Phys. Chem. Chem. Phys. 15 (2013) 9295-9299.

[200] H.C. Streit, M. Adlung, O. Shekhah, X. Stammer, H.K. Arslan, O. Zybaylo, T. Ladnorg, H. Gliemann, M. Franzreb, C. Wöll, C. Wickleder, Surface-anchored MOF-based photonic antennae, ChemPhysChem 13 (2012) 2699-2702.

[201] S. Chavan, J.G. Vitillo, D. Gianolio, O. Zavorotynska, B. Civalleri, S. Jakobsen, M.H. Nilsen, L. Valenzano, C. Lamberti, K.P. Lillerud, S. Bordiga, H_2 storage in isostructural UiO-67 and UiO-66 MOFs, Phys. Chem. Chem. Phys. 14 (2012) 1614-1626.

[202] J.H. Cavka, S. Jakobsen, U. Olsbye, N. Guillou, C. Lamberti, S. Bordiga, K.P. Lillerud, A new zirconium inorganic building brick forming metal organic frameworks with exceptional stability, J. Am. Chem. Soc. 130 (2008) 13850-13851.

[203] D. Farrusseng, C. Daniel, C. Gaudillère, U. Ravon, Y. Schuurman, C. Mirodatos, D. Dubbeldam, H. Frost, R.Q. Snurr, Heats of adsorption for seven gases in three metal−organic frameworks: systematic comparison of experiment and simulation, Langmuir 25 (2009) 7383-7388.

[204] J.A. Mason, M. Veenstra, J.R. Long, Evaluating metal−organic frameworks for natural gas storage, Chem. Sci. 5 (2014) 32-51.

[205] P. Horcajada, H. Chevreau, D. Heurtaux, F. Benyettou, F. Salles, T. Devic, A. Garcia-Marquez, C. Yu, H. Lavrard, C.L. Dutson, E. Magnier, G. Maurin, E. Elkaim, C. Serre, Extended and functionalized porous iron(iii) tri- or dicarboxylates with MIL-100/101 topologies, Chem. Commun. 50 (2014) 6872-6874.

3. Publications and Manuscripts

Insights into the Separation Performance of MOFs by High-Performance Liquid Chromatography and In-depth Modelling

Weiwei Qin, Martin E. Silvestre, Gerald Brenner-Weiss., Zhengbang Wang, Sophia Schmitt, Jonas Hübner, Matthias Franzreb

Separation and Purification Technology, **2015**, 156, 249-258.

DOI: http://dx.doi.org/10.1016/j.seppur.2015.10.008

ISSN: 1383-5866

Insights into Chromatographic Separation Using Core–Shell Metal–Organic Frameworks: Size Exclusion and Polarity Effects

Weiwei Qin, Martin E. Silvestre, Frank Kirschhöfer, Gerald Brenner-Weiss, Matthias Franzreb

Journal of chromatography A, **2015**, 1411, 77-83.

DOI: http://dx.doi.org/10.1016/j.chroma.2015.07.120

ISSN: 0021-9673

High Performance Liquid Chromatography of Substituted Aromatics with the Metal-organic Framework MIL-100(Fe): Mechanism Analysis and Model-based Prediction

Weiwei Qin, Martin E. Silvestre, Yongli Li, Matthias Franzreb

Journal of Chromatography A, **2016**, 1432, 84-91.

DOI: http://doi.org/10.1016/j.chroma.2016.01.006

ISSN: 0021-9673

Magnetic Microparticles@UiO-67 Core-Shell Composites as a Novel Stationary Phase for High Performance Liquid Chromatography

Weiwei Qin, Martin E. Silvestre, Matthias Franzreb.

Applied Mechanics and Materials, **2015**, 703, 73-76.

DOI: http://dx.doi.org/10.4028/www.scientific.net/AMM.703.73

ISSN: 1662-7482

4. Insights into the Separation Performance of MOFs by High–Performance Liquid Chromatography and In-depth Modelling

Weiwei Qin, Martin E. Silvestre, Gerald Brenner-Weiss, Zhengbang Wang, Sophia Schmitt, Jonas Hübner, Matthias Franzreb*

Institute of Functional Interfaces (IFG), Karlsruhe Institute of Technology (KIT), Hermann-von-Helmholtz-Platz 1, 76344 Eggenstein-Leopoldshafen, Germany

*Corresponding author: matthias.franzreb@kit.edu

Abstract Carboxyl functionalized magnetic cores coated homogeneously with UiO-67 metal–organic frameworks (MOFs) through a liquid phase epitaxy (LPE) process are introduced. Using the as-synthesized core-shell microparticles as stationary phase in HPLC runs with different phenol derivatives, good separation efficiencies can be achieved when applying an acetonitrile/water mobile phase. To understand the advantages and limitations of such MOF based stationary phases in more detail, the experimental elution profiles are compared with simulations from a powerful chromatography modeling software (ChromX) newly developed at the KIT. The simulation results reveal that the affinities of UiO-67 to the tested phenol derivatives strongly differ (2,6-dimethylphenol < benzene-1,3-diol < 2,6-dichlorophenol), while its maximum capacity remains identical for each derivative with 0.14 mol L^{-1}. The uptake kinetics are dominated by intraparticle diffusion while axial dispersion and film diffusion play only minor roles. The pore diffusivities of the phenol derivatives are found to be around $1.3 \cdot 10^{-13}$ m^2 s^{-1}. Based on single component data, the successful simulation of multicomponent isocratic pulse experiments is demonstrated. In summary, HPLC runs combined with in-depth modeling are a powerful tool to investigate the interactions between solute molecules and thin MOF films, and to reveal data about affinities, capacities and uptake kinetics.

Published in *Separation and Purification Technology, 156 (2015) 249-258*

4.1. Introduction

Metal-organic frameworks (MOFs) have emerged as a new class of highly ordered porous materials in the last two decades. They are built from inorganic units interconnected by functional organic linkers through strong bonds [1, 2]. Due to their particular properties, such as high surface area to volume ratio, tunable pore structures, high porosity, and good thermal stability, this novel class of hybrid inorganic-organic materials exhibits enormous potentials for applications in catalysis, optics, gas adsorption and storage, drug delivery, and sensing [3-6]. The unique combination of properties such as the absence of dead volume, a good solvent stability, and high loading capacity for solutes also makes MOFs an attractive material for preparative chromatographic separation [7, 8].

Several studies have investigated the performance of columns filled with bulk MOFs for liquid chromatography [9-12]. However, the results are mostly limited to validating a proof-of-concept for the separation of analyte mixtures and to demonstrating the influence of different parameters onto the observed retention times. More fundamental information about the interaction of the analytes with the MOF structure, especially the equilibrium isotherms and particle diffusion parameters, is often under-investigated, through this would allow an in-depth understanding of the performance of MOFs as stationary phases. One reason for this omission is that the used MOF material is often very heterogeneous with respect to particle size and morphology. Because of these unknown geometrical factors, it is practically impossible to derive quantitative kinetic data.

The recently introduced MOF fabrication by a liquid phase epitaxy (LPE) process [13] can produce highly ordered, oriented, and homogenous, surface-attached metal−organic framework thin films (SURMOFs) on a supporting template. A suitable functionalization of the template surface ensures the initial SURMOF nucleation and its attachment to the surface [14, 15]. Here, we report the first fabrication of well-defined core-shell structures by this LPE process, resulting in UiO-67 SURMOFs encrusting uniform magnetic microparticles (MPs). While the choice of micro particles having magnetic properties as carrier material has no effect on the chromatographic performance of the resulting core-shell particles, it greatly facilitates the frequent solid-liquid separation steps required during the synthesis of the MOF shell using the LPE method (Figure 4.1). Among the MOF family, the zirconium based UiO (University of Oslo) series [16], especially the UiO-66 and UiO-67, are of special interest due to their excellent thermal and chemical stability [17, 18]. UiO-66 is formed by a cubic framework of cationic zirconium nodes and 1,4-benzene-dicarboxylate (BDC) linkers (6.8 Å), leading to a three dimensional structure where each octahedral pore (11 Å) is connected to eight face-shared tetrahedral pores (8 Å) through accessible windows (6 Å) [19]. UiO-67 has the similar structure as UiO-66, but UiO-67 is obtained using zirconium nodes in combination with the longer 4,4′-biphenyldicarboxylate (BPDC) linkers (11.6 Å) and therefore, has larger pore dimensions (23 and 11.5 Å) and accessible windows (8 Å) (Figure 4.1, inset) [20]. One UiO-67 unit cell is occupied by four octahedral pores and eight

tetrahedral pores. UiO-67 has been successfully applied in gas adsorption [21] and catalysis [22]. Recently, several studies have reported the successful use of UiO-66 as stationary phases in HPLC [23-25]. However, to the best of our knowledge, no case of UiO-67 MOFs used in HPLC has been published so far. In this work, core-shell UiO-67 magnetic microparticles (MPs) were synthesized and packed into HPLC columns to investigate the interactions between SURMOFs and a set of dissolved phenol derivatives (Figure 4.2) at a more fundamental level by means of experimental and simulated HPLC.

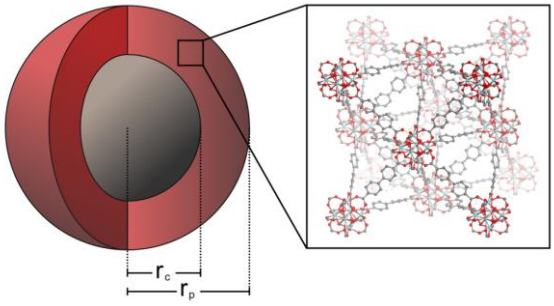

Figure 4.1. The schematic structure of UiO-67 shell grown on carboxyl-functionalized magnetic microparticles: r_c refers the radius of the magnetic particle and r_p defines the radius of the particle including the MOF shell. The structure of UiO-67 (inset) contains octahedral and face-shared tetrahedral pores.

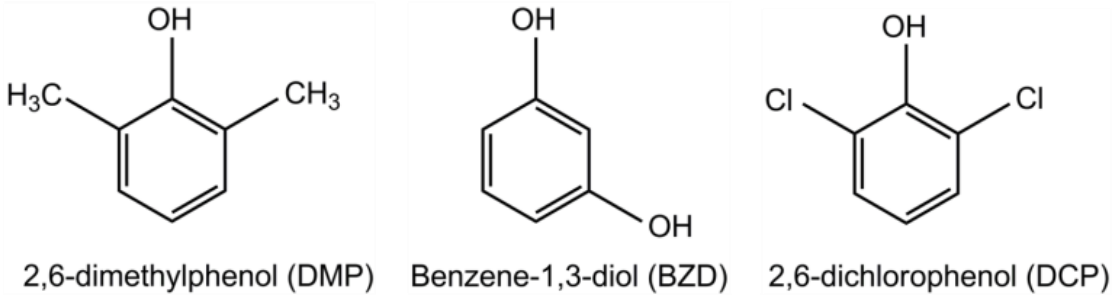

Figure 4.2. Structures of the phenol derivatives used for HPLC experiments. Due to the increasing electronegativity of the side groups, the polar character of the molecules increases in the following order: DMP < BZD < DCP.

4.2. Experimental

4.2.1. Materials and Reagents

Carboxyl-functionalized magnetic silica particles (MPs, Iron oxide > 15%) with narrow size distribution of 4.7±0.14 µm were purchased from the company microParticles GmbH, Berlin, Germany. Empty stainless steel HPLC column (200 mm × 1.0 mm i.d) was bought from VDS optilab Chromatographie Technik GmbH (order code: N1910 0000), Berlin, Germany. Zirconium(IV) propoxide solution ($Zr(OPr)_4$, 70%), methacrylic acid (99%), 4,4'-biphenyl-

dicarboxylate (BPDC, 97%), N,N-dimethylformamide (DMF, 99.8%), 2,6-dimethylphenol (DMP, 99%), benzene-1,3-diol (BZD, 99%), 2,6-dichlorophenol (DCP, 99%), dichloromethane (DCM, 99.8%), carbon tetrachloride (CCl_4, 99.9%) methanol(99.9%), acetonitrile (ACN, 99.9%), acetone (99.9%), and blue dextran were purchased from Sigma-Aldrich or Merck, Germany. All reagents and solvents were used as received without further purification. The phenol derivatives were dissolved in ACN and used as HPLC analytes.

4.2.2. Preparation of $Zr_6(OH)_4O_4(OMc)_{12}(PrOH)\cdot 3McOH$

Zirconium methacrylate oxocluster $Zr_6(OH)_4O_4(OMc)_{12}(PrOH)\cdot 3McOH$ was prepared according to G. Kickelbick *et al* [26, 27]. Typically, 10 mL of a 70% solution of $Zr(OPr)_4$ (0.2 mM) in *n*-propanol was mixed with 17 mL (200 mM) of methacrylic acid (Aldrich) under an nitrogen atmosphere and stored in a closed Schlenk tube at room temperature. The zirconium methacrylate oxocluster crystallized during 13 days as a colorless solid (3.8 g, 51% yield).

4.2.3. Synthesis of UiO-67 MPs Core−Shell Composites

UiO-67 was synthesized onto carboxyl-functionalized MPs with zirconium methacrylate oxocluster $Zr_6(OH)_4O_4(OMc)_{12}(PrOH)\cdot 3McOH$ as metal source and BPDC as organic linker using a liquid phase epitaxy process in a layer-by-layer fashion. All the fabrication procedures were manually done. Briefly, 25 mg of magnetic microparticles were alternately immersed into 2 mL $Zr_6(OH)_4O_4(OMc)_{12}(PrOH)\cdot 3McOH$ DMF solution (1.5 mM) and 2 mL BPDC DMF solution (1 mM) and kept on a thermoshaker (1350 rpm) at 45 °C for 7 min in each case. The magnetic microparticles were magnetically separated and washed thoroughly with 2 mL pure DMF solution between each immersion step for about 2 min. A defined thickness for the resulting UiO-67 layer is achieved by repeating this deposition cycle process. After 20 and 55 cycles, samples were magnetically separated and washed with methanol solution, dried in vacuum (120 °C, 12 h) for further use and characterizations.

4.2.4. Characterization Techniques

X-ray diffraction (XRD) data were recorded with a Bruker diffractometer. For the co-planar (out-of-plane, OP) orientation a Bruker D8-Advance equipped with a position sensitive detector (PSD) Lynxeye® in θ-θ geometry, a variable divergence slit, and a 2.3° Soller-slit on the secondary side was used. The XRD data were acquired over a 2θ range of 4 – 20°, with 126 seconds per 0.019° 2θ-step. Cu-anodes were used with the Cu Kα1,2-radiation (λ = 0.15419 nm).

Fourier transform infrared (FTIR) measurements were carried out with a Bruker Optics Tensor 27 spectrometer with a Bruker Optics Platinum® ATR (Attenuated total reflectance)

accessory and a deuterated tri-glycine sulfate (RT–DTGS) detector. The FTIR ATR spectra were recorded at room temperature (ca. 22 °C) with a resolution of 4 cm^{-1} using air as background.

Analyses of the morphology were recorded on a Philips XL30 scanning electron microscope (SEM) at 20.0 kV. Prior to the SEM measurement, the samples were dried at 60 °C for 12 hours.

4.2.5. Preparation of the HPLC Column and Conducted HPLC Experiments

Before packing the column, the as-synthesized UiO-67 MPs core-shell composites were treated by: (i) washing three times with DCM solution; (ii) washing five times with methanol solution; and (iii) drying at 120 °C for 12 h under vacuum in order to remove unreacted species from the MOF cavities. The dried composites were added into a mixture of CCl_4 and methanol (1:1, vol/vol) under ultrasonication for 5 min to ensure the even dispersion of UiO-67 MPs. Thereafter, the suspension was packed with a down-flow into a stainless steel HPLC column (200 mm × 1.0 mm i.d, column volume 157 µL) under 40 MPa for 10 min with methanol as the slurry solvent to obtain the home-made UiO-67 based column.

All chromatographic tests were performed with an Agilent 1100 series HPLC system (Agilent Technologies, USA) equipped with a variable wavelength UV detector and a micro (2 µL) flow cell at room temperature. Before the chromatographic experiments, the home-made MOF columns were equilibrated with ACN until a stable baseline was reached. ACN and H_2O were used to compose the mobile phase and to prepare the liquid samples.

4.2.6. Simulation of Chromatographic Runs Using the Software ChromX

The simulation software ChromX (Version 0.1.0a) was developed at the Institute of Process Engineering in Life Sciences Section IV: Biomolecular Separation Engineering of the Karlsruhe Institute of Technology (KIT) in 2012 [http://mab.blt.kit.edu/chromx.php]. It is a powerful, modular simulation toolbox written in C++ that solves chromatography models by means of the finite element method in space and time stepping with finite differences. Because we expected the mass transport resistance within the MOF-based chromatography columns to be dominated by intraparticle diffusion phenomena, we opted for a Langmuir model with single or multiple component equilibrium, and for a general rate approach which takes into account the effect of axial dispersion as well as film and pore diffusion. The resulting partial differential equations (Equations 4.1 & 4.2) are given below, and the required set of column and mass transfer parameters are presented in Figure 4.3.

$$-D_{ax}\frac{\partial^2 C_{bi}}{\partial z^2}+u\frac{\partial C_{bi}}{\partial z}+\frac{\partial C_{bi}}{\partial t}+\frac{3k_{film,i}(1-\varepsilon_b)}{\varepsilon_b r_p}(C_{bi}-C_{pi,r=r_p})=0 \tag{4.1}$$

$$(1-\varepsilon_p)\frac{\partial C_{pi}^{*}}{\partial t}+\varepsilon_p\frac{\partial C_{pi}}{\partial t}-\varepsilon_p D_{pi}\left[\frac{1}{r^2}\frac{\partial}{\partial r}\left(r^2\frac{\partial C_{pi}}{\partial r}\right)\right]=0 \tag{4.2}$$

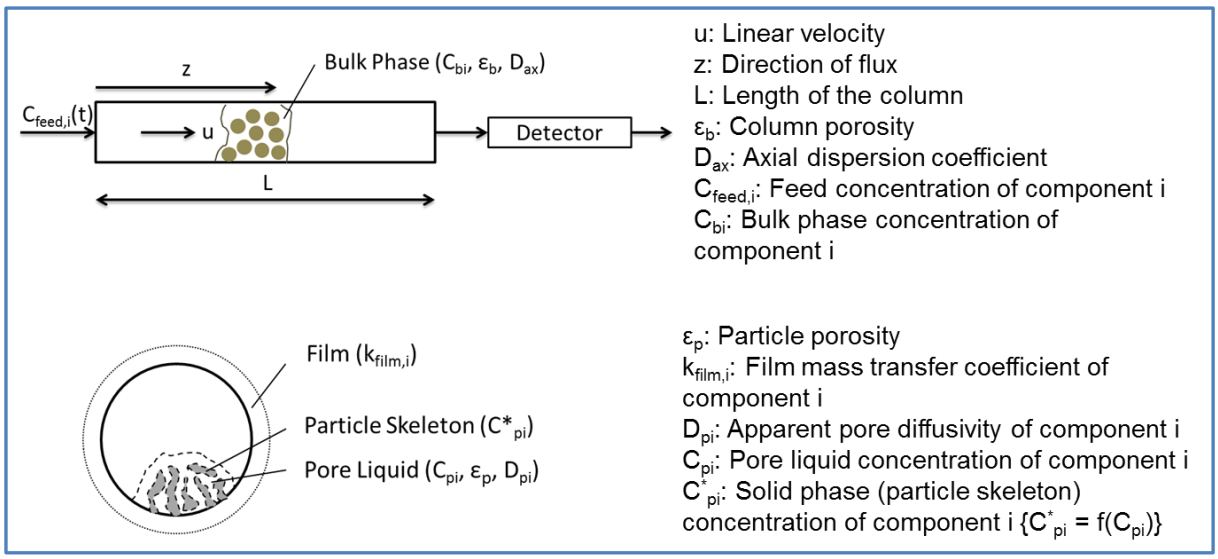

Figure 4.3. Column and mass transfer parameters for the simulation with ChromX.

In addition, the parameters of the multicomponent Langmuir isotherm are required and given by:

$$C_{pi}^{*}=C_{\max i}^{*}\frac{K_{Li}C_{pi}}{1+\sum_{j=1}^{Ns}K_{Lj}C_{pj}} \tag{4.3}$$

Here $C^*_{max,i}$ is the maximum capacity of component i within the solid phase and $K_{L,i}$ is the Langmuir coefficient of component i, which is a measure of its affinity towards the solid phase. When using this equation, one has to be aware that only the particle skeleton is viewed as solid phase. If the more common maximum capacity with respect to the particle volume is needed, disregarding the amount of component i within the pore liquid, it leads to the following relationship:

$$C_{V\max i}^{*}=\left(1-\varepsilon_p\right)\cdot C_{\max i}^{*} \tag{4.4}$$

Finally, ChromX, like many other LC simulation tools, limits the sorbent particle model to be homogenous while a more appropriate model in our case would be a spherical core-shell design defined by two radii, a core radius r_c and a total particle radius r_p (see Figure 4.1). Therefore, the true volumetric concentration within the MOF ($C^*_{MOFmax,i}$) must be calculated by means of the volume fraction ϕ_s of the shell (Equation 4.5 and 4.6):

$$\varphi_s=\frac{V_s}{V_p}=\frac{r_p^3-r_c^3}{r_p^3} \tag{4.5}$$

$$C^*_{MOF\max,i} = \frac{C^*_{V\max i}}{\varphi_s} \tag{4.6}$$

Extracting an approximation of the apparent pore diffusivity in the MOF from the simulation results is consequently more complex. Core-shell adsorbents have received great attention in recent years especially in the context of fast/ultrafast analytical HPLC separation in short and/or narrow bore columns. A recent review highlights the reasons behind this success and additionally investigates the differences in intraparticle mass transport of core-shell particles with non-porous cores with those of fully penetrable particles composed of the same shell material [28]. In dependence of the ratio between the core and the full particle radius, the following relation between the pore diffusivity in the shell $D_{p,shell}$ and the corresponding apparent pore diffusivity in an homogenous fully porous particle D_p can be derived (Equation 4.7).

$$\frac{D_{p,shell}}{D_p} = \frac{r_p^4 + 2r_p^3 r + 3r_p^2 r_c^2 - r_p r_c^3 - 5r_c^4}{\left(r_p^2 + r_p r_c + r_c^2\right)^2} \tag{4.7}$$

4.3. Results and Discussion

4.3.1. Characterization of UiO-67 Magnetic Microparticles Core-Shell Composites

The synthesized UiO-67 MPs core-shell composites were characterized by XRD, FTIR ATR, and SEM (Figure 4.4). The presence and intensity of diffraction peaks characteristic of UiO-67 at 5.6° and 9.2° after 20 and 55 deposition cycles respectively, prove the successful preparation of a UiO-67 shell (Figure 4.4A). Comparison shows that these peaks measured for our particles are identical to the simulated XRD peaks of UiO-67 at (111) and (220) positions. FTIR ATR spectra (Figure 4.4B) give another indication for the effective growth of the UiO-67 shell. The decrease of the peak intensity at 1780 – 1710 cm^{-1}, indicating a –COOH stretch, and the increase or appearance of UiO-67 characteristic bands at 1585, 1532, 1407 and 768 cm^{-1}, support the conclusion of a successful fabrication yielding UiO-67 MOFs chemically bonded onto the carboxyl functionalized surface of the magnetic microparticles [18]. The SEM images also clearly reveal the formation of the UiO-67 shell on the magnetic particles (Figure 4.4C, D and Figure S4.1). After applying 55 deposition cycles to grow the UiO-67 shell on the raw magnetic cores, the diameter of the UiO-67 MPs core-shell microspheres increased from 4.7 µm to 5.5 µm. These numbers result from measuring the diameter of more than twenty particles. The diameter of each particle was determined by calculating the average of the diameters measured for ten different angles. This indicates that approximately 0.4 µm thick SURMOFs shells were grown over the magnetic microparticles, resulting in a volume fraction for the shell ϕ_s of 38%. Moreover, thanks to their uniform

shapes and sizes, the as-prepared UiO-67 MPs composites are appropriate sorbent candidates for HPLC.

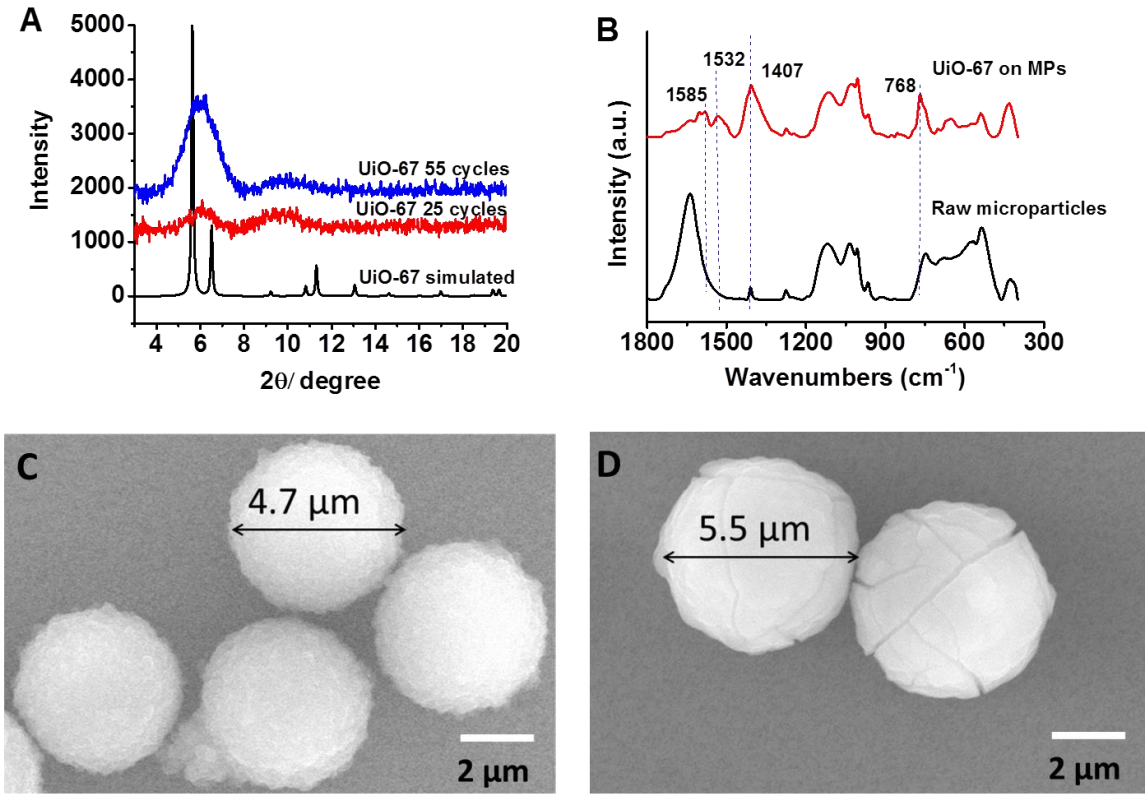

Figure 4.4. Characterization of the UiO-67 shell grown on carboxyl-functionalized magnetic micro-particles. (A) XRD patterns of as-synthesized UiO-67 MPs core-shell composites obtained after 20 and 55 deposition cycles. (B) FTIR-ATR spectra of raw magnetic microparticles and the as-synthesized UiO-67 MPs (55 cycles) core-shell composites. (C) SEM images of the raw magnetic microparticles and (D) UiO-67 MPs (55 cycles) core-shell composites. The cracks within the MOF-shell of the particles are probably an artifact from the previous drying procedure needed for SEM imaging.

Based on the XRD, FTIR ATR, and SEM results, the successful preparation of UiO-67 MPs core-shell composites by the LPE method is demonstrated. In contrast to MOF particles prepared by bulk synthesis, the synthesized core-shell particles showed a uniform size and a homogenous MOF shell covering the whole particle surface. These unique properties make the composite particles suitable for chromatographic applications and offer the possibility for detailed investigations regarding diffusion kinetics and binding isotherms within MOFs.

4.3.2. Determination of Column Characteristics

Tracer experiments with acetone and blue dextran were conducted in order to determine total and bed porosities of columns packed with the UiO-67 SURMOF-based composite particles, and estimate the resulting axial dispersion. Figure 4.5 shows the resulting chromatograms with the tracer peaks and the corresponding simulations using ChromX.

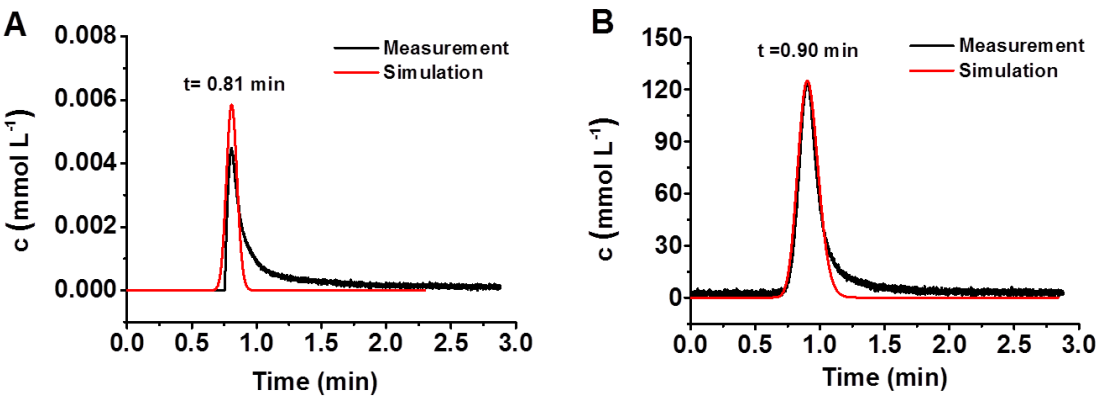

Figure 4.5. ChromX simulated (red lines) and experimental chromatograms (black lines) with a 0.2 µL injection of (A) blue dextran (0.5 µmol L^{-1}) and (B) acetone ($1.7 \cdot 10^4$ µmol L^{-1}) dissolved in ACN, eluted at a flow rate of 0.14 mL min^{-1}, and monitored with a UV detector at 280 nm (A) or 254 nm (B).

From the determined retention times of the peak maxima, total, bed and apparent particle porosities of 81%, 72%, and 32% were determined respectively. Given that the porosity of the composite support derives solely from the outer MOF shell and that the shell itself accounts for ~38% of the particle volume, the true porosity of the MOF UiO-67 shell is calculated as ~84%. Regarding the bed porosity, the value is unexpectedly high and indicates that although a high packing pressure was applied, high packing densities of the microparticles within the column of only 1.0 mm inner diameter were not achieved. The calculated axial dispersion coefficient is in the range of 10^{-6} m^2 s^{-1}, which is about an order of magnitude higher than the dispersion coefficient predicted by correlations for a well packed column of our particles [29]. This again agrees with a particle packing having an excessively large voidage. However, the value of axial dispersion is still acceptable, and allows the further investigation of equilibrium parameters and intraparticle mass transfer limitations within the column. Finally, for a feed rate of 0.14 mL min^{-1} the value of the film mass transfer coefficient is calculated to $4 \cdot 10^{-4}$ m s^{-1} using the correlation of Wilson and Geankoplis [30]. Nevertheless, simulations show that the film mass transfer resistance is negligible in the present case (Figure S4.2, Supporting Information).

4.3.3. Chromatographic Separation of Phenol Derivatives

To demonstrate the suitability of our UiO-67 MPs core-shell composites for liquid chromatography, the separation of a mixture of three phenol derivatives was tested. The phenol derivatives (DMP, BZD, and DCP) differ only in the type and position of one or two side groups (Figure 4.2). The same set of phenol derivatives has been used previously by Fu et al. [31] to probe the effect of the incorporation of submicron MOF UiO-66 particles into a porous polymer monolith made of polymethylacrylic acid-co-ethylene dimethacrylate (MAA-co-EDMA). While the incorporation of the MOF has clearly been shown to improve the separation performance of the monolith column, the investigations, restricted to analytical operation regime, did not provide maximum capacity or mass transfer limitation data.

In the present experiments, we applied a concentration gradient to the two component ACN/H_2O mobile phase, while maintaining a constant flow rate. First, the column packed with UiO-67 MPs (20 cycles) core-shell composites were tested at a flow rate of 0.14 mL min^{-1} (Figure 4.6A). Following injection of the sample (0.2 µL), DMP eluted rapidly (t = 1.0 min), immediately followed by a second peak (t ~ 1.7 min) comprising BZD and DCP. In stark contrast, UiO-67 MPs (55 cycles) core-shell composites resulted in baseline separation of DMP, BZD, and DCP (Fig 6B; R_s values for separation of the DMP and BZD, and BZD and DCP peaks were calculated as 1.7 and 1.5 respectively). On the one hand, the strong improvement of the separation which resulted from using composites with a thicker UiO-67 layer to pack the column proves that the UiO-67 shell is responsible for the separation phenomena. On the other hand, the difference between the UiO-67 MPs resulting from 20 and 55 cycles respectively is larger than expected. The most probable explanation is that at least in the beginning the growth of SURMOFs is not linear with the number of cycles, as shown in Figures 1, 2 and 6 of reference [32]. Due to the irregular arrangement of carboxyl groups on the initial surface, the first 5 to 10 cycles result in a SURMOF of worse crystallinity and lower thickness than the one calculated assuming a molecular layer per cycle.

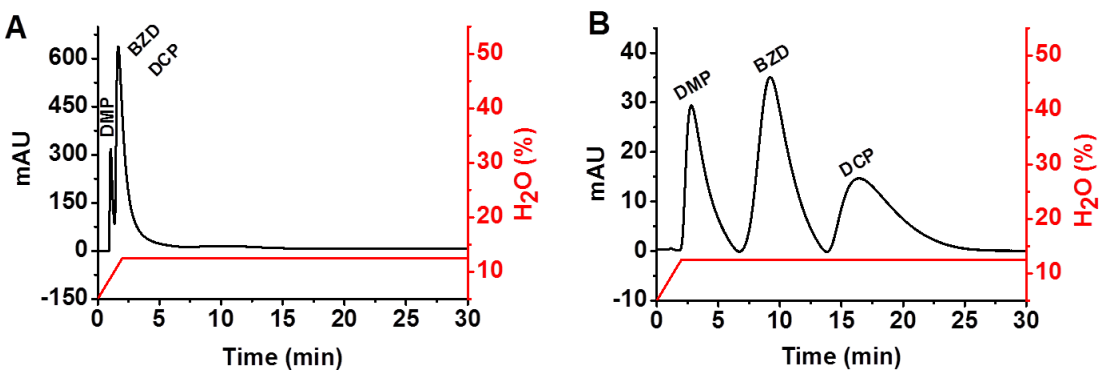

Figure 4.6. HPLC chromatograms resulting from the injection (0.2 µL) of a mixture of $8.19 \cdot 10^3$ µmol L^{-1} (1.0 g L^{-1}) DMP, $9.08 \cdot 10^3$ µmol L^{-1} (1.0 g L^{-1}) BZD and $1.27 \cdot 10^4$ µmol L^{-1} (2.0 g L^{-1}) DCP dissolved in ACN into the HPLC column (200 mm × 1.0 mm i.d.) packed with UiO-67 MPs core-shell composites of 20 (A) and 55 (B) cycles, respectively. The gradient of the mobile phase was as

follows: 0.00-2.00 min, ACN/H_2O (95:5 → 87.5:12.5); 2.01-30.00 min, ACN/H_2O (87.5:12.5) at a flow rate of 0.14 mL min^{-1}. The separations were performed at room temperature and monitored with a UV detector at 230 nm.

A noticeable difference in order of elution of the phenol derivatives observed here (DMP – BZD – DCP), with that reported by Fu et al. [31], (BDZ – DMP – DCP) employing UiO-66 incorporated within poly(MAA-co-EDMA) merits explanation. With their experimental setup, the elution order obtained correlates with the hydrophobicity ranking of the phenol derivatives. The incorporation of UiO-66 reinforces the weakly hydrophobic effect from their polymer matrix and enhances the separation performance. In comparison, our column system is highly hydrophobic with the effective sorbent being made only of UiO-67. However, DMP is eluted before BZD in our case. The diphenyl-4,4′-dicarboxylate linkers, compared to the 1,4-benzene-dicarboxylate of UiO-66, probably enable different and more important π-π interactions with the phenol derivatives. Stronger interactions, either hydrophobic and/or of π–π type, also explain the higher ACN concentration needed to elute the derivatives.

While the separation of a mixture of phenol derivatives by applying a gradient to the mobile phase shows the suitability of UiO-67 MPs core-shell composites for HPLC applications. In practice, however, it does not permit easy insight into the physical processes that dominate and also limit the observed performances. Therefore, a rigorous series of single and multicomponent chromatographic runs were conducted. The obtained data allow not only the extraction of a set of kinetic and equilibrium parameters which describe the interplay between our MOF and the phenol derivatives, but also permit *in-silico* predictions of the chromatographic performance.

4.3.4. Single Component Chromatography Runs with Isocratic Elution

The equilibrium parameters describing the adsorption isotherm between the phenol derivatives examined (DMP, BZD and DCP) and the UiO-67 stationary phase were determined by isocratic single component chromatography runs conducted in pulse injection and breakthrough mode modes, and the experimental and simulated chromatograms acquired are displayed in Figure 4.7.

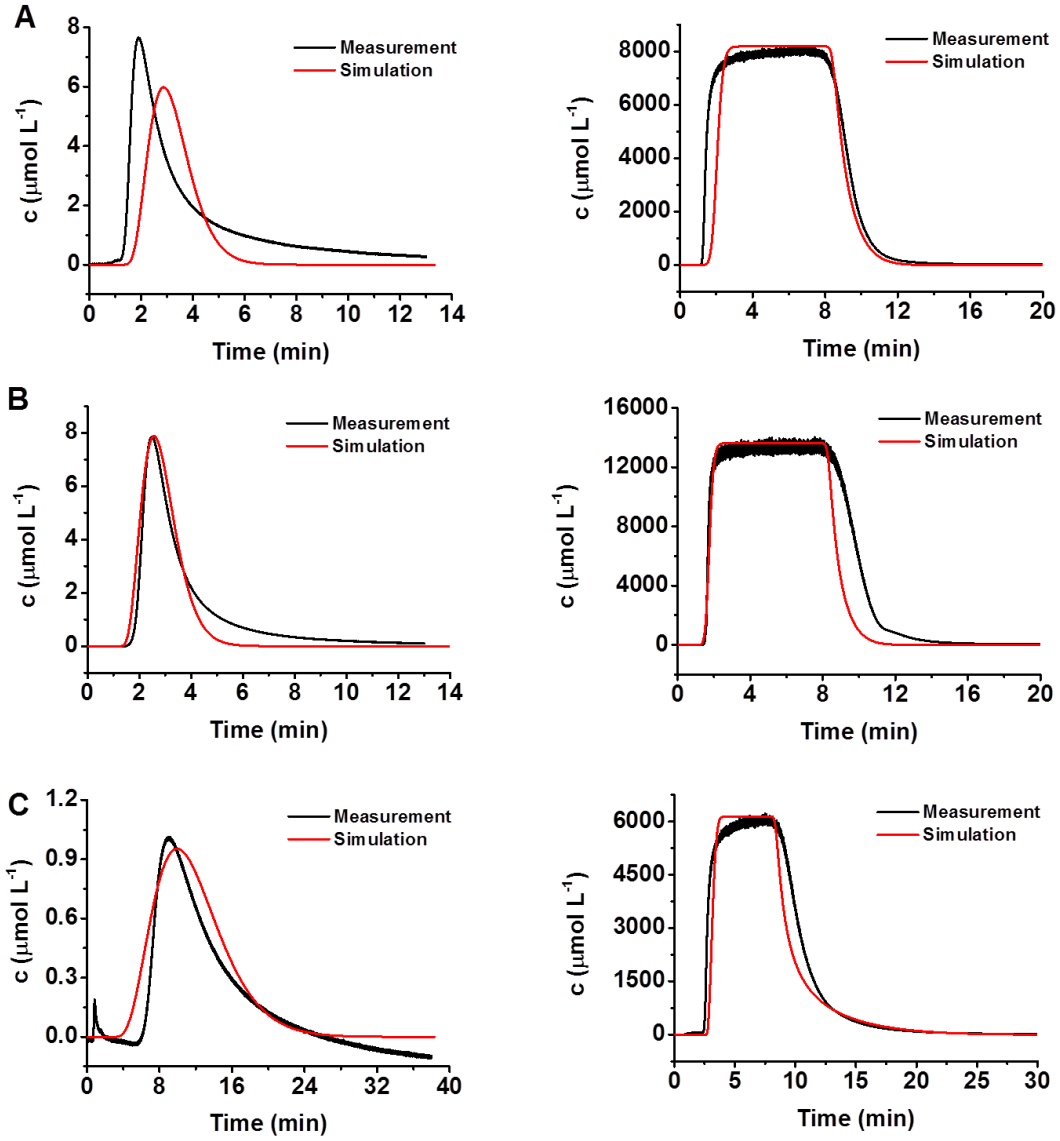

Figure 4.7. HPLC chromatograms of isocratic pulse (0.2 µL injected) and breakthrough (1 mL injected) experiments applying different phenol derivatives at a concentration of $8.19 \cdot 10^3$ µmol L^{-1} DMP (A), $9.08 \cdot 10^3$ µmol L^{-1} BZD (B) and $6.13 \cdot 10^3$ µmol L^{-1} DCP (C) (1 g L^{-1} each) onto a column (200×1.0 mm i.d.) packed with UiO-67 MPs (55 cycles) core-shell composites. Isocratic pulse chromatograms are on the left and breakthrough traces are on the right. All runs were performed at a flow rate of 0.14 mL min^{-1} and monitored with a UV detector at 230 nm. Black lines represent the experimental results whereas red lines show the results of the simulations using the software ChromX. DMP (A), BZD (B), and DCP (C) elutions using the mobile phase ACN/H_2O at 95:5, 90:10, and 85:15, respectively.

The retention time of the pulse experiments corresponds with the initial slope of the binding isotherm between the molecule and the stationary phase. In the case of a Langmuir behavior, this initial slope is given by the product of the saturation concentration $C^*_{MOFmax,i}$ and the Langmuir coefficient $K_{L,i}$ of the respective molecule. Therefore, pulse experiments within the analytical operation regime are normally not sufficient for determining the individual values of these parameters and additional breakthrough experiments have to be performed. When

these breakthrough experiments are done with concentrations at which the MOF loading approaches saturation, the resulting data combined with those of the pulse experiments permit an appropriate parameter evaluation to describe the equilibrium binding behavior within the complete concentration range. To extract the affinity coefficients (K_L) and the maximum capacities (C^*_{MOFmax}) for each phenol derivative, chromatograms were simulated by the software ChromX. As shown in Fig.4.7, good correlations between experimental (black line) and simulated data (blue line) were achieved in most cases with the equilibrium parameters being:

- K_L = 122 L mol^{-1} and C^*_{MOFmax} = 0.14 mol L^{-1} for DMP (Figure 4.7A);
- K_L = 99 L mol^{-1} and C^*_{MOFmax} = 0.14 mol L^{-1} for BZD (Figure 4.7B);
- K_L = 652 L mol^{-1} and C^*_{MOFmax} = 0.14 mol L^{-1} for DCP (Figure 4.7C).

While each of the simulated peaks for the pulse experiments exhibit an expected and almost perfect Gaussian shape, the experimental peak curves deviate clearly from any of those. This may be caused partly by backmixing within the rather high bed voidage and the Diode Array Detector (DAD) flow cell. The same phenomenon may also explain the notable tailing observed for the retention peak of the large tracer blue dextran (Figure 4.5). Nevertheless, the simulations show that the intraparticle mass transfer resistance has also a clear influence on the peak height and shape. Testing different apparent pore diffusion coefficient D_p reveals that the best fits in most cases are obtained with a value around $1.5 \cdot 10^{-12}$ m^2 s^{-1} for acetone and $5 \cdot 10^{-13}$ m^2 s^{-1} for the phenol derivatives. With Equation 7, the ratio between the real pore diffusion coefficients within the MOF shell ($D_{p,shell}$) and the apparent pore diffusion coefficient D_p within the simulated homogenous particles is evaluated to be around 0.25. Thus, we estimate pore diffusion coefficients within the MOF shell of ~$3.8 \cdot 10^{-13}$ m^2 s^{-1} and ~$1.31 \cdot 10^{-13}$ m^2 s^{-1} for acetone and the phenol derivatives respectively. Heinke *et al.* [33] determined these numbers compare well with the pore diffusivities that Heinke *et al*. have determined for cyclohexane within HKUST-1 thin films produced by a similar step-by-step LPE process. In case of pristine SURMOFs, a value of $6 \cdot 10^{-13}$ m^2 s^{-1} is reported. However, defects in the MOF structure, which can be caused by detrimental environmental conditions, can also strongly reduce the effective mass transfer. Taking into account a lower crystalline quality for our UiO-67 SURMOFs, pore diffusion values between 1 – $4 \cdot 10^{-13}$ m^2 s^{-1} are within the expected range.

Figure 4.8 shows three simulated chromatograms for the BZD pulse injection experiments with D_p values of $1 \cdot 10^{-12}$ m^2 s^{-1}, $5 \cdot 10^{-13}$ m^2 s^{-1} and $2 \cdot 10^{-13}$ m^2 s^{-1}, respectively, and demonstrates the sensitivity of the simulation results with respect to the pore diffusion coefficient. Simulation experiments with the initial D_p value doubled or halved clearly result in a reduced quality of the peak fit, both in peak shape and retention time. In contrast, variations of the film mass transfer coefficient (Figure S4.2, Supporting Information) or the

axial dispersion (Figure S4.3, Supporting Information) by the same order of magnitude show no, or only a minor, effect on the simulation results.

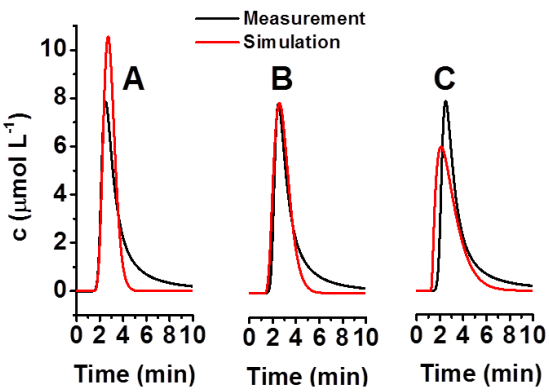

Figure 4.8. Sensitivity analysis of the simulation results with respect to the assumed intraparticle mass transfer. Different values of the apparent pore diffusion D_p ($1\cdot10^{-12}$ m^2 s^{-1}, $5\cdot10^{-13}$ m^2 s^{-1} and $2\cdot10^{-13}$ m^2 s^{-1}, for A, B, and C, respectively) were tested to fit the pulse injection experiment with $9.08\cdot10^3$ µmol L^{-1} (1 g L^{-1}) BZD (0.2 µL) using ACN/H_2O (90:10) as mobile phase. Black lines represent the experimental results and red lines show the results of the simulations by ChromX.

The chromatographic runs described above were optimized by adjusting the composition of the mobile phase to keep the retention times of the peaks from the pulse experiments within a time frame of less than 10 min. However, to compare the affinities of the different phenol derivatives towards the MOF UiO-67, it is necessary to run all samples under the same conditions. Therefore, a second set of single component chromatographic runs with isocratic elution was conducted with a mobile phase ACN/H_2O of constant composition (95:5). In this case, a good agreement between the measured black trace and simulated blue trace in Figure 4.9 data could be achieved with the following set of equilibrium parameters K_L and C^*_{MOFmax}:

- K_L = 122 L mol^{-1}and C^*_{MOFmax} = 0.14 mol L^{-1} for DMP (Figure 4.9A),
- K_L = 551 L mol^{-1} and C^*_{MOFmax} = 0.14 mol L^{-1} for BZD (Figure 4.9B),
- K_L = 2771 L mol^{-1} and C^*_{MOFmax} = 0.14 mol L^{-1} for DCP (Figure 4.9C).

From Figure 4.9B and C, it can be seen that using a mobile phase composition with a higher ACN concentration (ACN/H_2O at 95:5) results in stronger affinities for BZD and DCP, and therefore, longer retention times than those depicted by Figure 4.7. Nevertheless, the computer model is able to satisfactorily simulate the experimental results by simply changing the Langmuir coefficient K_L according to the increased affinities, while the maximum capacities remain unchanged. From this observation, it was interesting to realize the extent to which the sample molecules occupy the MOF pores when this maximum capacity is reached. Therefore, the theoretical capacity was calculated provided that each pore would be filled with one sample molecule.

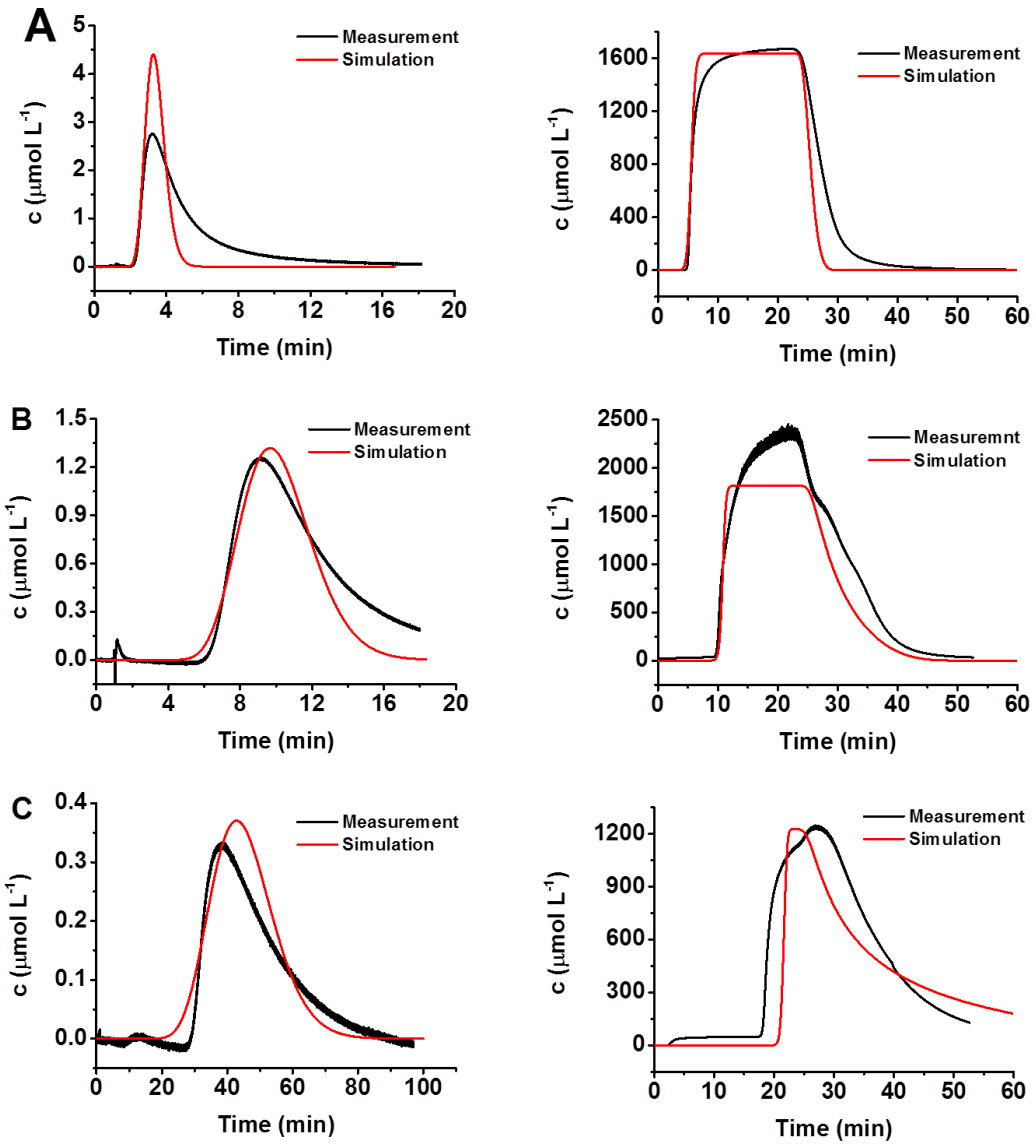

Figure 4.9. HPLC chromatograms of isocratic pulse (0.2 µL injected) and breakthrough (1 mL injected) experiments applying different phenol derivatives onto a column packed with UiO-67 MPs (55 cycles) core-shell composites. Isocratic pulse chromatograms are on the left and breakthrough traces are on the right. All runs were performed at a flow rate of 0.14 mL min^{-1} at a mobile phase composition ACN/H_2O (95:5) and monitored with a UV detector at 230 nm. Black lines represent the experimental results while red lines show the results of simulations using the software ChromX. Pulse experiments, column length 200 mm: (A) $4.09 \cdot 10^3$ µmol L^{-1} (0.5 g L^{-1}) DMP; (B) $4.54 \cdot 10^3$ µmol L^{-1} (0.5 g L^{-1}) BZD; (C) $6.13 \cdot 10^3$ µmol L^{-1} (1 g L^{-1}) DCP; breakthrough experiments, column length 140 mm: (A) $1.64 \cdot 10^3$ µmol L^{-1} (0.2 g L^{-1}) DMP; (B) $1.82 \cdot 10^3$ µmol L^{-1} (0.2 g L^{-1}) BZD; (C) $1.23 \cdot 10^3$ µmol L^{-1} (0.2 g L^{-1}) DCP.

The UiO-67 unit cell length and unit cell volume being $2.7 \cdot 10^{-9}$ m and $2 \cdot 10^{-26}$ m^3, respectively, the number of unit cells per 1 L that can be obtained is $5 \cdot 10^{22}$, equivalent to 83 mmol. In the case of the investigated phenol derivatives and the UiO-67 MOF, the condition of maximum capacity is characterized by a situation in which statistically approximately 1.7 phenol derivative molecules are incorporated per unit cell. This value is low in comparison to molecular loadings already reported, e.g. 4.0 pyridine and 2.5 chloroaniline isomers per

HKUST-1 unit cell [34]. A possible explanation for the discrepancy may again originate from imperfections in the crystallinity of our UiO-67 MOF shells.

4.3.5. Affinity Modulation through Mobile Phase Variation

Based on the observed effect that the mobile phase composition influences the binding affinity but not the maximum capacity of the UiO-67 MOF, a more detailed investigation of this relationship was performed as follows. Pulse experiments for the three phenol derivatives and ACN/H_2O mixtures containing between 2.5% and 20% of water were conducted. From the resulting retention times, K_L values were calculated using Equation 4.8 assuming a constant maximum capacity C^*_{MOFmax} of 0.14 mol L^{-1}. This C^*_{MOFmax} value corresponds to a maximum capacity per volume of particle skeleton of C^*_{max} = 0.33 mol L^{-1}.

$$K_L = \frac{k' \varepsilon_t}{(1-\varepsilon_t) \cdot C^*_{\max,i}} \tag{4.8}$$

Figure 4.10 shows the resulting retention factors (k′) and affinity parameters (K_L) for DMP, BZD and DCP. As observed there exists a critical point in each case beyond which k' and K_L rise steeply, i.e. *ca.* 3%, 5% and 10% for DMP, BZD and DCP respectively.

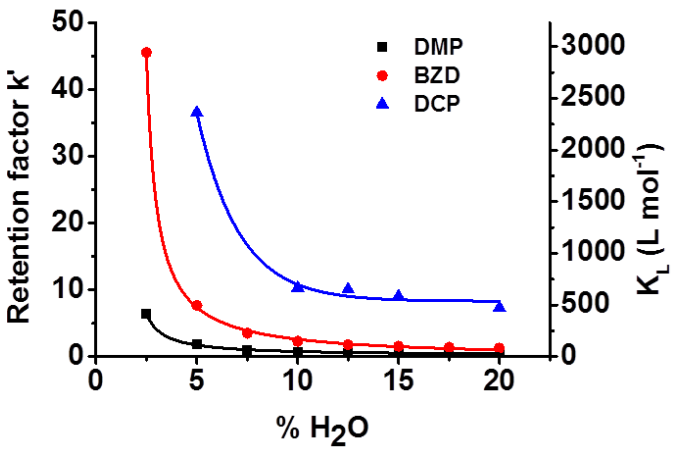

Figure 4.10. Variation of the retention factors (k′) and the Langmuir constants K_L with respect to the H_2O fraction in the ACN/H_2O mobile phase. All runs were performed at a flow rate of 0.14 mL min^{-1} injecting a pulse (0.2 µL) of either DMP (black curve), BZD (red curve), or DCP (blue curve).

4.3.6. Multicomponent Isocratic Pulse Experiments

Multicomponent isocratic pulse experiments were carried out with mobile phases of different compositions (Figure 4.11). The retention times of the phenol derivatives followed the order DMP < BZD < DCP for all eluent compositions used, indicating that the retention mechanism is in accordance with solute polarity. In the case of the mobile phase comprising 3% water, more than 100 min are needed to elute all analytes (Figure 4.11A). Applying a mobile phase

with 5% H_2O shortened the elution time of DMP and BZD to about 3 and 10 min, respectively, while DCP still needed about 38 min to pass the column (Figure 4.11B). Increasing the water content to 10% resulted in the three phenol derivatives eluting too fast, leading to overlapping poorly separated peaks (Figure 4.11C). The equilibrium and kinetic parameters determined for the individual phenol derivatives were integrated into a multicomponent simulation, in order to investigate whether the resulting ChromX model is able to predict the optimum performance of an isocratic separation at 5% water content. With the Langmuir coefficients data obtained from the single component chromatography runs conducted in pulse injection (Table S4.1, Supporting Information) and a constant maximum capacity of C^*_{MOFmax} of 0.14 mol L^{-1}, multicomponent isocratic runs were modeled by ChromX with ACN/H_2O ratios for the mobile phase composition at 97:3, 95:5, and 90:10 (Figure 4.11). Comparing the simulation results of the corresponding multicomponent isocratic pulse experiments against the experimental data demonstrated that the simulation achieved a good prediction of both peak maxima retention time and peak shape for both the retention times of the peak maxima and the overall peak shapes. The only noticeable deviation observed, i.e. in peak height, could not be modeled owing to baseline drift in some cases resulting in growing mismatch between the measured and simulated curves with increasing time. The successful transfer of single component equilibrium data into multicomponent simulations offers a valuable tool for optimizing the application of MOF based sorbents not only in the field of chromatography, but also in others such as sensor technology, where fast kinetics of solutes within MOF thin films are critical.

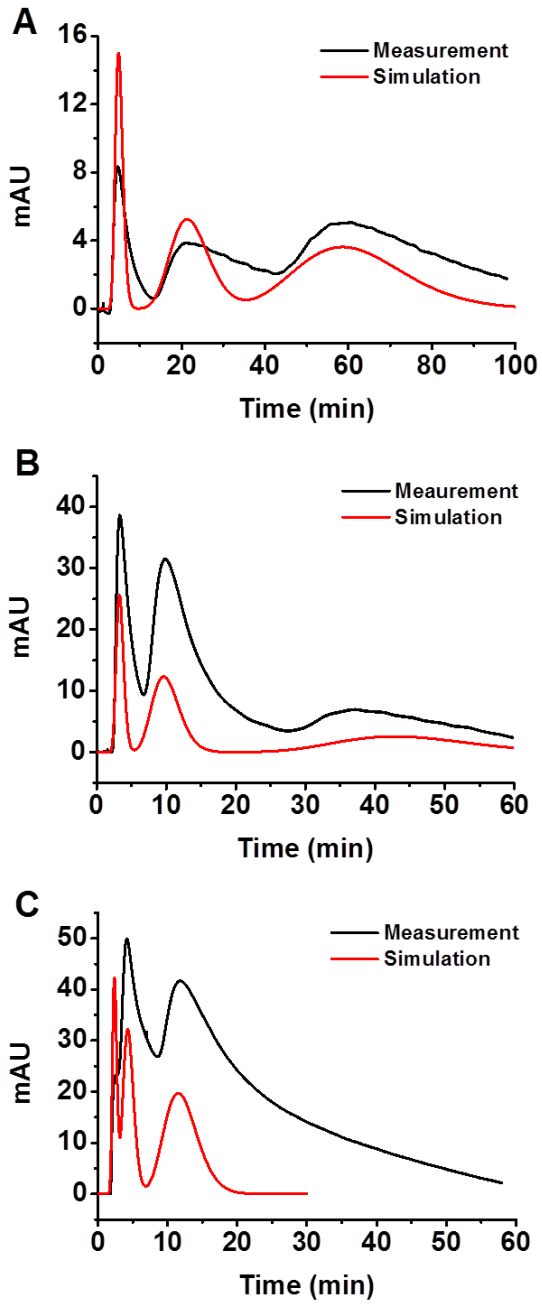

Figure 4.11. Experimental data (black line) and modeling results (red line) of multicomponent isocratic runs with a pulse injection (0.2 µL) of (A) $4.09 \cdot 10^3$ µmol L^{-1} (0.5 g L^{-1}) DMP, $4.54 \cdot 10^3$ µmol L^{-1} (0.5 g L^{-1}) BZD and $1.27 \cdot 10^4$ µmol L^{-1} (2 g L^{-1}) DCP, ACN/H_2O (97:3); (B) $4.09 \cdot 10^3$ µmol L^{-1} (0.5 g L^{-1}) DMP, $4.54 \cdot 10^3$ µmol L^{-1} BZD (0.5 g L^{-1}) and $6.13 \cdot 10^3$ µmol L^{-1} (1 g L^{-1}) DCP, ACN/H_2O (95:5); and (C) $4.09 \cdot 10^3$ µmol L^{-1} (0.5 g L^{-1}) DMP, $4.54 \cdot 10^3$ µmol L^{-1} (0.5 g L^{-1}) BZD and $1.27 \cdot 10^4$ µmol L^{-1} (2 g L^{-1}) DCP, ACN/H_2O (90:10). All runs were performed at a flow rate of 0.14 mL min^{-1} and monitored at 230 nm.

4.4. Conclusions

Shells of UiO-67 SURMOFs were synthesized by a LPE process on magnetic microparticle cores having carboxylic functional groups on the surface to nucleate and bind the first MOF layer. The obtained UiO-67 MPs core-shell composites were physically characterized and packed as a novel stationary phase in HPLC columns in order to investigate the binding properties and kinetics of the MOF sorbents for chromatographic applications. Detailed modeling of experimental data derived from pulse injection and breakthrough experiments conducted with three closely related phenol analytes permitted the extraction of binding equilibrium and pore diffusivity parameters. We found that in the case of these different phenol derivatives, the maximum molar loading capacities remained constant for different mobile phase compositions. In contrast, the affinities of the examined molecules varied and showed a strong dependence on the ACN/H_2O ratio employed. With values of $1 – 4 \cdot 10^{-13}$ m^2 s^{-1}, the determined pore diffusivities are around two to three orders of magnitude smaller than the reported pore diffusivities of phenol derivatives in e.g. activated carbon [35]. The MOF sorbent's slow intraparticle mass transfer kinetics and moderate binding capacities render it unsuitable for preparative chromatography where particle sizes of 30 – 90 µm are typically used.' However, the core-shell design affords acceptable kinetics at practicable operating pressures. Although a common pore diffusion model was applied in our simulations, our results suggest that within the MOFs, the mass transfer mechanism seems to be more elaborate, with significant surface diffusion and size exclusion effects occurring. Therefore, future work will be carried out with SURMOFs of pristine quality and improved models of the mass transfer to explore more comprehensively unique features offered by this highly porous but crystalline chromatographic material.

Acknowledgements

The authors acknowledge Frank Kirschhöfer (Institute of Functional Interfaces, Karlsruhe Institute of Technology, Germany) for the troubleshooting of HPLC issues during the experiments, and Moritz Ebeler (Institute of Functional Interfaces, Karlsruhe Institute of Technology, Germany) for the scanning electron microscope (SEM) measurements.

References

[1] H.C. Zhou, J.R. Long, O.M. Yaghi, Introduction to metal-organic frameworks, Chem. Rev. 112 (2012) 673-674.

[2] Q.L. Zhu, Q. Xu, Metal−organic framework composites, Chem. Soc. Rev. 43 (2014) 5468-5512.

[3] H. Furukawa, K.E. Cordova, M. O'Keeffe, O.M. Yaghi, The chemistry and applications of metal-organic frameworks, Science 341 (2013) 974.

[4] R. Ricco, L. Malfatti, M. Takahashi, A.J. Hill, P. Falcaro, Applications of magnetic metal−organic framework composites, J. Mater. Chem. B 1 (2013) 13033-13045.

[5] M.R. Lohe, K. Gedrich, T. Freudenberg, E. Kockrick, T. Dellmann, S. Kaskel, Heating and separation using nanomagnet-functionalized metal-organic frameworks, Chem. Commun. 47 (2011) 3075-3077.

[6] J. Yang, Y. Dai, X. Zhu, Z. Wang, Y. Li, Q. Zhuang, J. Shi, J. Gu, Metal–organic frameworks with inherent recognition sites for selective phosphate sensing through their coordination-induced fluorescence enhancement effect, J. Mater. Chem. B 3 (2015) 7445-7452.

[7] Y.B. Yu, Y.Q. Ren, W. Shen, H.M. Deng, Z.Q. Gao, Applications of metal-organic frameworks as stationary phases in chromatography, TrAC-Trends. Anal. Chem. 50 (2013) 33-41.

[8] Z.Y. Gu, C.X. Yang, N. Chang, X.P. Yan, Metal-organic frameworks for analytical chemistry: from sample collection to chromatographic separation, Acc. Chem. Res. 45 (2012) 734-745.

[9] A. Ahmed, M. Forster, R. Clowes, D. Bradshaw, P. Myers, H.F. Zhang, Silica SOS@HKUST-1 composite microspheres as easily packed stationary phases for fast separation, J. Mater. Chem. B 1 (2013) 3276-3286.

[10] W.W. Qin, M.E. Silvestre, M. Franzreb, Magnetic microparticles@UiO-67 core-Shell composites as a novel stationary phase for high performance liquid chromatography, Applied Mechanics and Materials 703 (2015) 73-76.

[11] R. Ahmad, A.G. Wong-Foy, A.J. Matzger, Microporous coordination polymers as selective sorbents for liquid chromatography, Langmuir 25 (2009) 11977-11979.

[12] K.A. Cychosz, R. Ahmad, A.J. Matzger, Liquid phase separations by crystalline microporous coordination polymers, Chem. Sci. 1 (2010) 293-302.

[13] O. Shekhah, H. Wang, S. Kowarik, F. Schreiber, M. Paulus, M. Tolan, C. Sternemann, F. Evers, D. Zacher, R.A. Fischer, C. Wöll, Step-by-step route for the synthesis of metal-organic frameworks, J. Am. Chem. Soc. 129 (2007) 15118-15119.

[14] M.E. Silvestre, M. Franzreb, P.G. Weidler, O. Shekhah, C. Wöll, Magnetic cores with porous coatings: growth of metal-organic frameworks on particles using liquid phase epitaxy, Adv. Funct. Mater. 23 (2013) 1210-1213.

[15] H.K. Arslan, O. Shekhah, J. Wohlgemuth, M. Franzreb, R.A. Fischer, C. Wöll, High-throughput fabrication of uniform and homogenous MOF coatings, Adv. Funct. Mater. 21 (2011) 4228-4231.

[16] J.H. Cavka, S. Jakobsen, U. Olsbye, N. Guillou, C. Lamberti, S. Bordiga, K.P. Lillerud, A new zirconium inorganic building brick forming metal organic frameworks with exceptional stability, J. Am. Chem. Soc. 130 (2008) 13850-13851.

[17] M. Kandiah, M.H. Nilsen, S. Usseglio, S. Jakobsen, U. Olsbye, M. Tilset, C. Larabi, E.A. Quadrelli, F. Bonino, K.P. Lillerud, Synthesis and stability of tagged UiO-66 Zr-MOFs, Chem. Mater. 22 (2010) 6632-6640.

[18] S. Chavan, J.G. Vitillo, D. Gianolio, O. Zavorotynska, B. Civalleri, S. Jakobsen, M.H. Nilsen, L. Valenzano, C. Lamberti, K.P. Lillerud, S. Bordiga, H_2 storage in isostructural UiO-67 and UiO-66 MOFs, Phys. Chem. Chem. Phys. 14 (2012) 1614-1626.

[19] Q. Yang, A.D. Wiersum, P.L. Llewellyn, V. Guillerm, C. Serre, G. Maurin, Functionalizing porous zirconium terephthalate UiO-66(Zr) for natural gas upgrading: a computational exploration, Chem. Commun. 47 (2011) 9603-9605.

[20] M.J. Katz, Z.J. Brown, Y.J. Colon, P.W. Siu, K.A. Scheidt, R.Q. Snurr, J.T. Hupp, O.K. Farha, A facile synthesis of UiO-66, UiO-67 and their derivatives, Chem. Commun. 49 (2013) 9449-9451.

[21] A.M. Ebrahim, B. Levasseur, T.J. Bandosz, Interactions of NO_2 with Zr-based MOF: Effects of the size of organic linkers on NO_2 adsorption at ambient conditions, Langmuir 29 (2013) 168-174.

[22] P.W. Siu, Z.J. Brown, O.K. Farha, J.T. Hupp, K.A. Scheidt, A mixed dicarboxylate strut approach to enhancing catalytic activity of a de novo urea derivative of metal−organic framework UiO-67, Chem. Commun. 49 (2013) 10920-10922.

[23] X.Q. Zhang, Q. Han, M.Y. Ding, One-pot synthesis of UiO-66@SiO_2 shell-core microspheres as stationary phase for high performance liquid chromatography, RSC Adv. 5 (2015) 1043-1050.

[24] Z.M. Yan, J.N. Zheng, J.F. Chen, P. Tong, M.H. Lu, Z. Lin, L. Zhang, Preparation and evaluation of silica-UIO-66 composite as liquid chromatographic stationary phase for fast and efficient separation, J. Chromatogr. A 1366 (2014) 45-53.

[25] W.W. Zhao, C.Y. Zhang, Z.G. Yan, L.P. Bai, X.Y. Wang, H.L. Huang, Y.Y. Zhou, Y.B. Xie, F.S. Li, J.R. Li, Separations of substituted benzenes and polycyclic aromatic hydrocarbons using normal- and reverse-phase high performance liquid chromatography with UiO-66 as the stationary phase, J. Chromatogr. A 1370 (2014) 121-128.

[26] G. Kickelbick, U. Schubert, Oxozirconium methacrylate clusters: $Zr_6(OH)_4O_4(OMc)_{12}$ and $Zr_4O_2(OMc)_{12}$ (OMc = methacrylate), Chem. Ber. Recl. 130 (1997) 473-477.

[27] G. Kickelbick, P. Wiede, U. Schubert, Variations in capping the $Zr_6O_4(OH)_4$ cluster core: X-ray structure analyses of $[Zr_6(OH)_4O_4(OOC\text{-}CH{=}CH_2)10]_2(\mu\text{-}OOC\text{-}CH{=}CH_2)_4$ and $Zr_6(OH)_4O_4(OOCR)_{12}(PrOH)$ (R = Ph, CMe = CH_2), Inorg. Chim. Acta 284 (1999) 1-7.

[28] S. Fekete, E. Olah, J. Fekete, Fast liquid chromatography: The domination of core-shell and very fine particles, J. Chromatogr. A 1228 (2012) 57-71.

[29] S.F. Chung, C.Y. Wen, Longitudinal dispersion of liquid flowing through fixed and fluidized Beds, AlChE J. 14 (1968) 857-866.

[30] E.J. Wilson, C.J. Geankopl, Liquid mass transfer at very low reynolds numbers in packed beds, Ind. Eng. Chem. Fundam. 5 (1966) 9-14.

[31] Y.Y. Fu, C.X. Yang, X.P. Yan, Incorporation of metal−organic framework UiO-66 into porous polymer monoliths to enhance the liquid chromatographic separation of small molecules, Chem. Commun. 49 (2013) 7162-7164.

[32] O. Shekhah, Layer-by-layer method for the synthesis and growth of surface mounted metal-organic frameworks (SURMOFs), Materials 3 (2010) 1302-1315.

[33] L. Heinke, Z.G. Gu, C. Wöll, The surface barrier phenomenon at the loading of metal-organic frameworks, Nat. Commun. 5 (2014) 1-6.

[34] W. Qin, M.E. Silvestre, F. Kirschhöfer, G. Brenner-Weiss, M. Franzreb, Insights into chromatographic separation using core–shell metal–organic frameworks: Size exclusion and polarity effects, J. Chromatogr. A 1411 (2015) 77-83.

[35] Z. Ma, R.D. Whitley, N.-H.L. Wang, Pore and surface diffusion in multicomponent adsorption and liquid chromatography systems, AlChE J. 42 (1996) 1244-1262.

4.5. Support Information

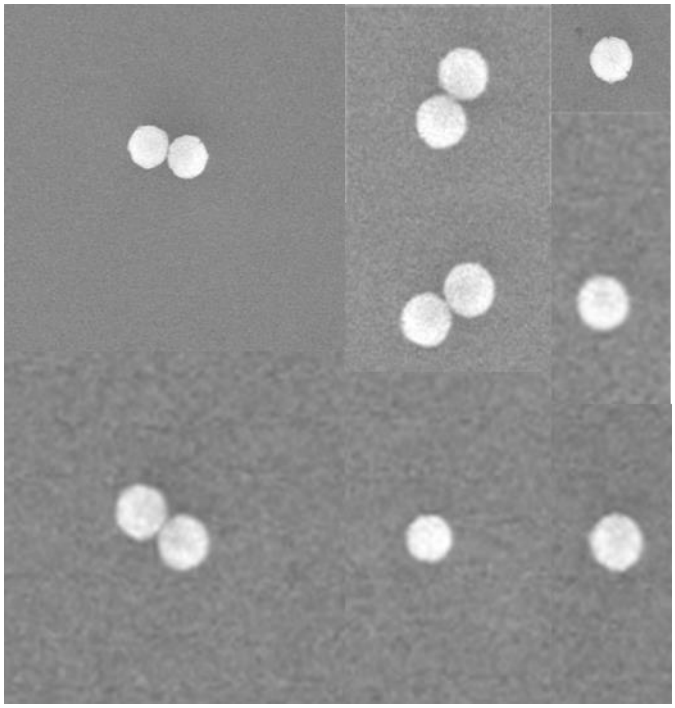

Figure S4.1. Collage of SEM images of UiO-67 MPs (55 cycles) using a lower magnification of 500x.

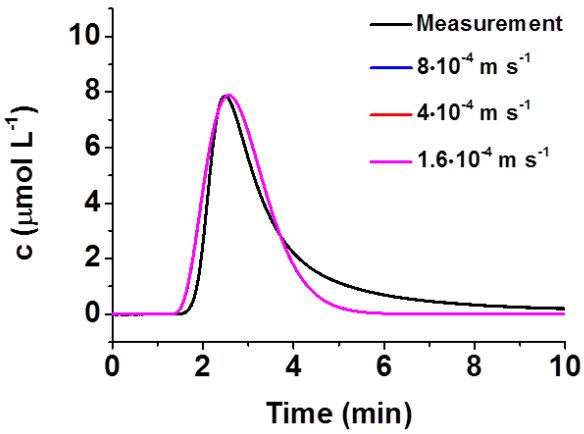

Figure S4.2. Sensitivity analysis of the simulation results with respect to the film mass transfer coefficient. Different values of the film mass transfer coefficient ($8\cdot10^{-4}$ m s^{-1}, $4\cdot10^{-4}$ m s^{-1} and $1.6\cdot10^{-4}$ m s^{-1}) were tested to fit the pulse injection experiment with $9.08\cdot10^{3}$ µmol L^{-1} (1 g L^{-1}) BZD (0.2 µL) using a ACN/H_2O (90:10) mobile phase. The experimental curves are depicted with black line while the simulated ones obtained using ChromX are colored. Due to perfect overlapping only one simulated curve seems visible.

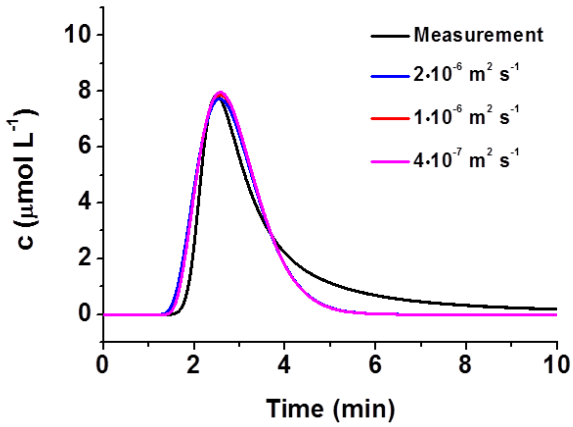

Figure S4.3. Sensitivity analysis of the simulation results with respect to the axial dispersion. Different values of the axial dispersion ($2\cdot10^{-6}$ m^2 s^{-1}, $1\cdot10^{-6}$ m^2 s^{-1} and $4\cdot10^{-7}$ m^2 s^{-1}) were tested to fit the pulse injection experiment with $9.08\cdot10^3$ µmol L^{-1} (1 g L^{-1}) BZD (0.2 µL) using a ACN/H_2O (90:10) mobile phase. Black lines represent the experimental results while the colored lines depict the results of the simulations with ChromX.

Table S4.1. Langmuir coefficients ($K_{L,i}$) for modeling multicomponent isocratic runs using ChromX with the ACN/H_2O mobile phase composition at 97:3, 95:5, and 90:10.

Parameters	ACN/H_2O (97:3)	ACN/H_2O (95:5)	ACN/H_2O (90:10)
$K_{L,DMP}$	244	122	73
$K_{L,BZD}$	1321	551	99
$K_{L,DCP}$	3830	2771	685

5. Insights into Chromatographic Separation Using Core–Shell Metal–Organic Frameworks: Size Exclusion and Polarity Effects

Weiwei Qin, Martin E. Silvestre, Frank Kirschhöfer, Gerald Brenner-Weiss, Matthias Franzreb*

Institute of Functional Interfaces (IFG), Karlsruhe Institute of Technology (KIT), Hermann-von-Helmholtz-Platz 1, 76344 Eggenstein-Leopoldshafen, Germany

*Corresponding author: matthias.franzreb@kit.edu

Abstract Porous metal–organic frameworks (MOFs) $[Cu_3(BTC)_2(H_2O)_3]_n$ (also known as HKUST-1; BTC, benzene-1,3,5-tricarboxylic acid) were synthesized as homogeneous shell onto carboxyl functionalized magnetic microparticles through a liquid phase epitaxy (LPE) process. The as-synthesized core-shell HKUST-1 magnetic microparticles composites were characterized by XRD and SEM, and used as stationary phase in high performance liquid chromatography (HPLC). The effects of the unique properties of MOFs onto the chromatographic performance are demonstrated by the experiments. First, remarkable separation of pyridine and bipyridine is achieved, although both molecules show a strong interaction between the Cu-ions in HKUST-1 and the nitrogen atoms in their heterocycles. The difference can be explained due to size exclusion of bipyridine from the well-defined pore structure of crystalline HKUST-1. Second, the enormous variety of possible interactions of sample molecules with the metal ions and linkers within MOFs allows for specifically tailored solid phases for challenging separation tasks. For example, baseline separation of three chloroaniline (CLA) isomers tested can be achieved without the need for gradient elution modes. Along with the experimental HPLC runs, in-depth modeling with a recently developed chromatography modelling software (ChromX) was applied and proofs the software to be a powerful tool for exploring the separation potential of thin MOF films. The pore diffusivity of pyridine and CLA isomers within HKUST-1 are found to be around $2.3 \cdot 10^{-15}$ m^2 s^{-1}. While the affinity of HKUST-1 to the tested molecules strongly differs, the maximum capacities are in the same range, with 0.37 mol L^{-1} for pyridine and 0.23 mol L^{-1} for CLA isomers, corresponding to 4.0 and 2.5 molecules per MOF unit cell, respectively.

Published in *Journal of Chromatography A, 1411 (2015) 77-83*

5.1. Introduction

The separation of aromatic mixtures of isomers, but also of compounds with relatively close structures, has always been a challenging task in the chemical industry due to similar physicochemical properties, and especially a similar boiling point. High performance liquid chromatography (HPLC) is one of the most commonly used techniques to separate similar synthetic chemicals owing to powerful adsorption columns (stationary phase) [1]. Being the heart of a HPLC system, a large number of stationary phases are already commercially available [2]. However, there is a growing demand for new materials to face the requisites and challenges of ever evolving analytical and industrial applications [3, 4].

As a new generation of stationary phases, metal-organic frameworks (MOFs) have recently exhibited a great feasibility in chromatography application [5, 6], due to their salient features of low density, high uptake capacity, and absence of dead volume. MOFs are highly ordered microporous and crystalline materials constructed by assembling metal ions or clusters with functional organic linkers via strong coordination bonds that have emerged in the past two decades [7, 8]. These materials are characterized by high specific surface area, inherent porosity, tunable pore size and chemical functionality. These features provide them a great potential for diverse applications [9, 10], ranging from gas storage and separation, to catalysis, sensor, and compound delivery.

Extensive studies have been carried out in gas chromatography (GC) since the bulk MOF-508 was first reported as stationary phases for GC in 2006 [11]. However, HPLC applications of MOFs are more complex due to the additional influence of the solvent and the sensitivity of many MOFs against e.g. water. Another major limitation for MOFs based phases in HPLC lies in the irregular shapes and wide size distributions of MOFs usually obtained by traditional solvothermal synthesis. These morphological variations result in suboptimal column packing, low column efficiency, and high column back pressure [12]. The recently established liquid phase epitaxy (LPE) process [13] with a step-by-step fashion is a promising method to produce homogenous MOF films with high (crystalline) quality, as well as well-controlled orientation and thickness on a suitably functionalized surface as a nucleation template [14]. Using nonporous, monodisperse spheres as a template (see Figure 5.1) the above mentioned problems of polydispersity can be solved while keeping the beneficial properties of MOFs as stationary phase [15-17].

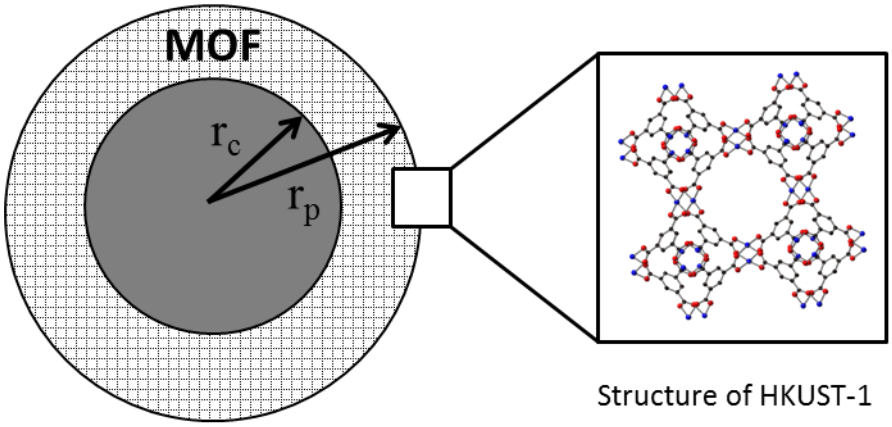

Figure 5.1. Schematic representation of the core–shell HKUST-1 magnetic microparticles. r_c refers to the radius of the magnetic particle and r_p to the radius of the particle including the MOF shell.

Since around ten years an increasing number of studies reporting about MOFs used as HPLC stationary phase have been published. Excellent overviews can be found, e.g. in the recent reviews of Yu and Yusuf, respectively [6, 18]. Most papers show the effective separation of analyte mixtures and demonstrate soundly the influence of several parameters on the observed retention times [19, 20]. Many classes of molecules have been separated, starting from relatively small alkylaromatic compounds using e.g. columns packed with MOFs of the MIL type [21-23], as well as substituted benzenes and polycyclic aromatic hydrocarbons on UiO-66 packed columns [24], up to the high-resolution separation of C_{60} and C_{70} achieved on a MIL-101(Cr) packed column (5 cm long × 4.6 mm i.d.) with dichloromethane/acetonitrile (98:2) as mobile phase [25]. Among the less frequently used MOFs in chromatography is the above mentioned HKUST-1, mainly because of its low stability against water. Nevertheless, effective separation of substituted aromatic hydrocarbons could be demonstrated using hexane as mobile phase [26]. However, fundamental information about the adsorption interaction between the analytes and the MOFs structure, and especially, the equilibrium isotherms and particle diffusion parameters, remain mostly undetermined, even though they would allow for an essential understanding of the performance of MOFs based stationary phases. The principal obstacles to this come from the geometrical factors that are unknown: the used MOF material is often very heterogeneous with respect to particle size and morphology, making it practically impossible to derive quantitative kinetic data. Several examples of core–shell MOF particles used as adsorbents have been reported, such as MOF–silica composites [12], or MOF–Fe_3O_4 microspheres [27]. However, also in these cases the MOF coating consists of an agglomeration of irregular shaped nanoparticles and the coverage of the base material is not homogenous.

In this work, we report on the synthesis of well-defined core–shell structures with a HKUST-1 layer grown evenly on uniform magnetic microparticles by the LPE process (Figure 5.1). HKUST-1 is a well-known functional MOF-material having a three-dimensional framework and a fairly large pore size of 0.9 nm (Figure 5.1, inset) [28]. The obtained core–shell

structured HKUST-1 magnetic microparticles were packed as stationary phase in HPLC columns, with the aim to demonstrate the effect of MOF specific properties onto chromatographic performance. Exemplarily, mixtures of aromatic compounds with similar chemical interaction with HKUST-1 (pyridine and 4,4′-bipyridine) or isomeric structures (chloroaniline isomers) were tested (Figure 5.2). Additionally, the interaction between the HKUST-1 core–shell solid phase and the analytes is investigated on a more fundamental level via simulation of the HPLC experiments.

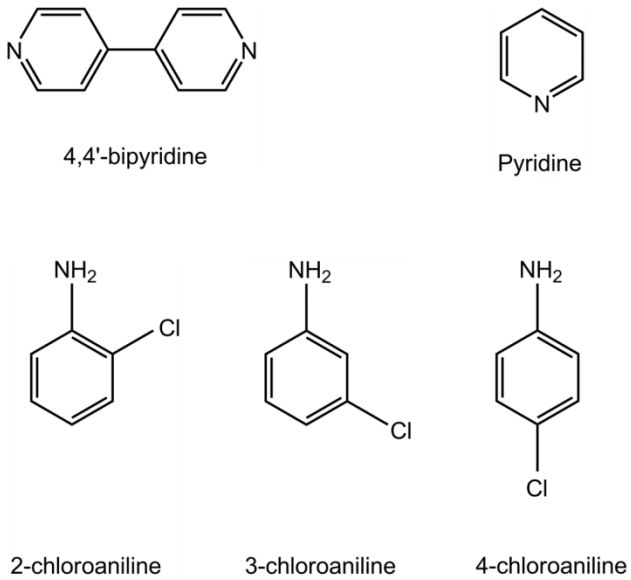

Figure 5.2. Structures of pyridine, 4,4’-bipyridine and chloroaniline isomers used for the HPLC experiments.

5.2. Experimental

5.2.1. Materials and Chemicals

Hydroxyl-functionalized magnetic silica microparticles (MPs, SiO_2-MAG-S1975-OH) with narrow size distribution of 3.55 ± 0.17 µm were purchased from microParticles GmbH, Berlin, Germany. The empty HPLC stainless steel column (50 mm long × 2.0 mm i.d.) was bought from VDS optilab Chromatographie Technik GmbH, Berlin, Germany. All chemicals were at least of analytical grade and purchased from Sigma–Aldrich or Merck KGaA, Germany. (3-Aminopropyl)triethoxysilane (APTES), ammonia aqueous, sodium hydroxide (NaOH), glutaraldehyde solution (GA) and potassium permanganate ($KMnO_4$) were used for particle treatments. Benzene-1,3,5-tricarboxylic acid (BTC, 98%), copper(II) acetate hydrate ($Cu(CH_3COO)_2 \cdot H_2O$), ethanol (CHROMASOLV® absolute for HPLC, 99.8%), carbon tetrachloride (CCl_4, 99.9%) and dichloromethane (DCM, 99.8%) were used to synthesize MOFs and prepare the column. The HPLC grade methanol (MeOH, 99.9%), ethanol (EtOH, 99.9%) and acetonitrile (ACN, 99.9%) were deoxygenated by bubbling through purified

nitrogen gas for at least 20 min prior to be used as HPLC mobile phase. Acetone (99.9%), toluene (anhydrous, 99.8%), pyridine (anhydrous, 99.8%), 4,4′-bipyridine (98%), 2-chloroaniline (2-CLA, 99.5%), 3-chloroaniline (3-CLA, 99%), 4-chloroaniline (4-CLA, 98%), 2,6-dimethylphenol (DMP, 99%), benzene-1,3-diol (BZD, 99%), 2,6-dichlorophenol (DCP, 99%) were dissolved in mobile phase aliquots used as HPLC samples. The molecular structures of pyridine, 4,4′-bypyridine and chloroaniline isomers (2-CLA, 3-CLA, 4-CLA) are shown in Figure 5.2.

5.2.2. Preparation of COOH-terminated MPs

Magnetic microparticles (MPs) were used as precursor for the synthesis of the solid phase. Due to their magnetic properties these particles are easy to separate from the liquid suspensions used during the following surface modification and LPE processes. To serve as a nucleation template, the hydroxyl surface functionalization of the MPs needed to be converted to a terminal carboxyl. This was achieved by a modified Stöber method [29]. 25 mg MPs were immersed into 2.5 mL EtOH, 4 mL deionized water and 0.1 mL 25% (v/v) ammonia. 0.4 mL APTES (0.1 mL per 20 min) was added into the MPs solution with a continuous shaking at 250 rpm for 1 h at room temperature. This resulted in an amino group ($–NH_2$) coating of the MPs. The NH_2-terminated MPs were washed with deionized water 5 times, and then, magnetically extracted. Thereafter, the freshly reacted MPs were dispersed into 4 mL 2% (v/v) GA aqueous solution. The pH was adjusted with 0.5 mol L^{-1} NaOH solution to pH 11 and the solution was then shaked for 1 h at room temperature to functionalize the surface with formyl groups (–CHO) by a derivatization reaction. Subsequently, the MPs were washed with deionized water 5 times and put into 4 mL 0.1 mol L^{-1} $KMnO_4$ solution with 1 h shaking at 40°C to oxidize the –CHO groups to –COOH groups. Finally, the obtained –COOH terminated MPs were washed with deionized water and ethanol, 5 and 2 times, respectively, and stored until further use.

5.2.3. Fabrication of HKUST-1 on MPs

HKUST-1 was synthesized onto the –COOH surface functionalized MPs using the liquid phase epitaxy process with $Cu(CH_3COO)_2·H_2O$, as metal source, and BTC, as organic linkers, deposited in a layer-by-layer fashion. Briefly, 25 mg of the obtained –COOH functionalized MPs were alternately immersed into 2 mL $Cu(CH_3COO)_2·H_2O$ in EtOH solution (5 mmol L^{-1}) and 2 mL BTC in EtOH solution (2 mmol L^{-1}) and kept on a shaker (1350 rpm) for 5 min. The MPs were magnetically separated and washed thoroughly with 2 mL pure EtOH solution between each immersion step for about 2 min. A desired thickness for the built HKUST-1 film was achieved by repeating the deposition process. All the solutions were kept at room temperature during the MOF thin film preparation. After 60 cycles the MOFs coated MPs

were magnetically separated, washed with EtOH solution, dried in vacuum, and stored until further use and characterizations.

5.2.4. Material Characterization

For X-ray diffraction (XRD) with co-planar (out-of-plane, OP) orientation acquisition, a Bruker D8 Advance equipped with a position sensitive detector (PSD) Lynxeye® in θ-θ geometry, variable divergence slit, and 2.3° Soller-slit on the secondary side was used. The data were acquired over a 2θ range of 5 – 20°, with 126 s per 0.019° 2θ-step. Cu-anodes were used with the Cu Kα1,2 radiation (λ = 0.15419 nm).

Scanning electron microscope (SEM) images were recorded using a Zeiss SUPRA60 VP (variable pressure, Carl Zeiss NTS GmbH Germany) at the Karlsruhe Nano Micro Facility, a Helmholtz Research Infrastructure at Karlsruhe Institute of Technology (KIT). Images were recorded at a beam voltage of 5.0 kV and varying magnifications (see scale bars for reference).

5.2.5. Preparation of the HPLC Column and HPLC Experiments

Before packing the column, the as-synthesized HKUST-1 MPs were washed five times with EtOH solution and dried at 120 °C for 12 h under vacuum in order to remove unreacted species in the MOF cavities. The dried composites were added into a mixture of CCl_4 and EtOH (1:1, by volume) under ultrasonication for 5 min. The suspension was then packed with down-flow into a stainless steel column (50 mm × 2.0 mm i.d., column volume 157 µL) under 40 MPa for 10 min with EtOH to obtain the home-made HKUST-1 column.

All chromatographic tests were performed with an Agilent 1100 series HPLC system (Agilent Technologies, USA) equipped with a variable wavelength UV detector and a micro (2 µL) flow cell at room temperature. All the signals were monitored at 254 nm. Before running the chromatographic experiments, the home-made MOF column was equilibrated with the mobile phase until the baseline was stabilized.

5.2.6. Simulation of Chromatographic Runs by the Software ChromX

The software ChromX (Version 0.1.0a) is a powerful tool for simulation of liquid chromatography experiments, developed at the Institute of Process Engineering in Life Sciences – Biomolecular Separation Engineering of the Karlsruhe Institute of Technology (KIT) [http://mab.blt.kit.edu/chromx.php]. Even in case of the freely available academic version, ChromX allows the application of different isotherm and kinetic models, including a so-called general rate model taking into account dispersion, film diffusion and pore diffusion mass transfer limitations. The methodology and equations employed with ChromX are

described previously [30, 31]. Applying a chromatography column model to our case encounters the problem, that the model assumes homogenous spherical particles instead of core–shell adsorbents. Therefore, the maximum loading capacities and pore diffusion coefficients resulting from the simulations have to be corrected by a factor taking into account the geometrical differences (see Supporting information). Although in case of the pore diffusion coefficients this approach is only an approximation, it is justified by the fact that the resulting error is smaller than the uncertainties given in experimental measurements or theoretical estimations of this parameter. Typically, a multicomponent Langmuir isotherm was selected in combination with a general rate kinetic model. Bed voidage ε_b was fixed to 0.4, as a typical value for column packings using monodisperse particles [32]. A particle porosity of ε_p = 0.75 was calculated from crystallographic data on HKUST-1 [33] and film mass transport coefficients were estimated by well-known correlations [34] for packed beds of spherical beads. Afterwards, equilibrium coefficients as well as axial dispersion and pore diffusion coefficients were extracted from single component experimental data by manual or automated fitting procedures included in ChromX. Simulation of multicomponent experiments was conducted on the basis of these parameters without further changes.

5.3. Results and Discussion

5.3.1. XRD and SEM Data

The HKUST-1 MPs (60 cycles), synthesized with the LPE method, were characterized by XRD and SEM experiments. The good agreement of XRD patterns of the as-synthesized HKUST-1 MPs with that of simulated bulk HKUST-1 confirmed the successful fabrication of a MOF shell grown on the MPs (Figure 5.3a). The SEM images obtained (Figure 5.3b and c) present a smooth, homogenous HKUST-1 shell on the magnetic particles. After applying 60 layers of HKUST-1 growth, the diameter of HKUST-1 MPs core-shell composites increased from 3.55 µm for raw MPs to 4.11 µm, indicating that a MOF shell of around 0.28 µm was grown over the MPs. The resulting volume fraction ϕ_s of the shell is 36%. Moreover, the uniform shapes and sizes observed for the as-prepared HKUST-1 MPs materials make them ideal candidates for applications as stationary phase in an HPLC system.

Based on the XRD and SEM results, it was concluded that MOF HKUST-1 shells were successfully fabricated onto the MPs by the LPE method. In contrast to MOF particles prepared by bulk synthesis [35], the synthesized HKUST-1 coated MPs present a uniform size distribution with each bead completely covered by a homogenous MOF shell. These unique properties make them specially suitable for chromatographic applications and offer the possibility for detailed investigations of diffusion kinetics within MOFs.

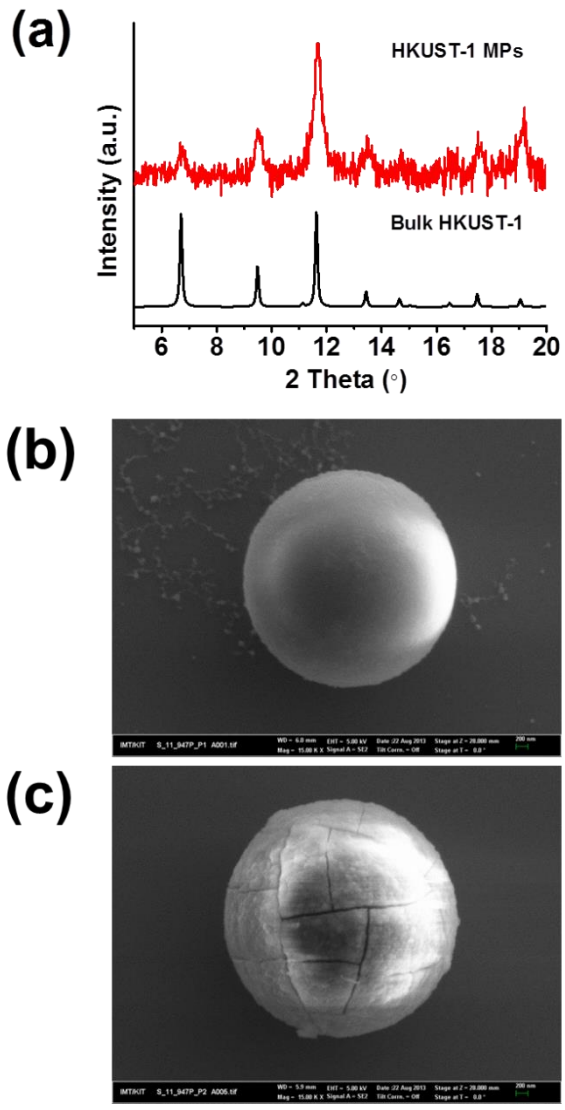

Figure 5.3. (a) Comparison of XRD patterns of as-synthesized HKUST-1 (60 cycles) MPs with the simulated bulk HKUST-1; (b) SEM image of a raw MP before MOFs nucleation; (c) SEM image of the HKUST-1 shell (60 cycles) deposited onto MPs with LPE. The cracks within the MOF–shell of the particles are artefacts from the drying procedure necessary for SEM imaging.

5.3.2. Determination of Column Characteristics

After packing the column, pulse experiments with toluene, and acetone samples were conducted using MeOH as mobile phase. It was expected that these analytes will show only weak or no interaction with the stationary phase and therefore are suitable for the determination of a first approximation of the axial dispersion and pore diffusivities within the column. Figure 5.4 shows the resulting peaks and the corresponding simulations assuming a neglectable interaction with the solid phase, an axial dispersion coefficient of 10^{-6} m^2 s^{-1} and pore diffusion coefficients within the MOF shell of approximately $2.3 \cdot 10^{-13}$ m^2 s^{-1}. Comparing the experimental results with the ChromX simulations revealed that the chosen kinetic parameters are able to give a good description of the peak shape. However both, toluene and acetone, show a weak interaction with HKUST-1, resulting in a short delay of the

peak maximum. The delay of the peaks cannot be explained by higher values of bed voidage or MOF shell porosities, because within a reasonable range of bed voidage (0.4 – 0.55) the required MOF shell porosities calculate to more than 100%. Another indication for a weak interaction of acetone with the HKUST-1 structure is the fact that its retention time differs from that of toluene. It should be mentioned, that for a feed rate of 0.3 mL min^{-1} the value of the film mass transfer coefficient is calculated to $5 \cdot 10^{-4}$ m s^{-1} using the correlation of Wilson and Geankoplis [34]. However, as shown by *in silico* experiments with varying film mass transfer coefficients, the influence of this parameter on column performance can be neglected in good approximation (see Figure S5.1).

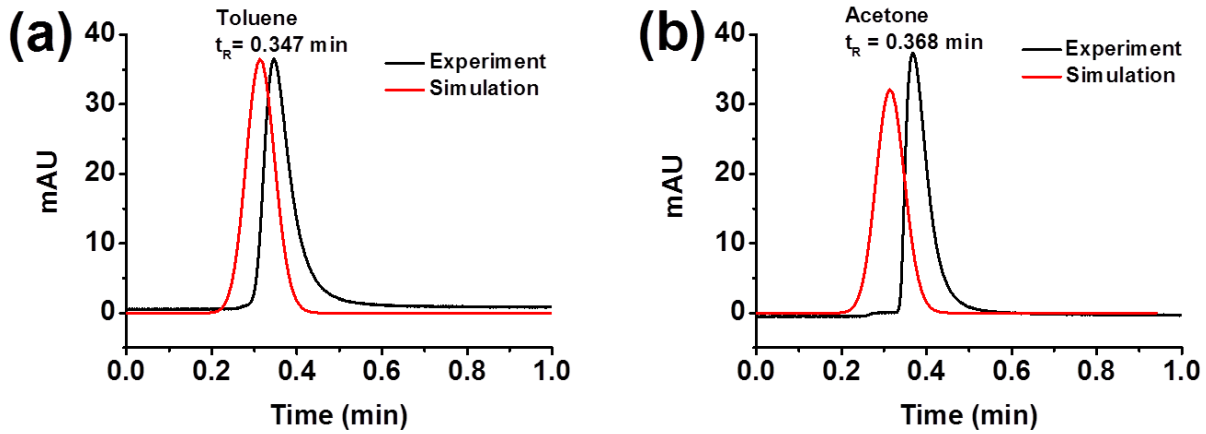

Figure 5.4. HPLC chromatograms of experimental (black lines) and simulated data (red lines) for various tracers on the HKUST-1 MPs packed column (50 mm long ×2.0 mm i.d.). (a) Toluene (9.44 mmol L^{-1}); (b) acetone (136.19 mmol L^{-1}). Conditions: Mobile phase, MeOH; injection volume, 0.2 µL each; flow rate, 0.3 mL min^{-1}.

5.3.3. Separation of Pyridine and 4,4′-bipyridine Using a HKUST-1 MPs Packed Column

Pyridine (kinetic diameter 0.6 nm) and 4,4′-bipyrdine (kinetic diameter 1.1 nm) were used as analytes to test the influence of molecule size onto chromatographic behavior within our column packed with HKUST-1 (pore size of 0.9 nm) core–shell beads. Both substances contain aromatic nitrogen heterocycles, which are known to strongly interact with the Cu-ions of HKUST-1 via both σ-donating nitrogen atoms and π-accepting molecular orbitals [36]. From Figure 5.5 it can be seen that the chromatographic response of pyridine follows this expectation of strong interaction with the HKUST-1 solid phase, corresponding with a retention time of almost 10 min. In contrast, 4,4′-bipyridne elutes immediately after around 15s without any noticeable interaction with HKUST-1 spheres. Therefore, 4,4′-bipyridine (1.1 nm) behaves like a large tracer molecule which is completely excluded from the MOF pores (0.9 nm) due to size exclusion. In our simulation this complete exclusion is realized in good approximation by setting the pore diffusions coefficient of bipyridine to a very small value of 10^{-26} m^2 s^{-1}, thus preventing the molecules from diffusing into the MOF pores.

Assuming bipyridine to be a large tracer, a bed voidage of 45% for the column can be calculated, which corresponds well with the assumption of 40% originally used.

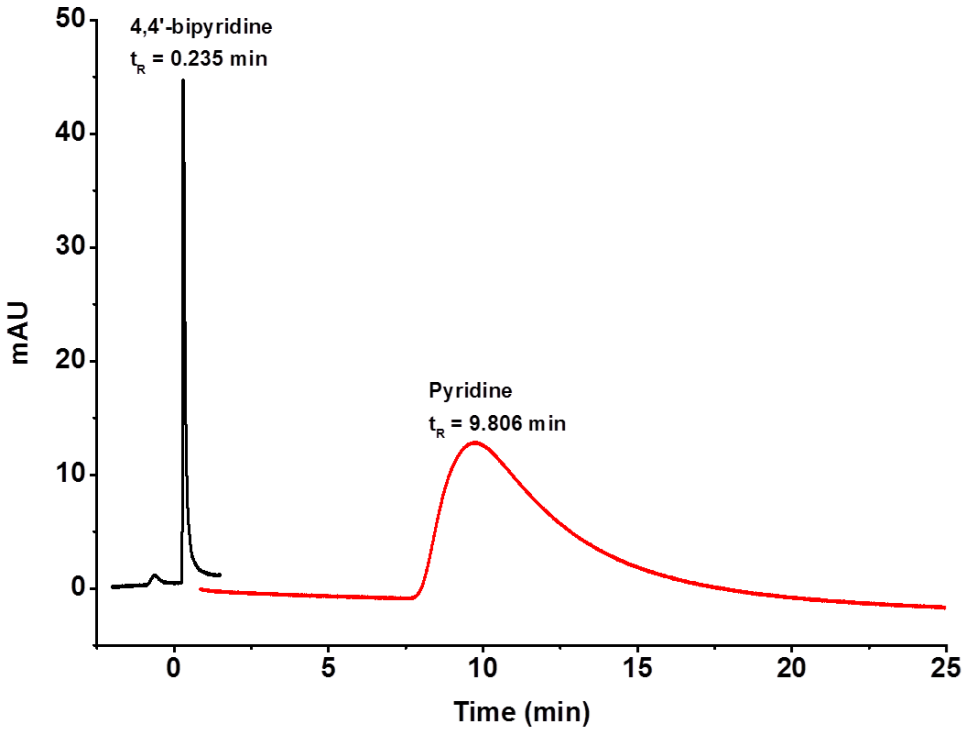

Figure 5.5. Chromatograms of pyridine (12.41 mmol L^{-1}) and 4,4′-bipyridine (6.40 mmol L^{-1}) on the HKUST-1 MPs packed column (50 mm long × 2.0 mm i.d.). Conditions: mobile phase, MeOH; injection volume, 0.2 µL each; flow rate, 0.3 mL min^{-1}.

While size exclusion effects are also known from conventional polymer-based chromatography media, the pore size distribution of these materials results in relatively broad transitions, resulting in only moderate ratios around 1.5 in the retention time of molecules with a ratio of two in their molecular weight. In contrast, our MOF material shows a ratio of the retention times of around 40 between pyridine and bipyridine.

In order to determine the equilibrium parameters of the interaction between pyridine and HKUST-1, pulse experiments with different concentrations (12.41 mmol L^{-1} and 124.1 mmol L^{-1}) were tested. The results show that a tenfold higher concentration leads to a clear shortening of the retention time, making it obvious that concentrations above 100 mmol L^{-1} are outside the linear range of the isotherm (Figure 5.6). From the simulation results, the values of the parameters K_L and C^*_{MOFmax} were determined to be 1187 L mol^{-1} and 0.37 mol L^{-1}, respectively. The pore diffusion coefficient $D_{p,shell}$ was determined to be $2.3 \cdot 10^{-15}$ m^2 s^{-1}, which is the same value as that in the case of acetone or toluene. Therefore, the $D_{p,shell}$ values we found for small organic molecules within HKUST-1 are remarkably smaller than the value of $6 \cdot 10^{-13}$ m^2 s^{-1} that Heinke et al. have determined for cyclohexane within pristine HKUST-1 SURMOF thin films produced by a similar step-by-step LPE process [37]. A

possible explanation could be the so-called surface barrier, that is, defects in the outermost MOF layers which can be caused by detrimental environmental conditions, and strongly reduce the effective mass transfer. As it has been shown by Heinke et al. using a Quartz Crystal Microbalance, such defects can reduce the mass transport into the MOF structure by several orders of magnitude.

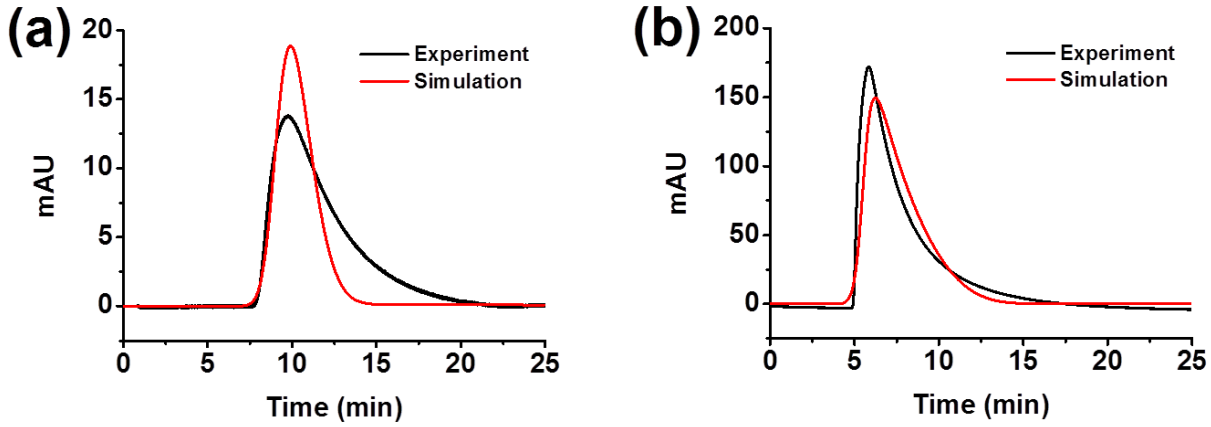

Figure 5.6. HPLC chromatograms of experimental results (black lines) and simulation data (red lines) for pyridine samples at different concentrations passed through the HKUST-1 MPs packed column (50 mm long × 2.0 mm i.d.). (a) 12.41 mmol L^{-1} pyridine; (b) 124.1 mmol L^{-1} pyridine (10 fold of sample concentration). Conditions: Mobile phase, MeOH; injection volume, 0.2 µL each; flow rate, 0.3 mL min^{-1}.

5.3.4. Separation of Chloroaniline Isomers Using a HKUST-1 MPs Packed Column

Three different chloroanilines were used as analytes to investigate the performance of our HKUST-1 MPs packed column with regard to the challenging separation of isomers. When MeOH was used as the mobile phase (Figure 5.7a), a poor separation of chloroaniline isomers was obtained with 2-choloraniline eluting first, followed by 3-, and then 4-chloroaniline. Both, the amino ($–NH_2$) and the chlorine (–Cl) groups, are electron-withdrawing substitutes; however the electronegativity of chlorine is clearly stronger. Consequently, the electronic cloud density of the nitrogen atom increased in the order as 2- < 3- < 4-chloroaniline, corresponding to an increasing distance of the chlorine atom. Thus, the interaction between the nitrogen atom in the analyte and the Cu active sites in HKUST-1 increases in the same order, resulting in the observed increasing retention time of the 2-, 3-, 4-chloroaniline. Ethanol was also tested as mobile phase and identical chromatograms were obtained. The separation performance can be improved by decreasing the analyte concentration (Figure S5.2a) or decreasing the flowrate (Figure S5.2b), but the former only provides a minor improvement and the latter comes with long sample run times.

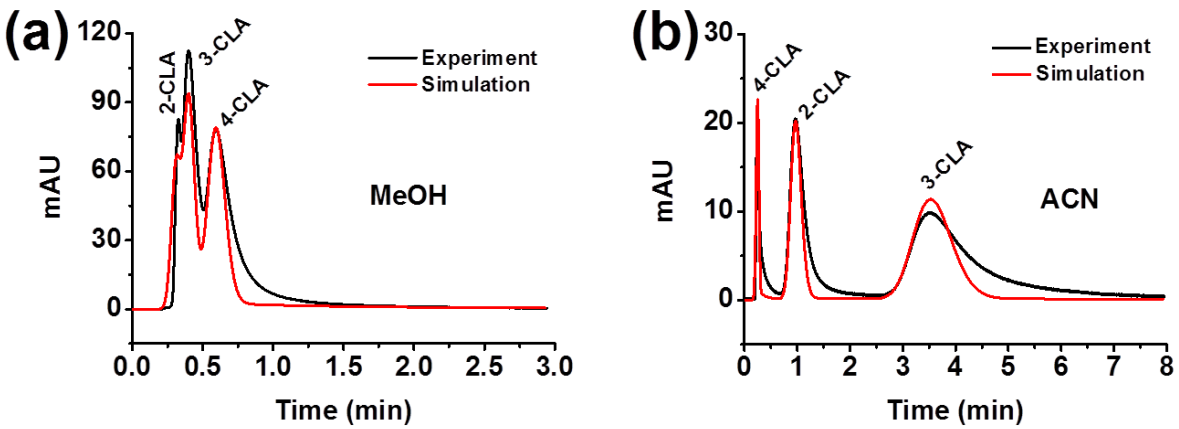

Figure 5.7. HPLC chromatograms of chloroaniline isomers (1.12 mmol L^{-1} in case of 2-CLA and 3-CLA, and 7.84 mmol L^{-1} 4-CLA) on the HKUST-1 MPs packed column (50 mm long × 2.0 mm i.d.). (a) Mobile phase, MeOH; (b) mobile phase, ACN. Conditions: flow rate, 0.3 mL min^{-1}.

In contrast, an excellent baseline separation within less than 8 min sample run time can be achieved when acetonitrile was used as the mobile phase (Figure 5.7b). Interestingly, the elution order was changed to 4- < 2- < 3-chloroaniline, which seems to follow the analyte hydrophobicity measured by means of solubility in water, while we assume that the influence of the specific interaction between the amine group of chloroanilines and Cu-ions in the MOF structure is weakened by the nitrile groups of the solvent. This switch of the dominant retention mechanism from a specific interaction between nitrogen and the metal ions of the MOF structure towards a more general hydrophobic interaction between the analytes and the BTC linkers shows the versatility of possible interactions of MOFs, mobile phase and the analytes. In this respect MOFs can be looked as a special type of mixed mode stationary phases, combining electrostatic and coordination interactions between the solute and the MOF metal ions, with the attractive forces resulting from hydrophobicities of the solute and MOF linker molecules, which usually contain an aromatic backbone.

The above observations show that the mobile phase has a great influence not only on the strength of the retention of chloroaniline isomers, but also on the selectivity of the HKUST-1 MPs packed column towards these molecules. The importance of the MOF type used becomes obvious, when we compare the separation performance of our HKUST-1 based column towards a mixture of phenol derivatives (2,6-dimethylphenol, benzene-1,3-diol and 2,6-dichlorophenol) with the performance of a comparable column based on the MOF UiO-67 reported earlier [20]. The HKUST-1 column showed very poor or no separation of phenol derivatives using ACN or MeOH as mobile phases (Figure S5.3), while the Zr-based MOF UiO-67 showed a good separation and distinctive affinity. A possible explanation could be, that on the one hand the phenol derivatives do not show a specific interaction with the metal ions of both MOFs, and on the other hand the hydrophobic interaction with the 4,4'-biphenyldicarboxylate (BPDC) linker of UiO-67 is stronger than with the BTC linker of HKUST-1 containing only one phenyl ring. In addition, UiO-67 has larger pores, enabling a

better penetration of the relatively large phenol derivatives. Although, these examples of screening different MOFs for the separation of structurally similar or isomeric molecules are rather limited in the moment, they show the potential of the high chemical variety in which MOFs exist for their application in chromatography. Up to today more than 20,000 different MOF structures [38] have been synthesized worldwide and it is easy to imagine that in future MOF based solid phases will be specially tailored for certain separation tasks.

In addition it should be emphasized that the chromatographic behavior of MOF based columns is highly predictable, applying state of the art simulation software. For the simulation of the separations shown in Figure 5.7, we first extracted the affinity coefficients (K_L) and the maximum capacities (C^*_{MOFmax}) for each analyte from simple, single component pulse experiments. Solely based on these single component data, the experimental multicomponent chromatograms were simulated with the software ChromX. As shown in Figure 5.7, a good correlation between the experimental (black line) and simulated data (red line) was achieved with the assumption of $D_{p,shell} = 2.3 \cdot 10^{-15}$ m^2 s^{-1}, and $C^*_{MOFmax} = 0.23$ mol L^{-1} for all CLA isomers, while the different interactions with the solid phase only reflect themselves in considerably different K_L values (Table 5.1).

Table 5.1 Langmuir coefficients ($K_{L,i}$) for chloroaniline isomers with MeOH and ACN as mobile phase.

Mobile Phase	$K_{L,\ 2\text{-CLA}}$ (L mol^{-1})	$K_{L,\ 3\text{-CLA}}$ (L mol^{-1})	$K_{L,\ 4\text{-CLA}}$ (L mol^{-1})
MeOH	7.02	25.5	65.1
ACN	140	644	<5

5.3.5. Theoretical Capacity of HKUST-1

To comprehend further to which extent the analyte molecules occupy the HKUST-1 pores when the maximum capacity is reached, the theoretical capacity was calculated assuming that each pore would be filled with one analyte molecule.

Starting with the HKUST-1 unit cell volume of $1.8 \cdot 10^{-26}$ m^3, obtained by the software Crystalmaker 2.5 using the HKUST-1 CIF file from Cambridge Crystallographic Data Centre (CCDC), the number of unit cells per 1 L that can be calculated to 5.6×10^{22}, or equivalent to 0.092 mol. Comparing the measured maximum capacities ($C^*_{MOFmax,pyridine} = 0.37$ mol L^{-1}, $C^*_{MOFmax,CLA} = 0.23$ mol L^{-1}) with this number, it shows that approximately 4.0 (pyridine) and 2.5 (CLA) analyte molecules fitted into a single HKUST-1 unit cell. These values show compare well with e.g. a maximum molecular loading of 1.7 phenol derivatives per unit cell we found for UiO-67 MOF, and the molecular loadings in MIL-47 already reported, e.g. by Alaerts et al. [21].

5.4. Conclusions

Crystalline HKUST-1 MOF thin films were coated onto magnetic microparticles having a COOH-terminated surface using the process of liquid-phase epitaxy (LPE). Chromatographic column packed with the as-synthesized HKUST-1 magnetic particles offered unusually sharp separation performance for the aromatic nitrogen heterocycles pyridine and 4,4′-bipyridine, due to size exclusion effects of the crystalline MOF material. In addition, the separation of chloroaniline isomers showed, that in combination with suitable mobile phases, the versatile chemistry of MOF-based solid phases offers a chance to identify sorbent materials well suited for challenging separation tasks. With assistance from the modern simulation software, the interactions and mass transfer mechanisms between dissolved molecules and MOF solid phases are easily revealed and will help to further rationalize the screening for optimum separation conditions in future.

References

[1] M. Kluska, D. Prukala, W. Prukala, A. Kondrzycka-Dada, M. Komasinska, K. Malkiewicz, Successful separation and determination of isomers of cytosine derivatives for HPLC, J. Liq. Chromatogr. Relat. Technol. 37 (2014) 2172-2181.

[2] L.R. Snyder, J.J. Kirkland, J.W. Dolan, Introduction to Modern Liquid Chromatography, third ed., 2009, John Wiley & Sons; New York.

[3] K. Ballschmiter, M. Wossner, Recent developments in adsorption liquid chromatography (NP-HPLC) – a review, Fresenius J. Anal. Chem. 361 (1998) 743-755.

[4] T.L. Chester, Recent developments in high-performance liquid chromatography stationary phases, Anal. Chem. 85 (2013) 579-589.

[5] Z.Y. Gu, C.X. Yang, N. Chang, X.P. Yan, Metal–organic frameworks for analytical chemistry: from sample collection to chromatographic separation, Acc. Chem. Res. 45 (2012) 734-745.

[6] Y.B. Yu, Y.Q. Ren, W. Shen, H.M. Deng, Z.Q. Gao, Applications of metal–organic frameworks as stationary phases in chromatography, TrAC-Trends. Anal. Chem. 50 (2013) 33-41.

[7] J.L.C. Rowsell, O.M. Yaghi, Metal–organic frameworks: a new class of porous materials, Micropor. Mesopor. Mater. 73 (2004) 3-14.

[8] Q.L. Zhu, Q. Xu, Metal–organic framework composites, Chem. Soc. Rev. 43 (2014) 5468-5512.

[9] H. Furukawa, K.E. Cordova, M. O'Keeffe, O.M. Yaghi, The chemistry and applications of metal–organic frameworks, Science 341 (2013) 974.

[10] O. Shekhah, J. Liu, R.A. Fischer, C. Wöll, MOF thin films: existing and future applications, Chem. Soc. Rev. 40 (2011) 1081-1106.

[11] B.L. Chen, C.D. Liang, J. Yang, D.S. Contreras, Y.L. Clancy, E.B. Lobkovsky, O.M. Yaghi, S. Dai, A microporous metal−organic framework for gas-chromatographic separation of alkanes, Ind. Eng. Chem. Res. 45 (2006) 1390-1393.

[12] A. Ahmed, M. Forster, R. Clowes, D. Bradshaw, P. Myers, H. Zhang, Silica SOS@HKUST-1 composite microspheres as easily packed stationary phases for fast separation, J. Mater. Chem. B 1 (2013) 3276.

[13] O. Shekhah, H. Wang, S. Kowarik, F. Schreiber, M. Paulus, M. Tolan, C. Sternemann, F. Evers, D. Zacher, R.A. Fischer, C. Wöll, Step-by-step route for the synthesis of metal-organic frameworks, J. Am. Chem. Soc. 129 (2007), 15118-15119.

[14] D. Zacher, O. Shekhah, C. Wöll, R.A. Fischer, Thin films of metal-organic frameworks, Chem. Soc. Rev. 38 (2009) 1418-1429.[15] M.E. Silvestre, M. Franzreb, P.G. Weidler, O. Shekhah, C. Wöll, Magnetic cores with porous coatings: growth of metal-organic frameworks on particles using liquid phase epitaxy, Adv. Funct. Mater. 23 (2013) 1210-1213.

[16] E. Biemmi, C. Scherb, T. Bein, Oriented growth of the metal organic framework $Cu_3(BTC)_2(H_2O)\cdot xH_2O$ tunable with functionalized self-assembled monolayers, J. Am. Chem. Soc. 129 (2007) 8054-8055.

[17] R. Makiura, S. Motoyama, Y. Umemura, H. Yamanaka, O. Sakata, H. Kitagawa, Surface nano-architecture of a metal-organic framework, Nat. Mater. 9 (2010) 565-571.

[18] K. Yusuf, A. Aqel, Z. ALOthman, Metal-organic frameworks in chromatography, J. Chromatogr. A 1348 (2014) 1-16.

[19] S.S. Liu, C.X. Yang, S.W. Wang, X.P. Yan, Metal-organic frameworks for reverse-phase high-performance liquid chromatography, Analyst 137 (2012) 816-818.

[20] W.W. Qin, M.E. Silvestre, M. Franzreb, Magnetic microparticles@UiO-67 core-shell composites as a novel stationary phase for high performance liquid chromatography, Appl. Mech. and Mater. 703 (2015) 73-76.

[21] L. Alaerts, C.E.A. Kirschhock, M. Maes, M.A. van der Veen, V. Finsy, A. Depla, J.A. Martens, G.V. Baron, P.A. Jacobs, J.E.M. Denayer, D.E. De Vos, Selective adsorption and separation of xylene isomers and ethylbenzene with the microporous vanadium(IV) terephthalate MIL-47, Ind. Eng. Chem. Res. 46 (2007) 4293-4297.

[22] C.X. Yang, X.P. Yan, Metal−organic Framework MIL-101(Cr) for high-Performance liquid chromatographic separation of substituted aromatics, Anal. Chem. 83 (2011) 7144-7150.

[23] Y.Y. Fu, C.X. Yang, X.P. Yan, Metal−organic framework MIL-100(Fe) as the stationary phase for both normal-phase and reverse-phase high performance liquid chromatography, J. Chromatogr. A 1274 (2013) 137-144.

[24] W.W. Zhao, C.Y. Zhang, Z.G. Yan, L.P. Bai, X.Y. Wang, H.L. Huang, Y.Y. Zhou, Y.B. Xie, F.S. Li, J.R. Li, Separations of substituted benzenes and polycyclic aromatic hydrocarbons using normal- and reverse-phase high performance liquid chromatography with UiO-66 as the stationary phase, J. Chromatogr. A 1370 (2014) 121-128.

[25] C.X. Yang, Y.J. Chen, H.F. Wang, X.P. Yan, High-performance separation of fullerenes on metal−organic framework MIL-101(Cr), Chem. Eur. J. 17 (2011) 11734-11737.

[26] R. Ahmad, A.G. Wong-Foy, A.J. Matzger, Microporous coordination polymers as selective sorbents for liquid chromatography, Langmuir 25 (2009) 11977-11979.

[27] X.F. Chen, N. Ding, H. Zang, H. Yeung, R.S. Zhao, C.G. Cheng, J.H. Liu, T.W.D. Chan, Fe_3O_4@MOF core-shell magnetic microspheres for magnetic solid-phase extraction of polychlorinated biphenyls from environmental water samples, J. Chromatogr. A 1304 (2013) 241-245.

[28] S.S.Y. Chui, S.M.F. Lo, J.P.H. Charmant, A.G. Orpen, I.D. Williams, A chemically functionalizable nanoporous material $[Cu_3(TMA)_2(H_2O)_3]_n$, Science 283 (1999) 1148-1150.

[29] W. Stöber, A. Fink, E. Bohn, Controlled growth of monodisperse silica spheres in micron size range, J. Colloid Interface Sci. 26 (1968) 62-68.

[30] T.C. Huuk, T. Hahn, A. Osberghaus, J. Hubbuch, Model-based integrated optimization and evaluation of a multi-step ion exchange chromatography, Sep. Purif. Technol. 136 (2014) 207-222.

[31] T. Hahn, A. Sommer, A. Osberghaus, V. Heuveline, J. Hubbuch, Adjoint-based estimation and optimization for column liquid chromatography models, Comput. Chem. Eng. 64 (2014) 41-54.

[32] M.N. Gupta, Methods for Affinity-based Separations of Enzymes and Proteins, first ed., 2002, Birkhäuser; Basel.

[33] P.J. Ryan, O.K. Farha, L.J. Broadbelt, R.Q. Snurr, Y.S. Bae, In: USPTO, (Ed.), Patent Application Publication, 2014, Northwestern University, Evanston, IL, United States, 1-22.

[34] E.J. Wilson, C.J. Geankopl, Liquid mass transfer at very low reynolds numbers in packed beds, Ind. Eng. Chem. Fundam. 5 (1966) 9-14.

[35] L. Ge, L. Wang, V. Rudolph, Z.H. Zhu, Hierarchically structured metal-organic framework/vertically-aligned carbon nanotubes hybrids for CO_2 capture, RSC Adv. 3 (2013) 25360-25366.

[36] O. Zybaylo, O. Shekhah, H. Wang, M. Tafipolsky, R. Schmid, D. Johannsmann, C. Wöll, A novel method to measure diffusion coefficients in porous metal-organic frameworks, Phys. Chem. Chem. Phys. 12 (2010) 8092-8097.

[37] L. Heinke, Z.G. Gu, C. Wöll, The surface barrier phenomenon at the loading of metal-organic frameworks, Nat. Commun. 5 (2014) 1-6.

[38] M. Zhang, M. Bosch, T. Gentle III, H.C. Zhou, Rational design of metal-organic frameworks with anticipated porosities and functionalities, CrystEngComm 16 (2014) 4069-4083.

5.5 Support Information

Correction factors between shell–core and homogenous sphere geometries

ChromX calculates maximum particle loadings in form of mass or mol per particle skeleton volume ($C^*_{max,i}$). In order to calculate maximum loadings with respect to the entire particle volume ($C^*_{V\,max,i}$) this number has to be multiplied by the solid phase fraction of the particle, which depends on the particle porosity (ε_p):

$$C^*_{V\,max,i} = \left(1 - \varepsilon_p\right) \cdot C^*_{max,i} \tag{S5.1}$$

In case of shell-core particles where only the MOF shell contributes to the loading capacity, the true maximum volumetric concentration within the MOF ($C^*_{MOFmax,i}$) must be calculated by means of the volume fraction ϕ_s of the shell (Equation S5.2 and S5.3).

$$\varphi_s = \frac{V_s}{V_p} = \frac{r_p^3 - r_c^3}{r_p^3} \tag{S5.2}$$

$$C^*_{MOF\,max,i} = \frac{C^*_{V\,max,i}}{\varphi_s} \tag{S5.3}$$

In dependence of the ratio between the core and the full particle radius, the relation between the pore diffusivity in the shell ($D_{p,shell}$) and the corresponding apparent pore diffusivity in an homogenous fully porous particle (D_p) can be derived from Equation S5.4 [1].

$$\frac{D_{p,shell}}{D_p} = \frac{r_p^4 + 2r_p^3 r_c + 3r_p^2 r_c^2 - r_p r_c^3 - 5r_c^4}{\left(r_p^2 + r_p r_c + r_c^2\right)^2} \tag{S5.4}$$

Effect of the variation of the film mass transfer coefficient onto the chromatographic behavior

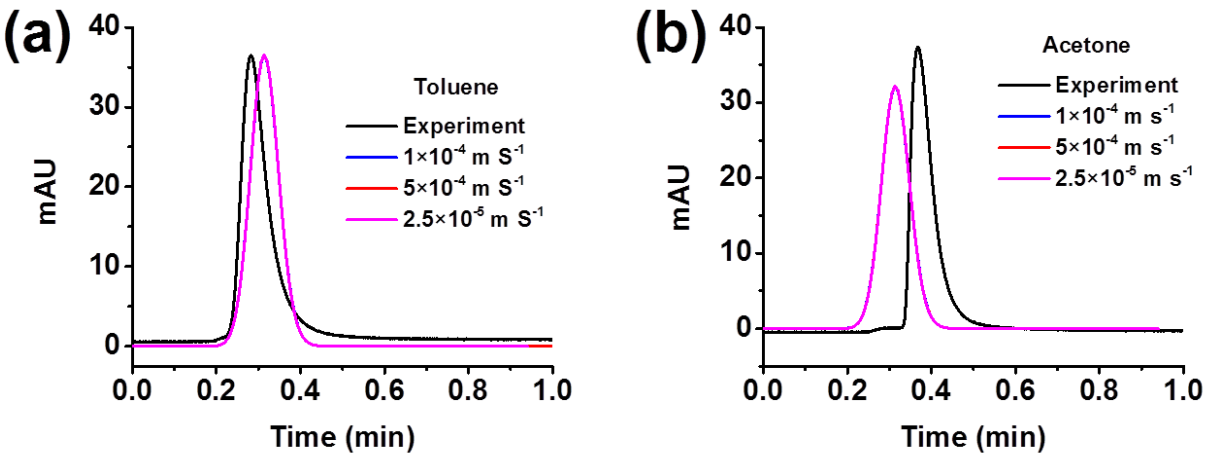

Figure S5.1. Sensitivity analysis of the simulation results with respect to the film mass transfer coefficient. Different values of the film mass transfer coefficient (1×10^{-4} m s^{-1}, 5×10^{-4} m s^{-1} and 2.5×10^{-5} m s^{-1}) were tested to fit the pulse injection experiment with (a) toluene (9.44 mmol L^{-1}); (b) acetone (136.19 mmol L^{-1}). The experimental curves are depicted with black line while the simulated ones obtained using ChromX are colored. Due to perfect overlapping only one simulated curve seems visible. Conditions: Mobile phase, MeOH; injection volume, 0.2 µL each; flow rate, 0.3 mL min^{-1}.

Separation performance of chloroaniline isomers using HKUST-1 as solid phase and MeOH as mobile phase

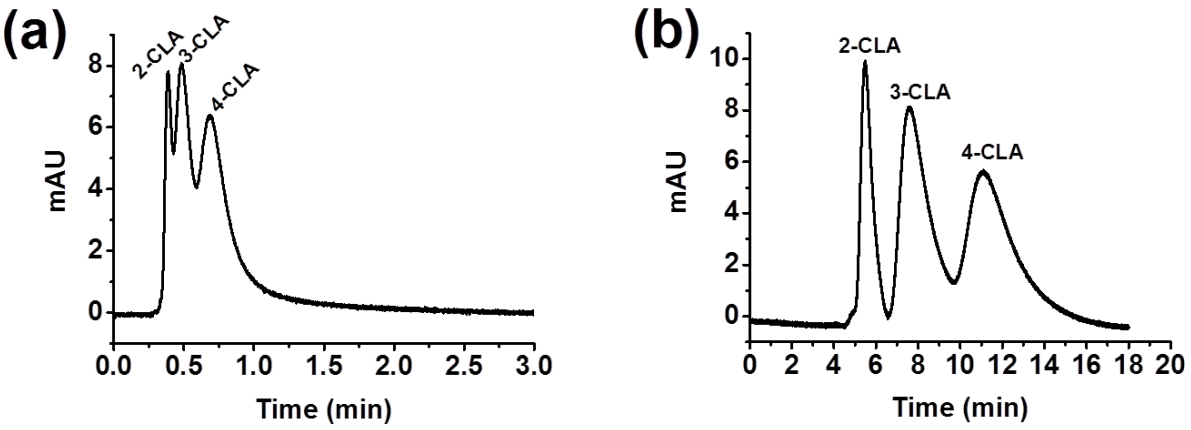

Figure S5.2. Separation improvement by decreasing: (a) sample concentration (0.11 mmol L^{-1} 2-CLA and 3-CLA, and 0.78 mmol L^{-1} 4-CLA); and (b) flowrate (0.02 mL min^{-1}). Conditions: Mobile phase, methanol.

Separation performance of phenol derivatives using HKUST-1 as solid phase

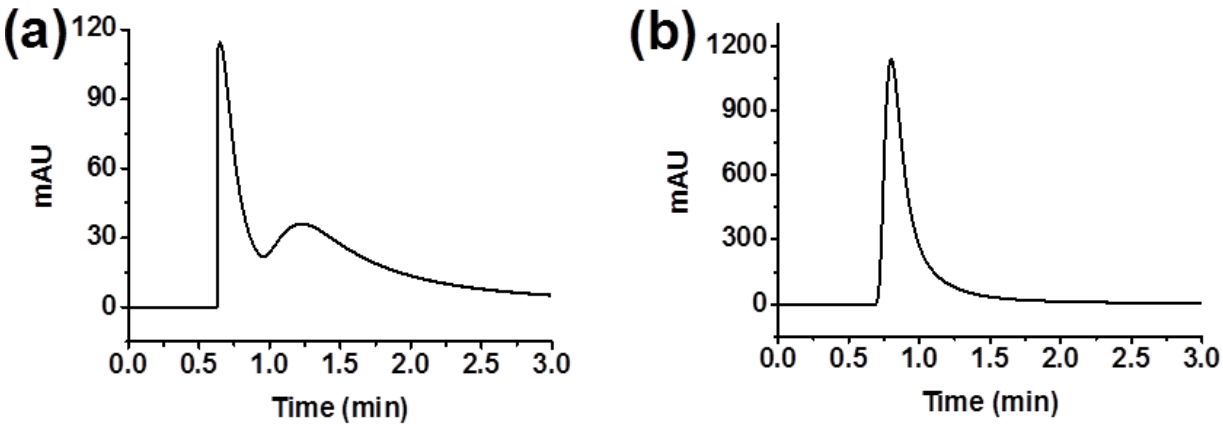

Figure S5.3. Separation performance of phenol derivatives of 2,6-dimethylphenol (4.09 mmol L^{-1}), benzene-1,3-diol (4.54 mmol L^{-1}), and 2,6-dichlorophenol (3.07 mmol L^{-1}): (a) using acetonitrile as the mobile phase at a flow rate of 0.3 mL min^{-1}; (b) using methanol as the mobile phase at a flow rate of 0.1 mL min^{-1}.

Additional References

[1] S. Fekete, E. Olah, J. Fekete, Fast liquid chromatography: The domination of core–shell and very fine particles, J. Chromatogr. A 1228 (2012) 57-71.

6. High Performance Liquid Chromatography of Substituted Aromatics with the Metal-Organic Framework MIL-100(Fe): Mechanism Analysis and Model-based Prediction

Weiwei Qin[a], Martin Eduardo Silvestre[b], Yongli Li[a], Matthias Franzreb[a,*]

[a]*Institute of Functional Interfaces (IFG), Karlsruhe Institute of Technology (KIT), Hermann-von-Helmholtz-Platz 1, 76344 Eggenstein-Leopoldshafen, Germany*

[b]*Roche Diagnostics GmbH, DXRERA7D6164, Nonnenwald 2, 82377 Penzberg, Germany*

∗ Corresponding author: matthias.franzreb@kit.edu

Abstract Metal−organic framework (MOF) MIL-100(Fe) with well-defined thickness was homogenously coated onto the outer surface of magnetic microparticles via a liquid-phase epitaxy method. The as-synthesized MIL-100(Fe) was used as stationary phase for high-performance liquid chromatography (HPLC) and separations of two groups of mixed aromatic hydrocarbons (toluene, styrene and p-xylene; acetanilide, 2-nirtoaniline and 1-naphthylamine) using methanol/water as mobile phase were performed to evaluate its performance. Increasing water content of the mobile phase composition can greatly improve the separations on the expense of a longer elution time. Stepwise elution significantly shortens the elution time of acetanilide, 2-nirtoaniline and 1-naphthylamine mixtures, while still achieving a baseline separation. Combining the experimental results and in-depth modeling using a recently developed chromatographic software (ChromX), adsorption equilibrium parameters, including the affinities and maximum capacities, for each analyte towards the MIL-100(Fe) are obtained. In addition, the pore diffusivity of aromatic hydrocarbons within MIL-100(Fe) was determined to be 5×10^{-12} m^2 s^{-1}. While the affinities of MIL-100(Fe) toward the analyte molecules differs much, the maximum capacities of the analytes are in a narrow range with $q^*_{MOFmax,toluene}$ = 3.55 mol L^{-1}, $q^*_{MOFmax,styrene\ or\ p\text{-}xylene}$ = 3.53 mol L^{-1}, and $q^*_{MOFmax,anilines}$ = 3.12 mol L^{-1} corresponding to approximately 842 toluene and 838 styrene or p-xylene, and 740 aniline molecules per MIL-100(Fe) unit cell, respectively.

Published in Journal of Chromatography A, 1432 (2016) 84-91

6.1. Introduction

Metal–organic frameworks (MOFs), also called porous coordination polymers (PCPs), are an emerging class of crystalline porous materials constructed with inorganic metals ions and organic functional linkers [1, 2]. A key fascinating feature of MOFs is that their structures (pore sizes, geometrics and chemical properties) can be rationally designed for specific targets [3], a possibility which does not exist in other porous materials to the same degree. The versatility of different MOFs leads to a wide range of promising applications in gas storage [4], separation [5, 6], catalysis [7], biomedicine [8], and so on [9]. Besides their tunable structures, the absence of dead volume, high specific surface area, high loading capacity of guest species and inherent porosity make MOFs promising materials as chromatographic stationary phases [10, 11]. Recently, several MOFs have been successfully employed as high-performance liquid chromatography (HPLC) stationary phases to separate dissolves molecules, such as MIL-101(Cr) [12, 13], HKUST-1 [14, 15], UiO-66 [16] and UiO-67 [17]. However, most of the previous studies are focused on MOF synthesis and present the chromatographic performance as ‘proof-of-concept’. What is often missing is the fundamental information about the adsorption interaction between the dissolved solutes and the MOF-based stationary phase, especially the equilibrium isotherms and diffusion parameters. However, for practical applications and model based optimization of the use of MOF based columns in HPLC systems these parameters are of great importance and must be known for in-depth understanding. Instead of the broad size and shape distribution of MOF powders fabricated by traditional solvothermal methods, the recently developed layer-by layer liquid-phase epitaxy (LPE) process [18, 19] is a promising method to prepare homogenous MOF coatings, so-called surface-mounted MOFs (SURMOFs), with controllable thickness on the surface of a suitable functionalized substrate [20, 21].

In present work, MIL-100(Fe) was selected from the wide range of possible MOFs due to its suitability to generate SURMOFs and its stability in the presence of water. The reaction of iron(III) chloride ($FeCl_3$) and 1,3,5-tricarboxylic acid (BTC) leads to a rigid 3D crystal structure with large pores, named MOF-100(Fe) by Serre et al. in 2007 [22]. Compared to other metal ions, Fe(III) is an ideal candidate to be used as the metal nodes in the assembling of MOFs, because of its low toxicity, easily accessible, and most importantly, its robust Lewis acidity, which gives rise to strong coordinate covalent bonds with the organic linkers to form more stable MOFs. The MIL-100(Fe) structure (Figure 6.1, inset) consists of 2.5 nm and 2.9 nm mesoporous pores with window diameters of ca. 0.47 – 0.55 nm and 0.86 nm, respectively. Moreover, MIL-100(Fe) possesses large accessible and permanent pores, and exhibits a remarkable thermal (> 270 °C) and chemical stability (organic solvents or water). Additionally, the presence of the accessible coordinately unsaturated metal sites in the walls of MIL-100(Fe) structure allows the strong coordination of guest molecules. MIL-100(Fe) has been intensively studied for applications in separation [23], catalysis [24], and drug delivery [25].

In this work, we present the synthesis of homogenous MIL-100(Fe) coatings onto the surface of magnetic microparticles (MPs) by a LPE process in order to yield a core-shell architecture (Figure 6.1). The core-shell structured MIL-100(Fe) MPs were used as HPLC stationary phase to illustrate the MOF separation performance and mechanism of mixed aromatic hydrocarbons. The interaction between the organic linkers of the inner surface of the MOF shell and aromatic compounds results in their different affinities towards the stationary phase. First, these affinities were determined independently by single component HPLC experiments. Afterwards, the separation of mixtures of three different aromatic compounds was demonstrated using isocratic and stepwise elution modes. In this context, the capability of a recently published chromatographic software ChromX [http://mab.blt.kit.edu/chromx.php] to predict the chromatographic behavior of mixtures on the basis of single component equilibrium and kinetic data is shown. This allows an *in-silico* optimization of the separation as well as an in-depth understanding of the limiting parameters, pointing the way for future developments of MOF based stationary phases.

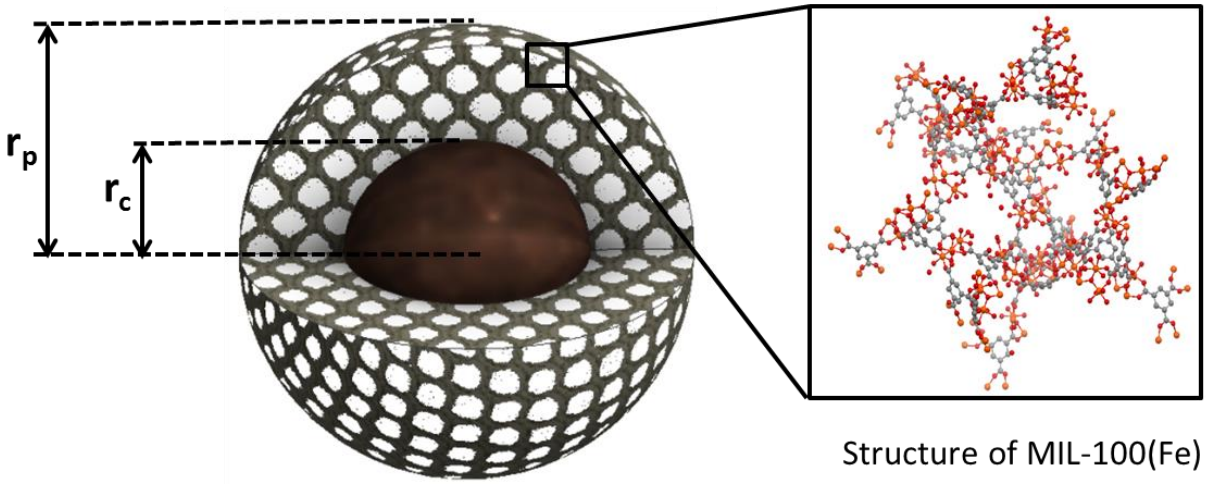

Figure 6.1. Schematic illustration of the structure of the synthesized core-shell MIL-100(Fe) magnetic microparticles. r_c refers to the radius of the magnetic particle and r_p refers to the radius of the particle including the MOF-shell.

6.2. Materials and Methods

6.2.1. Chemicals and Reagents

Carboxyl-functionalized magnetic silica particles (SiO_2-MAG-S1964-COOH), with narrow size distribution of 4.7 ± 0.14 µm were purchased from microParticles GmbH, Berlin, Germany. Empty stainless steel HPLC columns (200 mm long × 1.0 mm i.d., column volume 180 µL, order code: N1910 0000) were bought from VDS optilab Chromatographie Technik GmbH, Berlin, Germany.

All reagents were at least analytical grade and used without further purification. Iron(III) chloride hexahydrate ($FeCl_3 \cdot 6H_2O$, 99%), benzene-1,3,5-tricarboxylic acid (BTC), carbon tetrachloride (CCl_4, 99.9%), methanol (MeOH, 99.9%), dichloromethane (DCM, 99.8%), acetone (99.9%), toluene (anhydrous, 99.8%), styrene (99.9%), p-xylene (99%), acetanilide (99%), 2-nitroaniline (98%), 1-naphthylamine (99%) were purchased from Sigma-Aldrich, WVR or Merck, Germany. MeOH and deionized water (H_2O) were deoxygenated by bubbling through purified nitrogen gas for at least 20 min prior to be used as HPLC mobile phase. The chemical structures of the HPLC analytes used in this study are shown in Figure 6.2.

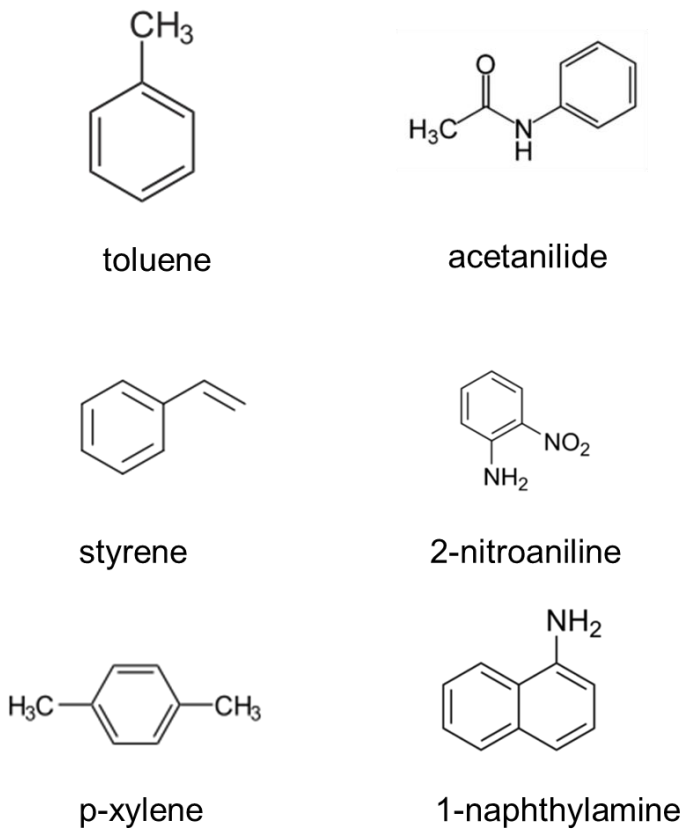

Figure 6.2. Chemical structures of the used HPLC analytes.

6.2.2. Fabrication and Activation of MIL-100(Fe) Magnetic Microparticles

MIL-100(Fe) was deposited onto carboxyl-functionalized MPs (SiO_2-MAG-S1964-COOH, 4.7±0.14 µm) using the LPE process with $FeCl_3 \cdot 6H_2O$ as metal source and BTC as organic linker according to Chen et al. [26]. Briefly, 25 mg MPs were alternately immersed into 2 mL $FeCl_3 \cdot 6H_2O$ ethanol solution (10 mmol L^{-1}) for 15 min and 2 mL BTC ethanol solution (10 mmol L^{-1}) for 30 min and kept on a thermostated shaker (1350 rpm, 70 °C) in each case. The MPs were magnetically separated and washed thoroughly with 2 mL pure ethanol solution between each immersion step for about 2 min. A defined thickness for the built MIL-100(Fe)

film was achieved by repeating the deposition process. After 55 cycles, the MIL-100(Fe) coated MPs were magnetically separated, washed with ethanol solution, dried in vacuum, and stored until further use and characterizations.

6.2.3. Characterization Techniques

X-ray diffraction (XRD) patterns were recorded with Bruker diffractometer. For the co-planar (out-of-plane, OP) orientation a Bruker D8 Advance equipped with a position sensitive detector (PSD) Lynxeye® in θ-θ geometry, variable divergence slit of V12, and 2.3° Soller-slit on the secondary side was used. The XRD data were acquired over a 2θ range of 3 – 20°, with 84 s per 0.019° 2θ-step. Cu-anodes were used with the Cu Kα1,2 radiation (λ = 0.15419 nm).

Analyses of the morphology were recorded using a Philips XL 30 Field Emission Gun Environmental Scanning Electron Microscope (FEG-ESEM) at 20.0 kV at the Institute of Functional Interfaces (IFG), Karlsruhe Institute of Technology (KIT). The diameters of MPs and MIL-100(Fe) MPs were respectively measured and averaged by software ImageJ based on a representative sample of twenty particles in ten different angles.

6.2.4. Preparation of the HPLC Column and Conducted HPLC Experiments

The column was packed according to the previous reports of our group [15, 17]. Typically, the as-synthesized MIL-100(Fe) MPs were first treated by washing three times with DCM solution and washing five times with methanol solution. The composites were then dried at 120 °C for 12 h under vacuum to remove unreacted substances from the MOF cavities. The dried MIL-100(Fe) MPs were added into a mixture of CCl_4 and methanol (1:1, vol/vol) and ultra-sonicated for 5 min. Afterwards, the suspension was packed with a down-flow into the stainless steel HPLC column (200 mm × 1.0 mm i.d.) under 40 MPa for 10 min with methanol to obtain the home-made MIL-100(Fe) based column.

All HPLC tests were carried out on an Agilent 1100 series chromatographic system (Agilent Technologies, USA) equipped with a variable wavelength UV detector at room temperature. All the signals were monitored at 254 nm. Before running the chromatographic experiments, the home-made MOF column was equilibrated with methanol until a stable baseline was reached. The mobile phase was used to prepare the liquid samples containing different aromatic analytes. The samples were injected with a manual injector (Rheodyne LabPro PR700-100-01 switcher valve, USA).

6.2.5. Simulation of Chromatographic Runs Using the Software ChromX

The software ChromX is a powerful tool for liquid chromatography simulation, exploited by the Institute of Process Engineering in Life Sciences – Biomolecular Separation Engineering of the Karlsruhe Institute of Technology (KIT). ChromX offers different isotherm and kinetic models, including a so-called general rate model taking into account dispersion, film diffusion and pore diffusion mass transfer limitations. The methodology and equations employed with ChromX were described previously [27, 28].

The freely available academic version of ChromX (Version 0.1.0a) used in our earlier work is limited to the assumption that the stationary phase consists of homogenous spherical particles. In this work, we use for the first time an updated version (ChromX_shell_core) specifically adapted to our case. The equations used in this model take into account the shell-core structure of the adsorbents, eliminating the need for an artificial approximation of such a case using reduced capacities and lumbed-rate diffusivities. This reduces the work-load of the simulation considerably and improves the quality of the simulations. Typically, a multicomponent Langmuir isotherm was selected in combination with a general rate kinetic model and the column parameters were determined by fitting the simulations to the experiments. Thus, equilibrium coefficients as well as axial dispersion and pore diffusion coefficients were extracted from single component experimental data by manual or automated fitting procedures included in ChromX. Simulation of multicomponent experiments was conducted on the basis of these parameters without further changes.

6.3. Results and Discussion

6.3.1. Characterization of Synthesized MIL-100(Fe) MPs

The as-synthesized MIL-100(Fe) MPs were characterized by XRD and SEM experiments. The successful growth of a MIL-100(Fe) shell onto the MPs is validated by the good agreement between the XRD pattern of the obtained MIL-100(Fe) MPs and the simulated one (Figure 6.3a). The SEM images of the raw MPs and the prepared MIL-100(Fe) MPs are shown in Figure 6.3b and 3c, respectively. Figure S6.1 shows the images of these uniform uncoated and coated MPs with more numbers under a lower magnification. Figure 6.3c displays a smooth, homogenous MIL-100(Fe) shell on the MPs. After applying 55 layers of MIL-100(Fe) deposition with the LPE method, the diameter of composites increases from 4.7 µm for raw MPs to 6.0 µm, indicating that a MOF shell of 0.65 µm is assembled on the MPs. The resulting volume fraction ϕ_s of the shell is 52%. In addition, the uniform shapes and sizes observed for the obtained MIL-100(Fe) MPs materials make them well-suited for use as stationary phase in chromatography.

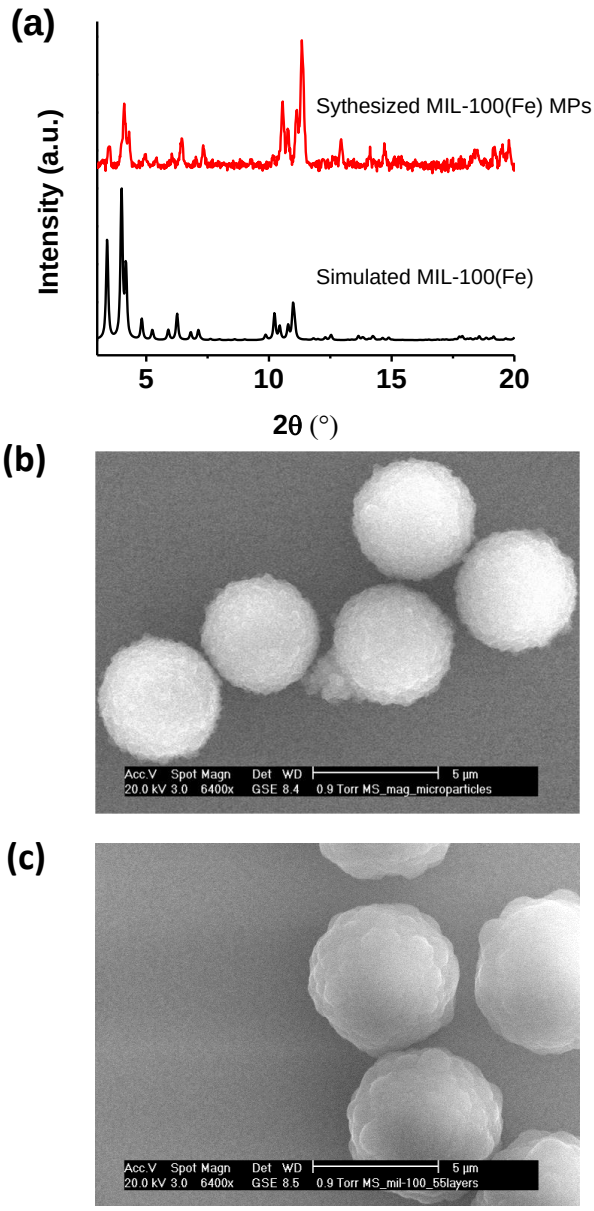

Figure 6.3. (a) XRD patterns of the simulated MIL-100(Fe) and the prepared MIL-100(Fe) MPs; SEM images of (b) the raw MPs and (c) the synthesized MIL-100(Fe) MPs.

The XRD and SEM results confirm the successful formation of MOF MIL-100(Fe) shells onto the MPs via the LPE method. Different from MOF powders produced via bulk synthesis [29,30], the MIL-100(Fe) coated MPs features a uniform size distribution and each bead being completely covered by a homogenous MOF shell, which make them ideal materials for chromatographic applications and provide the possibility of investigating in detail diffusion kinetics within MOFs.

6.3.2. Determination of Column Characteristics

After packing the column, pulse experiments with blue dextran and acetone samples were conducted using MeOH as mobile phase. These two analytes show only weak or no interaction with the stationary phase and therefore are suitable for the determination of column void fraction, particle porosity and a first approximation of the axial dispersion coefficient within the column.

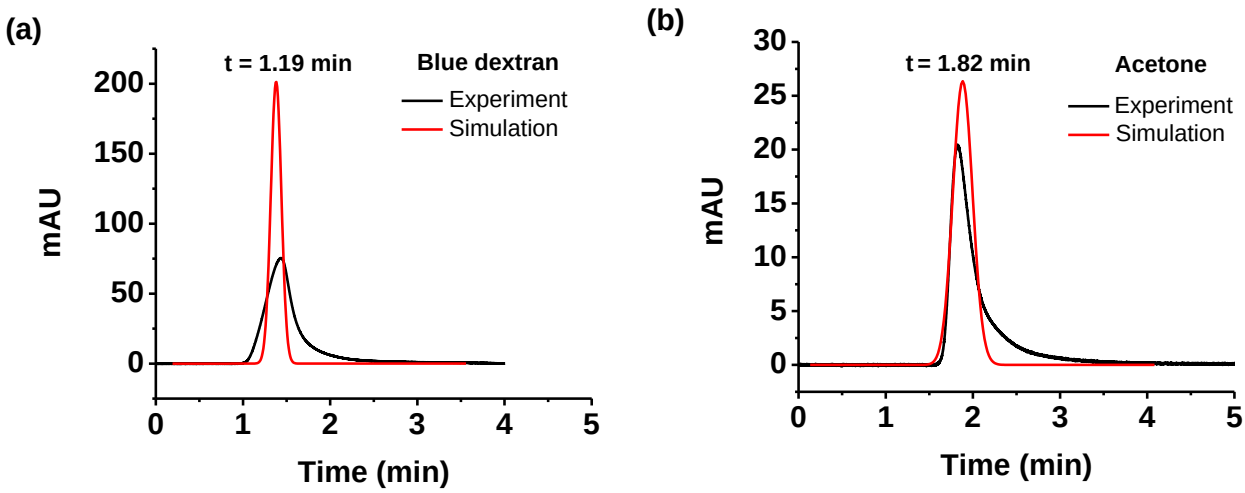

Figure 6.4. HPLC chromatograms of experimental for blue dextran (5×10^{-7} mol L^{-1}) and acetone (0.04mol L^{-1}) on the MIL-100(Fe) MPs packed column (2 cm long ×1.0 mm i.d.). Conditions: Mobile phase, MeOH; injection volume, 1 µL each; flow rate, 0.07 mL min^{-1}.

Figure 6.4 shows the resulting chromatographic peaks of blue dextran and acetone and their corresponding simulations. Compared to the simulated curves, the experimental curves show considerable tailing, probably caused by imperfect column packing and backmixing within UV and conductivity detectors. Assuming a neglectable interaction with the solid phase, the bed porosity (ε_b) and the total porosity (ε_t) are calculated to be 46.3% and 70.0%, respectively, from the retention of the large tracer blue dextran and the small tracer acetone, resulting in the calculated values of the average particle porosity (ε_p) to be 44.2% and MOF shell porosity ($\varepsilon_{p,MOF}$) to be 85.0%, which is in the realistic range.

With ChromX, an axial dispersion coefficient of 10^{-6} m^2 s^{-1} was determined. Besides, the pore diffusion coefficient for acetone within the MOF shell was approximated to be 5×10^{-12} m^2 s^{-1}. Comparing the experimental results with the ChromX simulations reveals that the determined parameters are able to give a good description of the hydrodynamic column behavior. For the feed rate of 0.07 mL min^{-1} a film mass transfer coefficient of 4×10^{-4} m s^{-1} can be estimated from the known correlations [31]. However, as we showed previously for UiO-67 and HKUST-1 columns [15,32], film mass transfer can be neglected in case of MOF based chromatographic material of a few micrometers in size.

6.3.3. Determination of Equilibrium Parameters

To determine the equilibrium parameters of the adsorption isotherm between the analytes (neutral analytes: toluene, styrene and p-xylene; basic analytes: acetanilide, 2-nitroaniline and 1-naphthylamine) and the MIL-100(Fe) MPs stationary phase, isocratic elution of single component runs was conducted in pulse injection and breakthrough mode with MeOH/H_2O as mobile phase. The experimental (black lines) as well as the simulated HPLC chromatograms (red lines) of isocratic runs using pulse injection are shown in Figure 6.5 for the neutral analytes and Figure 6.6 for the basic analytes, respectively.

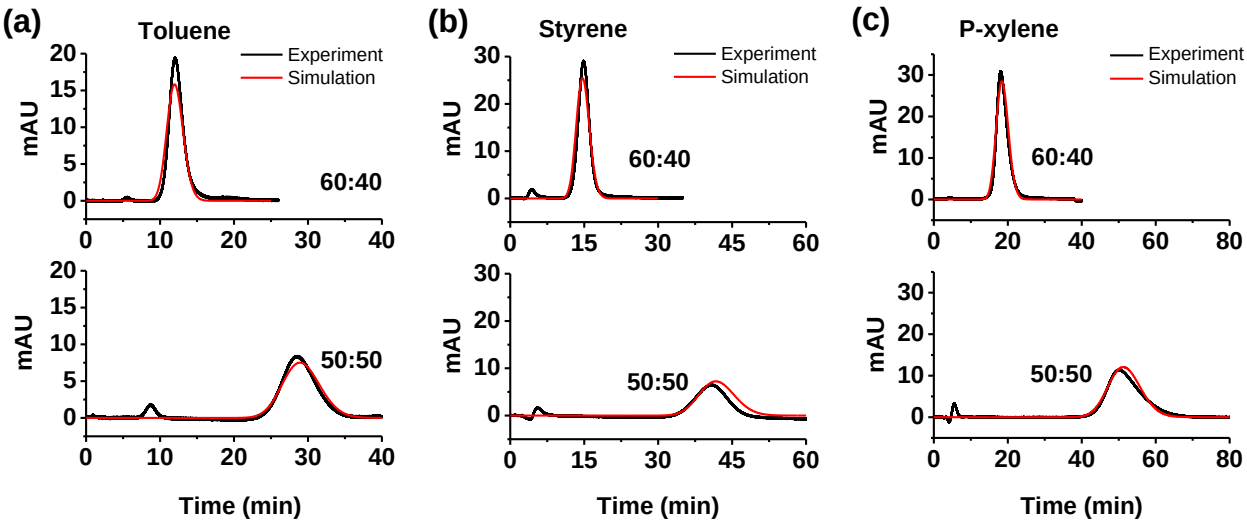

Figure 6.5. Isocratic elution chromatograms (experiment and simulation) of single components (neutral analytes) on the MIL-100(Fe) MPs packed column (2 cm long ×1.0 mm i.d.): (a) toluene (14.16 mmol L^{-1}); (b) styrene (0.26 mmol L^{-1}); (c) p-xylene (24.30 mmol L^{-1}). Conditions: Mobile phase: MeOH/H_2O (60:40) and (50:50), respectively; injection volume, 1 µL each; flow rate, 0.07 mL min^{-1}.

MIL-100(Fe) exhibits hydrophobic properties resulting from the aromatic ring within the linkers of the framework. Comparing the chromatograms of Figure 6.5 within a fixed row**,** it can be seen that the retention time increases with the following order: toluene < styrene < p-xylene in the case of both mobile phase compositions MeOH/H_2O 60:40 and 50:50. These three neutral analytes are all very weak polar substances with the polarity order: toluene > styrene > p-xylene. Taking into account their weak polarities, higher methanol fractions within the mobile phase should increase the tendency of all three analytes to stay in solution; therefore, shortening their retention time (comparing chromatograms within the same column). The measured retention time is in accordance with both described dependencies showing that the polarity of the analytes determines their interaction with the stationary and mobile phase.

The equilibrium parameters of K_L and $q^*_{MOF,max}$ derived from the simulations using ChromX are shown in Table 6.1. Here it should be noted that the value of the maximum capacity

$q^*_{MOF,max}$ remains the same for the individual components in different mobile phase compositions of MeOH/H_2O (60:40, 50:50 and 40:60). In addition there is only a tiny difference in the maximum capacity $q^*_{MOF,max}$ for toluene (3.55 mol L^{-1}), styrene (3.53 mol L^{-1}) and p-xylene (3.53 mol L^{-1}), which is within the experimental error. However, the affinity increases strongly with increasing water content of the mobile phase and also shows clear differences between the different analytes. The values of the affinity coefficients (K_L) are increasing in the order: toluene, styrene, and p-xylene when the mobile phase is kept constant. This indicates that, on the one hand, for isocratic elution the components of a mixture will elute in accordance with their affinities. And on the other hand, the separation efficiency and times can be optimized by adjusting the mobile phase composition.

Table 6.1 Equilibrium parameters K_L and $q^*_{MOF,max}$ of benzene derivatives obtained from experimental and simulation results of single components (Figure 6.5).

Sample	Toluene			Styrene			P-xylene		
MeOH/H_2O	60:40	50:50	40:60	60:40	50:50	40:60	60:40	50:50	40:60
$q^*_{MOF,max}$ (mol L^{-1})	3.55	3.55	3.55	3.53	3.53	3.53	3.53	3.53	3.53
K_L (L mol^{-1})	7.19	21.2	50.7	9.17	29.2	78.1	11.9	38.2	111

Isocratic elution of the single components of the basic analytes (acetanilide, 2-nitroaniline, and 1-napthyamine) was carried out to further demonstrate the utilization of MIL-100(Fe) MPs as stationary phase in combination with three different mobile phase compositions of MeOH/H_2O (60:40, 50:50 and 40:60) **(**Figure 6.6**)**. The retention time increases in the order of acetanilide < 2-nitroaniline < 1-napthyamine applying the same mobile phase composition. Again, the results can be simulated assuming increasing affinities, but the same maximum capacity of 3.12 mol L^{-1} (Table 6.2). The fast elution of acetanilide can be explained by the weak interaction between the methyl group (–CH_3) of acetanilide and the carboxyl group (–COOH) of MIL-100(Fe) [33,34]. The higher retention of 2-nitroaniline than that of acetanilide indicates a stronger interaction caused by an additional hydrogen bond between the nitro group (–NO_2) of 2-nitroaniline and the hydroxyl group (–OH) of MIL-100(Fe) [35]. The highest affinity of the MIL-100(Fe) towards the 1-naphthylamine attributes to the π–π interaction between the naphthalene substituent of 1-naphthylamine and the aromatic ring walls of MIL-100(Fe) [36]. For each analyte, an increase of the water content of the mobile phase results in longer retention times and broader peaks, notably for 1-naphthylamine (Figure 6.6c) which has stronger interactions with the MIL-100(Fe) framework.

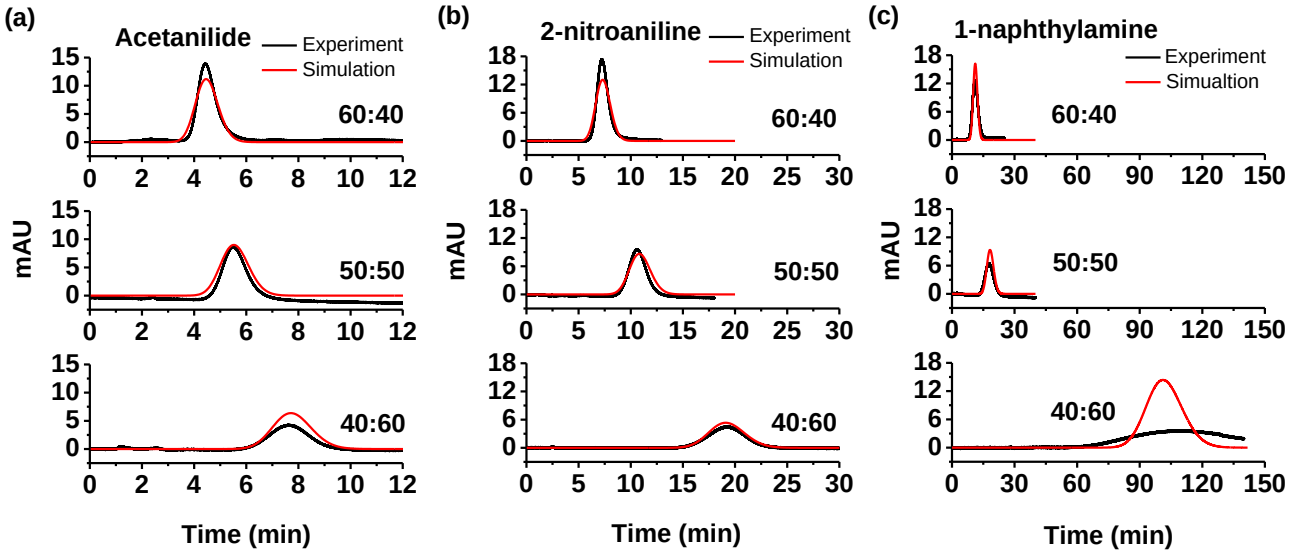

Figure 6.6. Isocratic elution chromatograms (experiment and simulation) of single components (basic analytes) on the MIL-100(Fe) MPs packed column (2 cm long ×1.0 mm i.d.): (a) Acetanilide (0.07 mmol L^{-1}); (b) 2-nitroaniline (0.72 mmol L^{-1}); (c) 1-naphthylamine (0.35 mmol L^{-1}). Conditions: mobile phase, MeOH/H_2O (60:40), (50:50) and (40:60), respectively; injection volume, 1 µL each; flow rate, 0.07 mL min^{-1}.

Table 6.2 Equilibrium parameters K_L and $q^*_{MOF,max}$ of anilines obtained from experimental and simulation results of single components (Figure 6.6).

Sample	Acetanilide			2-nitroaniline			1-naphthylamine		
MeOH/H_2O	60:40	50:50	40:60	60:40	50:50	40:60	60:40	50:50	40:60
$q^*_{MOF,\ max}$ (mol L^{-1})	3.12	3.12	3.12	3.12	3.12	3.12	3.12	3.12	3.12
K_L (L mol^{-1})	2.05	2.91	5.13	4.38	7.24	15.31	7.50	13.3	81.4

Applying the obtained $q^*_{MOF,max}$ and K_L values from single component pulse experiments, ChromX was used to simulate experimental breakthrough curves (Figure 6.7 and S6.2). Although the applied analyte amounts and the resulting concentrations within the column are orders of magnitude higher in these experiments, the determined equilibrium and kinetic parameters allowed good simulations of the breakthrough curves. The only exception is 1-napthyamine, where the experimental breakthrough time is substantially higher than the simulated one. A possible explanation is that the low effluent concentrations and long retention time of this analytes in the pulse experiments limit the accuracy of the calculated equilibrium parameters.

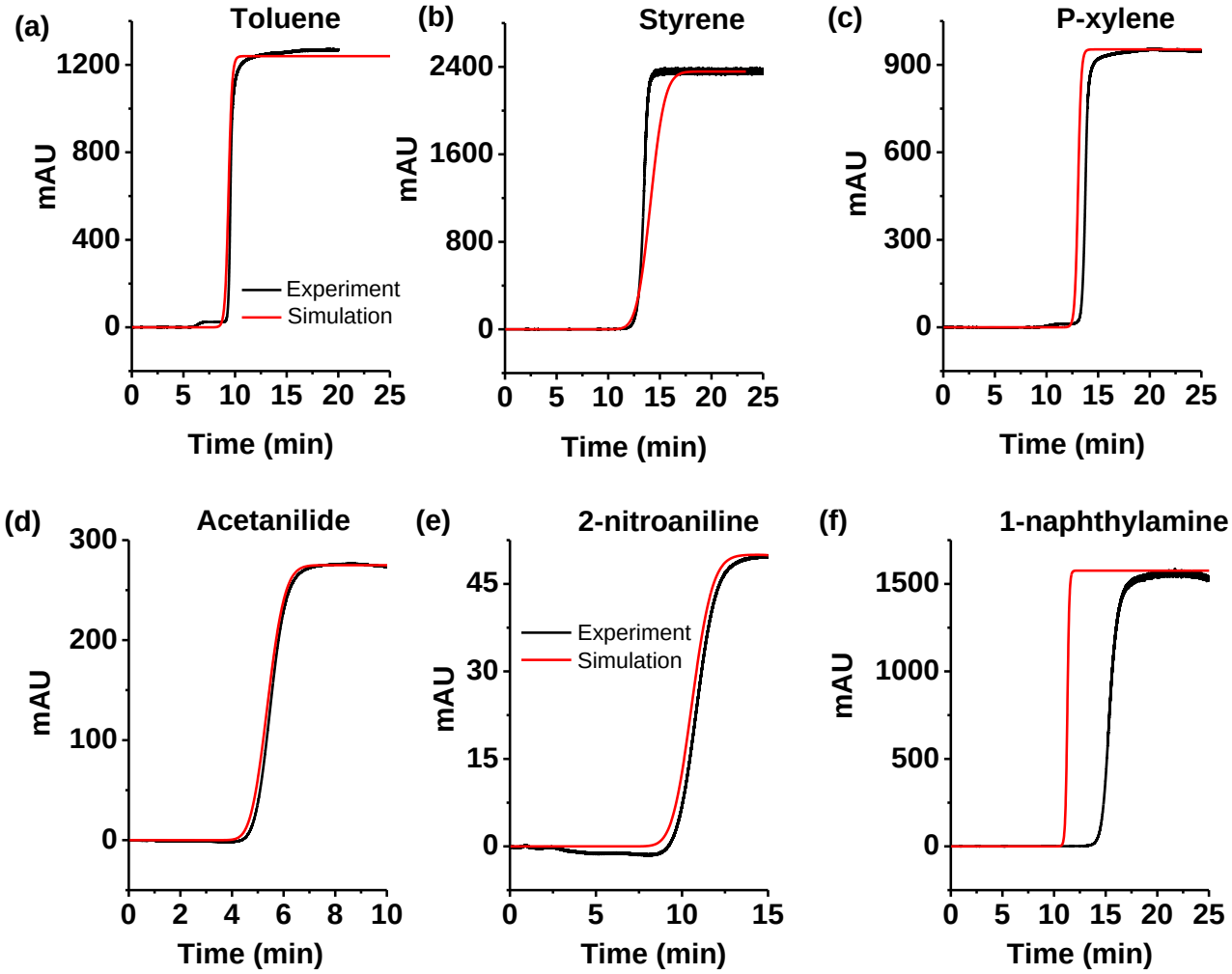

Figure 6.7. Chromatograms of breakthrough experiments of different analytes using a MIL-100(Fe) MPs packed column (2 cm long ×1.0 mm i.d.): (a) toluene (47.2 mmol L^{-1}); (b) styrene (43.6 mmol L^{-1}); (c) p-xylene (40.5 mmol L^{-1}); (d) (0.148 mmol L^{-1}) acetanilide; (e) 2-nitoaniline (0.724 mmol L^{-1}); (f) 1-naphthylamine (0.349 mmol L^{-1}). Conditions: mobile phase, (a-c) MeOH/H_2O (60:40) and (d-f) MeOH/H_2O (50:50); flow rate, 0.07 mL min^{-1}.

6.3.4. Mixture Separation on MIL-100(Fe) MPs Column with Isocratic and Stepwise Elution

With the guidance of the mass transfer and equilibrium parameters from single component experiments, the separation of mixtures of the analytes were predicted and experimentally verified. The separation of a mixture of toluene, styrene, and p-xylene is illustrated in Figure 6.8a and the separation of anilines is shown in Figure 6.8b. For both group of analytes the simulated chromatograms (red lines) fit very well the experimental ones (black lines). As expected, increasing the water content improves the separation performance but strongly extends elution time. For the neutral analytes using MeOH/H_2O (40:60) as mobile phase it needs 200 min to achieve a satisfying separation. Applying MeOH/H_2O (50:50) as mobile phase the separation run requires less than 30 min, but the peaks show a clear overlap, which was also predicted by the simulation. Regarding the separation of anilines, an excellent

baseline separation can be achieved when using MeOH/H_2O (40:60) as mobile phase within an elution time of about 180 min. However, looking at the chromatogram (Figure 6.8b) it shows that the time lag between the second peak (2-nirtoaniline) and the third peak (1-naphthylamine) is unnecessarily large. Therefore, a stepwise elution method was tested and simulated shortening the duration of the baseline separation drastically to 60 min. In detail, from 0 min to 25min the mobile phase MeOH/H_2O (40:60) is used to elute the first two peaks (acetanilide and 2-nitroaniline). Afterwards the elution of 1-naphthyamine is accelerated by stepwise changing the mobile phase composition from MeOH/H_2O (40:60) to (100:0).

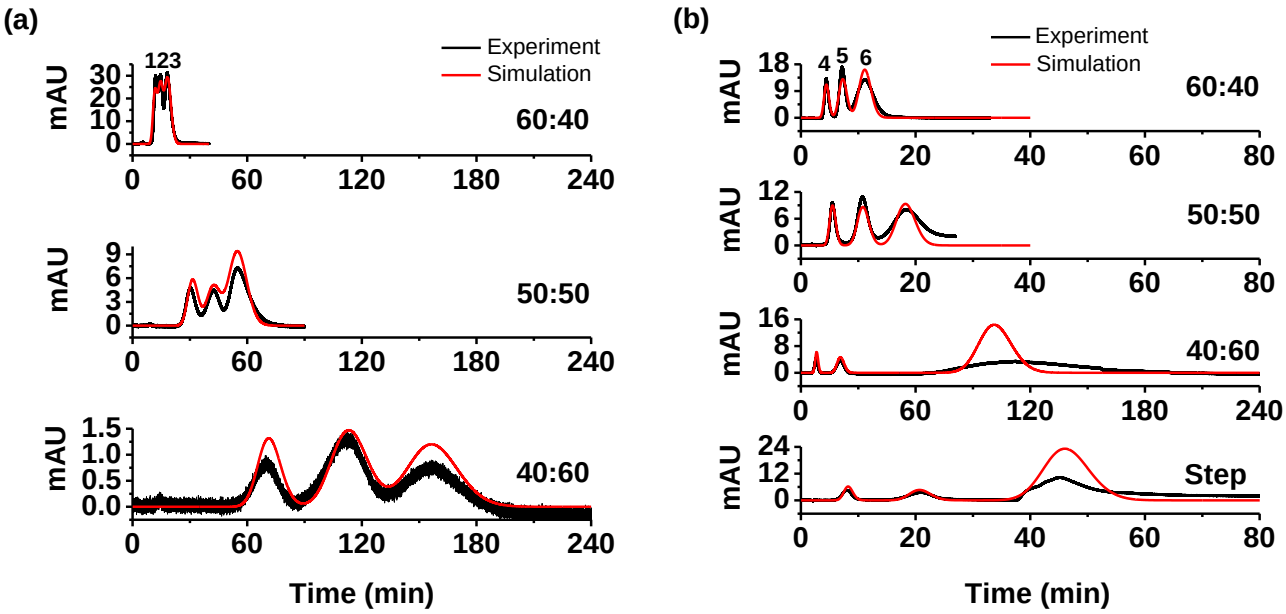

Figure 6.8. (a) Chromatographic separation of a mixture of toluene (14.2 mmol L^{-1}), styrene (0.260 mmol L^{-1}) and p-xylene (24.3 mmol L^{-1}) with isocratic elution applying MeOH/H_2O (60:40, 50:50, 40:60) as mobile phase, respectively; (b) Chromatographic separation of a mixture of acetanilide (0.070 mmol L^{-1}), 2-nitroaniline (0.720 mmol L^{-1}) and 1-naphthylamine (0.350 mmol L^{-1}) with isocratic elution applying MeOH/H_2O (60:40), (50:50) and (40:60) as mobile phase, respectively, as well as stepwise elution applying a constant composition of MeOH/H_2O (40:60) in 0-25 min followed by a step to (100:0) after 25 min. Conditions: injection volume, 1 µL each; flow rate, 0.07 mL min^{-1}. Peak identity: 1, toluene; 2, styrene; 3, p-xylene; 4, acetanilide; 5, 2-nirtroaniline; 6, 1-naphthylamine.

6.3.5. Capacity of MIL-100(Fe)

To comprehend further to which extent the analyte molecules occupy the MIL-100(Fe) pores when the maximum capacity is reached, the number of molecules per MIL-100(Fe) unit cell is calculated.

Starting with the large MIL-100(Fe) unit cell volume of 3.94×10^{-25} m^3 [37], the number of unit cells per liter that can be calculated to 2.56×10^{21}, equivalent to 4.26 mmol. If this number is compared with the measured maximum capacities ($q^*_{MOFmax,toluene}$ = 3.55 mol L^{-1}, $q^*_{MOFmax,styrene\ or\ p\text{-}xylenne}$ = 3.53 mol L^{-1}, $q^*_{MOFmax,anilines}$ = 3.12 mol L^{-1}), it shows that approximately 842 (toluene), 838 (styrene or p-xylene) and 740 (aniline derivatives) analyte

molecules fit into a single MIL-100(Fe) unit cell. These values show promising solute adsorption of MIL-100(Fe) and are more than two orders of magnitude higher than the numbers of analyte molecules per unit cell found for phenol derivatives (1.7) loaded in UiO-67 [32], or pyridine and chloroaniline isomer molecules loaded in HKUST-1 [15] (4.0 and 2.5, respectively) measured in our previous studies, or the ones reported for MIL-53 in combination with ethyltoluene (2.4), o-cymene (0.6) [38], o-xylene (4.0), styrene and ethylbenzene (2.0, respectively) [39]. In order to get a clearer picture of the properties of different MOFs with respect to their use as liquid chromatographic media, we summarized them in Table 6.3.

Table 6.3 Different characteristics of UiO-67, HKUST-1 and MIL-100(Fe).

MOF name	Metal nodes	Linker	pore diameter (Å)	Windows (Å)	Unit cell volume [nm^3]	Molecule number density [nm^{-3}]	Maximum capacity (mol L^{-1})	Pore diffusivity (m^2 s^{-1})
UiO-67 [32, 40]	Zr	(BPDC)[a]	11.5; 23	8	19.9	0.085 (phenols)	0.14 (phenols)	1.3×10^{-13}
HKUST-1 [15, 41]	Cu	BTC	5, 9	3.5	18.3	0.14 (pyridine); 0.22 (chloroanilines)	0.23 (pyridine); 0.37 (chloroanilines)	2.3×10^{-15}
MIL-100(Fe) [42]	Fe	BTC	25; 29	4.7-5.5; 8.6	394.5	1.88 (anilines); 2.13 (benzene hydrocarbon)	3.1 (anilines); 3.55 (benzene hydrocarbon)	5×10^{-12}

[a] 4,4'-biphenyl-dicarboxylate

Table 6.3 shows that MIL-100(Fe) not only has the largest pores but also by far the largest unit cell volume, simply because of the complex structure of the unit cell. Therefore, a big part of the high number of molecules per unit cell is simply a consequence of the size of the unit cell. Nevertheless, if the number of molecules is divided by the unit cell volume, the packing density in MIL-100(Fe) is still clearly higher than in the other MOFs. At least a part of this observation can be related to the known fluctuations in packing density if e.g. spheres of a certain diameter should be packed into cylinders. If the diameter of the cylinder is less than twice the sphere diameter, low packing densities can result. In addition adsorbed molecules may block small pores and therefore prevent the loading of free volume deeper inside the MOF. The influence of the pore diameter can also be seen in the pore diffusivities we approximated for the different MOFs. While UiO-67 and MIL-100(Fe) result in pore diffusivities in the range of 10^{-12} m^2 s^{-1}, for HKUST-1 we found a value in the range of 10^{-14}

– 10^{-15} m^2 s^{-1}. Therefore, besides its higher chemical stability it shows that MIL-100(Fe) has superior capacity and kinetic properties, making it the most suitable MOF for chromatographic purposes we studied so far.

6.4. Conclusions

Crystalline MIL-100 (Fe) SURMOF thin films were coated onto magnetic microparticles having a COOH-terminated surface using the process of liquid-phase epitaxy (LPE). Chromatographic columns packed with the as-synthesized MIL-100(Fe) magnetic particles offer improved separation performance for aromatic hydrocarbons with increasing water content of the mobile phases ($MeOH/H_2O$), due to the change of the affinity strength between the analytes and the crystalline MOF-based solid phase. Additionally, the equilibrium parameters and mass transfer mechanisms between the MIL-100(Fe) and analytes are obtained from the experiments and the simulation using modern chromatographic modeling software. Notably, MIL-100(Fe) exhibits high adsorption capacities for aromatic molecules compared to the previous reported MOFs used in chromatography. This important finding should have a significant impact on applying MOFs as adsorbents in industrial separation and purification processes.

References

[1] H.C. Zhou, J.R. Long, O.M. Yaghi, Introduction to metal-organic frameworks, Chem. Rev. 112 (2012) 673-674.

[2] Q.L. Zhu, Q. Xu, Metal−organic framework composites, Chem. Soc. Rev. 43 (2014) 5468-5512.

[3] W.G. Lu, Z.W. Wei, Z.Y. Gu, T.F. Liu, J. Park, J. Park, J. Tian, M.W. Zhang, Q. Zhang, T. Gentle, M. Bosch, H.C. Zhou, Tuning the structure and function of metal-organic frameworks via linker design, Chem. Soc. Rev. 43 (2014) 5561-5593.

[4] L.J. Murray, M. Dinca, J.R. Long, Hydrogen storage in metal-organic frameworks, Chem. Soc. Rev. 38 (2009) 1294-1314.

[5] S.L. Qiu, M. Xue, G.S. Zhu, Metal−organic framework membranes: from synthesis to separation application, Chem. Soc. Rev. 43 (2014) 6116-6140.

[6] J.R. Li, R.J. Kuppler, H.C. Zhou, Selective gas adsorption and separation in metal-organic frameworks, Chem. Soc. Rev. 38 (2009) 1477-1504.

[7] L.Q. Ma, J.M. Falkowski, C. Abney, W.B. Lin, A series of isoreticular chiral metal-organic frameworks as a tunable platform for asymmetric catalysis, *Nat. Chem.* 2 (2010) 838-846.

[8] P. Horcajada, R. Gref, T. Baati, P.K. Allan, G. Maurin, P. Couvreur, G. Ferey, R.E. Morris, C. Serre, Metal-organic frameworks in biomedicine, Chem. Rev. 112 (2012) 1232-1268.

[9] H. Furukawa, K.E. Cordova, M. O'Keeffe, O.M. Yaghi, The chemistry and applications of metal-organic frameworks, Science 341 (2013) 974.

[10] K. Yusuf, A. Aqel, Z. ALOthman, Metal-organic frameworks in chromatography, J. Chromatogr. A 1348 (2014) 1-16.

[11] Y.B. Yu, Y.Q. Ren, W. Shen, H.M. Deng, Z.Q. Gao, Applications of metal-organic frameworks as stationary phases in chromatography, TrAC-Trends. Anal. Chem. 50 (2013) 33-41.

[12] C.X. Yang, Y.J. Chen, H.F. Wang, X.P. Yan, High-performance separation of fullerenes on metal−organic framework MIL-101(Cr), Chem. Eur. J. 17 (2011) 11734-11737.

[13] C.X. Yang, X.P. Yan, Metal−organic framework MIL-101(Cr) for high-performance liquid chromatographic separation of substituted aromatics, Anal. Chem. 83 (2011) 7144-7150.

[14] A. Ahmed, M. Forster, R. Clowes, D. Bradshaw, P. Myers, H. Zhang, Silica SOS@HKUST-1 composite microspheres as easily packed stationary phases for fast separation, J. Mater. Chem. B 1 (2013) 3276.

[15] W. Qin, M.E. Silvestre, F. Kirschhöfer, G. Brenner-Weiss, M. Franzreb, Insights into chromatographic separation using core–shell metal–organic frameworks: Size exclusion and polarity effects, J. Chromatogr. A 1411 (2015) 77-83.

[16] Z.M. Yan, J.N. Zheng, J.F. Chen, P. Tong, M.H. Lu, Z. Lin, L. Zhang, Preparation and evaluation of silica-UIO-66 composite as liquid chromatographic stationary phase for fast and efficient separation, J. Chromatogr. A 1366 (2014) 45-53.

[17] W.W. Qin, M.E. Silvestre, M. Franzreb, Magnetic microparticles@UiO-67 core-Shell composites as a novel stationary phase for high performance liquid chromatography, Appl. Mech. Mater. 703 (2015) 73-76.

[18] O. Shekhah, H. Wang, S. Kowarik, F. Schreiber, M. Paulus, M. Tolan, C. Sternemann, F. Evers, D. Zacher, R.A. Fischer, C. Wöll, Step-by-step route for the synthesis of metal-organic frameworks, J. Am. Chem. Soc. 129 (2007) 15118-15119.

[19] H. Gliemann, C. Wöll, Epitaxially grown metal-organic frameworks, Mater. Today 15 (2012) 110-116.

[20] D. Zacher, O. Shekhah, C. Wöll, R.A. Fischer, Thin films of metal-organic frameworks, Chem. Soc. Rev. 38 (2009) 1418-1429.

[21] O. Shekhah, J. Liu, R.A. Fischer, C. Wöll, MOF thin films: existing and future applications, Chem. Soc. Rev. 40 (2011) 1081-1106.

[22] P. Horcajada, S. Surble, C. Serre, D.Y. Hong, Y.K. Seo, J.S. Chang, J.M. Greneche, I. Margiolaki, G. Ferey, Synthesis and catalytic properties of MIL-100(Fe), an iron(III) carboxylate with large pores, Chem. Commun. (2007) 2820-2822.

[23] A.M. Ribeiro, M.C. Campo, G. Narin, J.C. Santos, A. Ferreira, J.S. Chang, Y.K. Hwang, Y.K. Seo, U.H. Lee, J.M. Loureiro, A.E. Rodrigues, Pressure swing adsorption process for the separation of nitrogen and propylene with a MOF adsorbent MIL-100(Fe), Sep. Purif. Technol. 110 (2013) 101-111.

[24] P. Wang, H.M. Zhao, H. Sun, H.T. Yu, S. Chen, X. Quan, Porous metal−organic framework MIL−100(Fe) as an efficient catalyst for the selective catalytic reduction of NOx with NH3, RSC Adv. 4 (2014) 48912-48919.

[25] V. Agostoni, R. Anand, S. Monti, S. Hall, G. Maurin, P. Horcajada, C. Serre, K. Bouchemal, R. Gref, Impact of phosphorylation on the encapsulation of nucleoside analogues within porous iron(III) metal−organic framework MIL-100(Fe) nanoparticles, J. Mater. Chem. B 1 (2013) 4231-4242.

[26] X.F. Chen, N. Ding, H. Zang, H. Yeung, R.S. Zhao, C.G. Cheng, J.H. Liu, T.W.D. Chan, Fe_3O_4@MOF core-shell magnetic microspheres for magnetic solid-phase extraction of polychlorinated biphenyls from environmental water samples, J. Chromatogr. A 1304 (2013) 241-245.

[27] T.C. Huuk, T. Hahn, A. Osberghaus, J. Hubbuch, Model-based integrated optimization and evaluation of a multi-step ion exchange chromatography, Sep. Purif. Technol. 136 (2014) 207-222.

[28] T. Hahn, A. Sommer, A. Osberghaus, V. Heuveline, J. Hubbuch, Adjoint-based estimation and optimization for column liquid chromatography models, Comput. Chem. Eng. 64 (2014) 41-54.

[29] A. Dhakshinamoorthy, M. Alvaro, Y.K. Hwang, Y.-K. Seo, A. Corma, H. Garcia, Intracrystalline diffusion in metal organic framework during heterogeneous catalysis: Influence of particle size on the activity of MIL-100 (Fe) for oxidation reactions, Dalton Trans. 40 (2011) 10719-10724.

[30] M.G. Plaza, A.M. Ribeiro, A. Ferreira, J.C. Santos, U.H. Lee, J.-S. Chang, J.M. Loureiro, A.E. Rodrigues, Propylene/propane separation by vacuum swing adsorption using Cu-BTC spheres, Sep. Purif. Technol. 90 (2012) 109-119.

[31] E.J. Wilson, C.J. Geankopl, Liquid mass transfer at very low reynolds numbers in packed beds, Ind. Eng. Chem. Fundam. 5 (1966) 9-14.

[32] W. Qin, M.E. Silvestre, G. Brenner-Weiss, Z. Wang, S. Schmitt, J. Hübner, M. Franzreb, Insights into the separation performance of MOFs by high-performance liquid chromatography and in-depth modelling, Sep. Purif. Technol. DOI: 10.1016/j.seppur.2015.10.008.

[33] L. Heinke, M. Tu, S. Wannapaiboon, R.A. Fischer, C. Wöll, Surface-mounted metal-organic frameworks for applications in sensing and separation, Microporous Mesoporous Mater. 216 (2015) 200-215.

[34] J.X. Liu, W.C. Zhou, S. Walheim, Z.B. Wang, P. Lindemann, S. Heissler, J.X. Liu, P.G. Weidler, T. Schimmel, C. Wöll, E. Redel, Electrochromic switching of monolithic prussian blue thin film devices, Opt. Express 23 (2015) 13725-13733.

[35] S. Schmitt, M. Silvestre, M. Tsotsalas, A.L. Winkler, A. Shahnas, S. Grosjean, F. Laye, H. Gliemann, J. Lahann, S. Brase, M. Franzreb, C. Wöll, Hierarchically functionalized magnetic core/multishell particles and their postsynthetic conversion to polymer capsules, Acs Nano 9 (2015) 4219-4226.

[36] Y.Y. Fu, C.X. Yang, X.P. Yan, Metal−organic framework MIL-100(Fe) as the stationary phase for both normal-phase and reverse-phase high performance liquid chromatography, J. Chromatogr. A 1274 (2013) 137-144.

[37] J.W. Yoon, Y.K. Seo, Y.K. Hwang, J.S. Chang, H. Leclerc, S. Wuttke, P. Bazin, A. Vimont, M. Daturi, E. Bloch, P.L. Llewellyn, C. Serre, P. Horcajada, J.-M. Grenèche, A.E. Rodrigues, G. Férey, Controlled reducibility of a metal–organic framework with coordinatively unsaturated sites for preferential gas sorption, Angew. Chem. Int. Ed. 49 (2010) 5949-5952.

[38] L. Alaerts, M. Maes, L. Giebeler, P.A. Jacobs, J.A. Martens, J.F.M. Denayer, C.E.A. Kirschhock, D.E. De Vos, Selective adsorption and separation of ortho-substituted alkylaromatics with the microporous aluminum terephthalate MIL-53, J. Am. Chem. Soc. 130 (2008) 14170-14178.

[39] M. Maes, F. Vermoortele, L. Alaerts, S. Couck, C.E.A. Kirschhock, J.F.M. Denayer, D.E. De Vos, Separation of styrene and ethylbenzene on metal-organic frameworks: analogous structures with different adsorption mechanisms, J. Am. Chem. Soc. 132 (2010) 15277-15285.

[40] M.J. Katz, Z.J. Brown, Y.J. Colon, P.W. Siu, K.A. Scheidt, R.Q. Snurr, J.T. Hupp, O.K. Farha, A facile synthesis of UiO-66, UiO-67 and their derivatives, Chem. Commun. 49 (2013) 9449-9451.

[41] A. Vishnyakov, P.I. Ravikovitch, A.V. Neimark, M. Bülow, Q.M. Wang, Nanopore structure and sorption properties of cu−btc metal−organic framework, Nano Lett. 3 (2003) 713-718.

[42] P. Horcajada, S. Surble, C. Serre, D.Y. Hong, Y.K. Seo, J.S. Chang, J.M. Greneche, I. Margiolaki, G. Ferey, Synthesis and catalytic properties of MIL-100(Fe), an iron(iii) carboxylate with large pores, Chem. Commun. (2007) 2820-2822.

6.5. Supporting Information

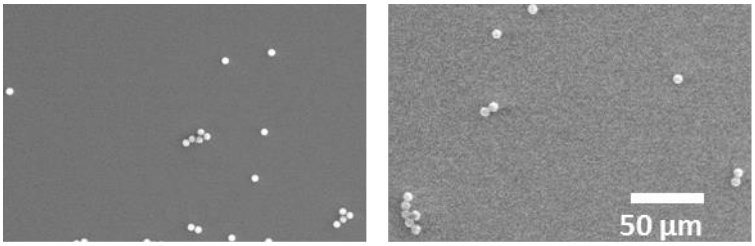

Figure S6.1. SEM images of uniform raw MPs (left) and MIL-100(Fe) MPs (right, 55 cycles) using a low magnification (500×).

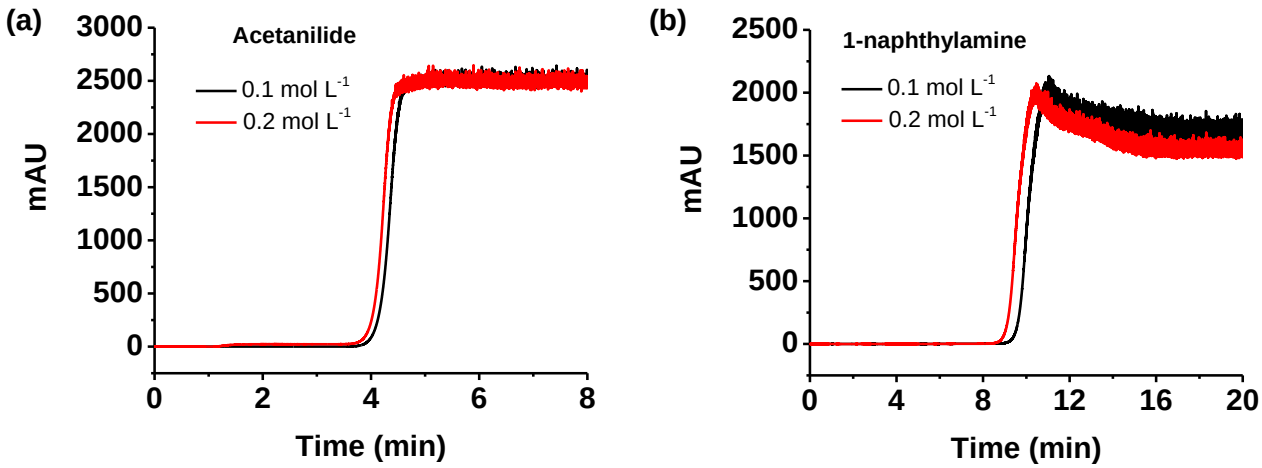

Figure S6.2. Break through chromatograms with high concentrations of analytes on the MIL-100(Fe) packed column (2 cm long ×1.0 mm i.d.): (a) 0.1 and 0.2 mol L^{-1} acetanilide; (b) 0.1 and 0.2 mol L^{-1} 1-naphthylamine. Conditions: mobile phase, MeOH/H_2O (50:50); flow rate, 0.07 mL min^{-1}.

7. Magnetic Microparticles@UiO-67 Core−Shell Composites as a Novel Stationary Phase for High Performance Liquid Chromatography

Weiwei Qin[1, a], Martin E. Silvestre [2,b] and Matthias Franzreb [3,c]

[1,2,3]*Institute of Functional Interfaces (IFG), Karlsruhe Institute of Technology (KIT), Hermann-von-Helmholtz-Platz 1, 76344 Eggenstein-Leopoldshafen, Germany*

[a]weiwei.qin@partner.kit.edu, [b]martin.silvestre@kit.edu, [c]matthias.franzreb@kit.edu

Abstract Metal−organic framework UiO-67 was explored as a novel stationary phase for high performance liquid chromatography (HPLC). UiO-67 was, for the first time, homogeneously coated on carboxyl functionalized magnetic silica microparticles at low temperature (45 °C) by using a recently introduced liquid phase epitaxy (LPE) process. HPLC runs using the synthesized core-shell microparticles as stationary phase showed baseline separation for three phenol derivatives, applying gradient elution using acetonitrile and water as mobile phase. It also showed that UiO-67 has the largest affinity for 2,6-dichlorophenol among the phenol derivatives tested. The comparison of core-shell microparticles with 20 and 55 layers, respectively, of UiO-67 grown on the magnetic silica core proof that the UiO-67 shell determines separation behavior. Therefore, the use of UiO-67 core-shell microparticles as a stationary phase combines the advantages of a thin, homogenous MOF shell showing fast kinetics and good separation efficiency with the advantages of spherical silica microparticle cores offering high mechanical robustness and moderate pressure drop.

Publisched in *Applied Mechanics and Materials* ***2015****, 703, 73-76.*

7.1. Introduction

Metal-organic frameworks (MOFs) emerged as a new class of highly ordered porous coordination polymers about twenty years ago [1]. This novel class of hybrid material consists of two building units: metal centers or clusters and functionalized organic linkers. MOFs have drawn special interest due to their potential applications in gas storage, catalysis, drug delivery and sensors [2]. The unique properties of large surface to volume ratios, diverse structures and high porosity also make MOFs an interesting candidate for high-performance liquid chromatography (HPLC) [3]. However, a major limitation of the application of MOFs in the field of HPLC lies in the irregular shapes and wide size distributions of MOF particles synthesized by traditional solvothermal processes, resulting in bad column packing, low column efficiency and high column back pressure. In contrast, the recently proposed liquid phase epitaxy (LPE) process [4] can produce high quality, oriented and homogenous surface-attached metal−organic framework thin films (SURMOFs) on a suitable functionalized surface as a nucleation template.

Here we report the first fabrication of well-defined core-shell UiO-67 SURMOFs coated on uniform magnetic microparticles by LPE process. Among the MOF family UiO-67 is especially suited for HPLC applications due to its high stability and large pore dimensions [5]. However, to the best of our knowledge, no UiO-67 MOFs used in HPLC have been reported so far. In this work, UiO-67 core-shell magnetic microparticles were synthesized and assembled into HPLC columns to investigate their chromatographic performance.

7.2. Experimental

7.2.1. Chemicals and Reagents

Carboxyl-functionalized magnetic silica particles (SiO_2-MAG-COOH) with narrow size distribution of 4.7±0.14 µm were purchased from microParticles GmbH, Berlin, Germany. Zirconium(IV) propoxide solution ($Zr(OPr)_4$, 70%), methacrylic acid (99%), 4,4'-biphenyl-dicarboxylate (BPDC, 97%), N,N-Dimethylformamide (DMF, 99.8%), 2,6-dimethylphenol (DMP, 99%), resorcinol (RSC, 99%), 2,6-dichlorophenol (DCP, 99%), acetone (99.9%), dichloromethane (DCM, 99.8%), carbon tetrachloride (CCl_4, 99.9%) methanol(99.9%), 2-propanol (99.5%) and acetonitrile (ACN, 99.9%) were purchased from Sigma-Aldrich or Merck , Germany. All reagents and solvents were used as received without further purification. The HPLC grade ACN and ultrapure water (H_2O) were adopted for HPLC tests. The phenol derivatives (Figure 7.1) were dissolved in ACN and used as HPLC analytes.

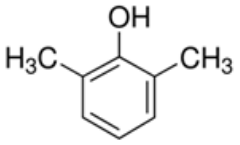

2, 6-dimethylphenol

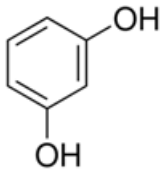

resorcinol

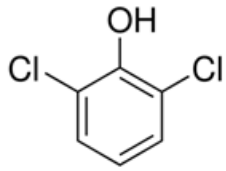

2, 6-dichlorophenol

Figure 7.1. Structures of the phenol derivatives used for HPLC experiments.

7.2.2. Instrumentation

X-ray diffraction (XRD) data was recorded with a Bruker diffractometer using Cu Kα1,2-radiation (λ = 0.15419 nm). Fourier transform infrared (FTIR) measurements were carried out with a Bruker Optics Tensor 27 spectrometer with a Bruker Optics Platinum® ATR (Attenuated total reflectance) accessory and a deuterated tri glycine sulfate (RT–DTGS) detector. The FTIR ATR spectra were recorded with a resolution of 4 cm^{-1} using air as background. Analyses of the morphology were recorded on a Philips XL30 scanning electron microscope (SEM) at 20.0 kV.

All chromatographic tests were performed with an Agilent 1100 series HPLC system (Agilent Technologies, USA) equipped with a variable wavelength UV detector and a micro (2 µL) flow cell at room temperature (ca. 22 °C).

7.2.3. Synthesis of Magnetic Microparticles@UiO-67 Core–shell Composites

UiO-67 was synthesized onto SiO_2-MAG-COOH magnetic microparticles using zirconium methacrylate oxocluster $Zr(OH)_4O_4(OMc)_{12}$ as metal source [6], and 4,4'-biphenyldicarboxylate (BPDC) as organic linker using a liquid phase epitaxy process in a layer-by-layer fashion. 25 mg of magnetic microparticles were dispersed in 2 mL of $Zr(OH)_4O_4(OMc)_{12}$ DMF solution (1.5 mM) for 7 min and then in 2 ml BPDC DMF solution (1 mM) for 7 min at 45 °C. Between each step, the magnetic microparticles were magnetically separated and washed with 2 ml DMF once. A desired thickness of the resulting UiO-67 thin film can be achieved by repeating the deposition steps. After 20 and 55 cycles, respectively, the samples were washed with methanol and dried in vacuum for further use and characterizations.

7.2.4. Preparation of the HPLC Column

Before packing the column, the as-synthesized magnetic microparticles@UiO-67 core-shell composites were treated by: (i) washing three times with DCM; (ii) washing five times with methanol; and (iii) drying at 120 °C for 12 h under vacuum, in order to remove unreacted species in the MOF cavities. The dried composites were added into a mixture of CCl_4 and methanol (1:1, vol) under ultrasonication for 5 min, and then the suspension was packed with down-flow into a stainless steel column (200 mm × 1.0 mm i.d) under 40 MPa for 10 min with methanol as the slurry solvent to obtain the home-made UiO-67 column.

7.3. Results and Discussion

7.3.1. Characterization of the Synthesized UiO-67

The synthesized microparticles@UiO-67 core-shell composites were characterized by XRD, FTIR ATR and SEM experiments. The existence and increase of the characteristic diffraction peak of UiO-67 at 2Θ = 5.4-6.7° in the XRD patterns of the particles obtained after 20 and 55 layers respectively proof the successful preparation of a UiO-67 shell (Figure 7.2A). FTIR ATR spectra (Figure 7.2B) give another indication for the growth of the UiO-67 shell. The decrease of the peak intensity at 1780-1710 cm^{-1}, characteristic for –COOH stretch, and the increase of the appearance of the characteristic bands of UiO-67 at 1585, 1532, 1407 and 768 cm^{-1} support the conclusion of a successful fabrication of UiO-67 MOF chemically bound on the surface of the magnetic microparticles. Finally, the SEM results clearly reveal the formation of a UiO-67 shell on the magnetic particles (Figure 7.2C). After applying fifty five layers of UiO-67 growth, the diameter of microparticles@UiO-67 core-shell composites increased from 4.7 µm for raw magnetic microparticles to 5.5 µm, indicating that a SURMOFs shell of around 0.4 µm thickness has grown on the magnetic microparticles. Moreover, the uniform shapes and sizes of the as-prepared microparticles@UiO-67 core-shell composites make them suitable for HPLC.

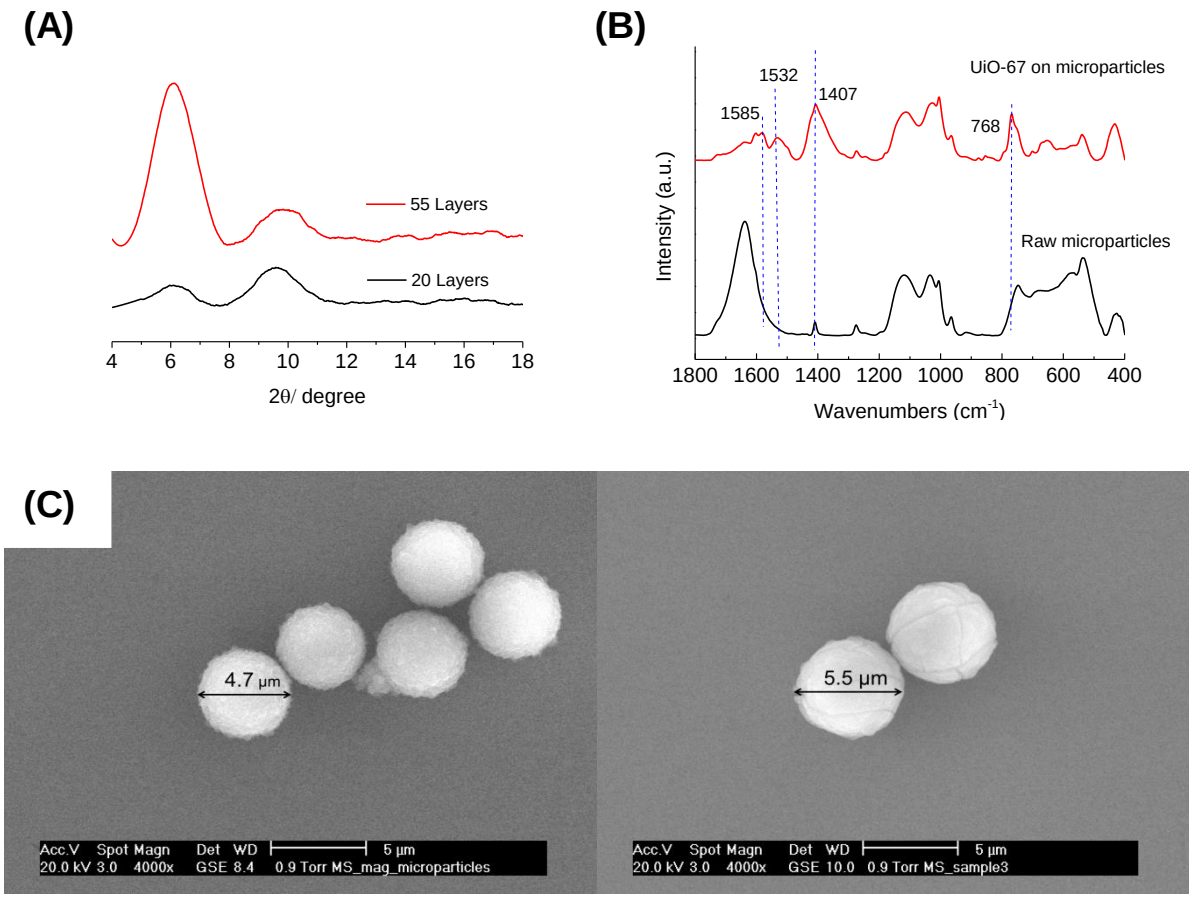

Figure 7.2. Characterization of the UiO-67 shell grown on COOH-functionalized magnetic micro particles. (A) XRD pattern of microparticles@UiO-67 core-shell composites (20 and 55 layers

respectively). (B) FTIR ATR spectra of raw magnetic microparticles and the as-synthesized microparticles@UiO-67 core-shell composites (55 layers). (C) SEM images of the raw magnetic microparticles and microparticles@UiO-67 core-shell composites (55 layers).

7.3.2. HPLC Separation of Dissolved Phenol Derivatives on Microparticles@UiO-67 Core−Shell Composites

We tested the column packed with microparticles@UiO-67 core-shell composites for the separation of phenol derivatives using solvent gradient elution at a flow rate of 0.14 ml min^{-1} (Figure 7.3). With the composites synthesized applying 20 layers of UiO-67 LPE, the retention of all phenol derivatives is weak, resulting in the elution of RSC and DCP as a single peak (Figure 7.3A). However, a good separation of DMP, RSC and DCP can be achieved by the application of composites synthesized with 55 layers of UiO-67 LPE (Figure 7.3B), reaching resolutions of 1.7 (DMP/RSC) and 1.5 (RSC/DCP) respectively. The strong improvement of the separation performance resulting from a column packed with composites with a higher number of UiO-67-LPE layers applied, demonstrates that the UiO-67 shell indeed dominates the separation process.

The elution of phenol derivatives followed the sequence DMP < RSC < DCP, indicating that the retention mechanism is in accordance with the polarity of the analytes. With the increase of the polarity of phenol derivatives, the hydrophilic interaction between the analyte and the UiO-67 increases, resulting in a stronger retention.

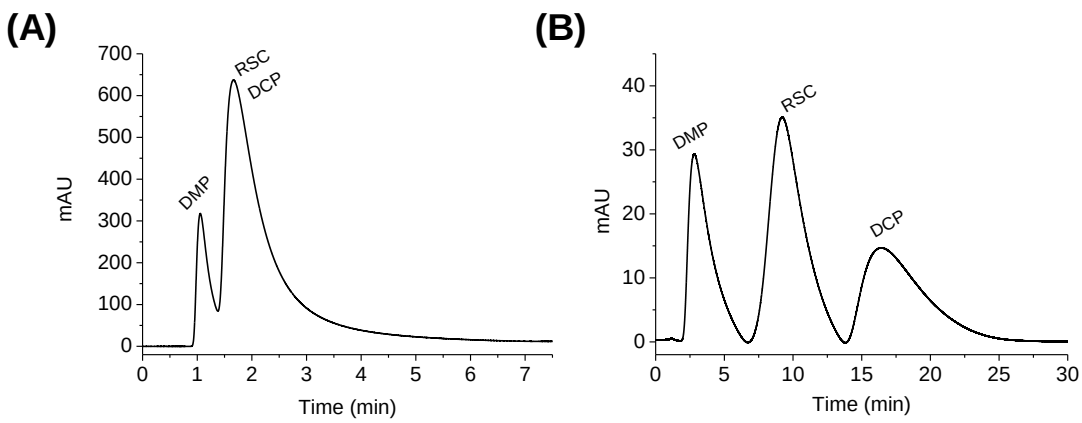

Figure 7.3. HPLC chromatograms resulting from the injection (0.2 µl) of a mixture of DMP, RSC and DCP (1.6 nmol, 1.8 nmol and 2.6 nmol, respectively) dissolved in ACN into HPLC columns (200 mm ×1.0 mm i.d.) packed with microparticles@UiO-67 core-shell composites synthesized with 20 (A) and 55 (B) layers UiO-67 LPE respectively. The gradient program was as follows: 0.00-2.00 min, ACN-H_2O (95:5 → 87.5:12.5); 2.01-30.00 min, ACN-H_2O (87.5:12.5) at a flow rate of 0.14 ml min^{-1}. The separations were performed at room temperature and monitored with a UV detector at 254 nm.

7.4 Conclusions

The authors have synthesized microparticles@UiO-67 core-shell composites having a UiO-67 MOF shell of around 0.4 µm thickness attached to magnetic silica microparticles of ca. 5 µm in diameter. The as-prepared uniform and homogenous UiO-67 shells are shown to be feasible as novel stationary phase in HPLC. The hydrophilic interactions between analytes and the UiO-67 shells provide the composites a unique chromatographic performance compared to other MOF-based stationary phases showing classical reversed phase characteristics [7].

References

[1] J.L.C. Rowsell, O.M. Yaghi, Metal-organic frameworks: a new class of porous materials, Micropor. Mesopor. Mat. Vol. 73 (2004), p. 3-14

[2] G. Ferey, Hybrid porous solids: past, present, future, Chem. Soc. Rev. Vol. 37 (2008), p. 191-214

[3] Z.Y. Gu, C.X. Yang, N. Chang, X.P. Yan, Metal-Organic Frameworks for Analytical Chemistry: From Sample Collection to Chromatographic Separation, Accounts. Chem. Res. Vol. 45 (2012), p. 734-745

[4] O. Shekhah, H. Wang, S. Kowarik, F. Schreiber, M. Paulus, M. Tolan, C. Sternemann, F. Evers, D. Zacher, R.A. Fischer, C. Woll, Step-by-step route for the synthesis of metal-organic frameworks, J. Am. Chem. Soc. Vol. 129 (2007), p. 15118-15119

[5] S. Chavan, J.G. Vitillo, D. Gianolio, O. Zavorotynska, B. Civalleri, S. Jakobsen, M.H. Nilsen, L. Valenzano, C. Lamberti, K.P. Lillerud, S. Bordiga, H-2 storage in isostructural UiO-67 and UiO-66 MOFs, Phys. Chem. Chem. Phys. Vol. 14 (2012), p. 1614-1626

[6] G. Kickelbick, U. Schubert, Oxozirconium methacrylate clusters: $Zr_6(OH)_4O_4(OMc)_{12}$ and $Zr_4O_2(OMc)_{12}$ (OMc = methacrylate), Chem. Ber. Recl. Vol. 130 (1997), p. 473-477

[7] A. Centrone, E.E. Santiso, T.A. Hatton, Separation of Chemical Reaction Intermediates by Metal-Organic Frameworks, Small. Vol. 7 (2011), p. 2356-2364

8 Conclusions & Outlook

This work has brought to light a better understanding of the relationship between the properties of different MOFs and their abilities to serve as stationary phase in HPLC setups in order to separate small aromatic molecules. Three different MOFs, UiO-67 (chapter 4 and 7), HKUST-1 (chapter 5), and MIL-100(Fe) (chapter 6), have been screened for selected analytes using pulse as well as breakthrough experiments. With the assistance of the newly developed chromatographic software ChromX, adsorption equilibrium data and mass transfer parameters have been derived from the experiments and simulations. The theoretical capacities of different MOFs were also discussed.

In order to get efficient MOF based stationary phases, shells of UiO-67, HKUST-1 and MIL-100(Fe) SURMOFs were successfully fabricated by a LPE process onto magnetic microparticle cores having functional groups on the surfaces to nucleate and bind the first MOF layer. The resulting homogenous MOF MPs core-shell composites were physically characterized and packed into columns with the same column volume. It is remarkable that all these MOF based columns showed good separation performance towards analytes with closely related properties if the mobile phases were appropriately chosen. Detailed modeling of experimental data allowed us to extract the mass transfer kinetics, binding equilibrium and pore diffusivity parameters. MIL-100(Fe) sorbents exhibit clearly the highest molecular loadings and fastest kinetics compared to UiO-67 and HKUST-1. As the main reason for this superior chromatographic behavior the comparable large cages and connecting windows of the crystal structure of this MOF could be identified. Another interesting fact is that for the same MOF the maximum molar loading capacities remained constant or in a narrow range for different analytes and mobile phase compositions. This shows that the achievable maximum molar loadings are closely related to the structure and the pore size of the MOF, and less to the nature of the aromatic analytes as long they are of approximately the same molecular weight. In contrast, the affinities of the examined analytes varied strongly and showed also a clear dependence on the mobile phase composition. Nevertheless, for each group of aromatic molecules examined a combination of MOF and mobile phase could be identified, which allowed good separation of the mixture. Therefore, our results suggest that the versatile chemistry of MOF based solid phases offer an interesting opportunity to screen and find optimum adsorbents for difficult separation tasks in HPLC. In addition, the well-defined crystalline structure of MOFs allows sharp size exclusion effects, even for analytes with a size ratio of two or less.

In future, these unique features of MOFs should be systematically studied and simulated in even more detail using molecular dynamics models. For this, a series of MOFs having the same metal atom and crystal type but linkers of different length should be synthesized and their chromatographic behavior compared. Next, MOFs with the same linker but different metal atoms should be synthesized and investigated. Finally, MOFs with identical metal atom and linker type could be realized, however, with varying side groups of the linker. Having

such a library of MOF sorbents and data about their chromatographic properties a rational design of tailored chromatographic media for difficult separation tasks comes into reach. Using even more sophisticated, multifunctional MOFs, such as homochiral MOFs, improved sorbents for enantioselective separations have also been reported and should be further investigated. Regarding mass transfer within MOF sorbents our studies reveal that it is limited by intra particle diffusion. Future work should further investigate the underlying mechanisms. E.g. will small pores be blocked by bound analyte molecules or are bound molecules able to further migrate into the MOF by surface diffusion? What is the role of solvent molecules regarding the overall mass transfer? Do we have to switch to a Stefan Maxwell description of fluxes instead of Fick's law?

Besides these more fundamental questions, a practical hurdle for the commercial use of well-defined shell-core MOF sorbents is the laborious way they are synthesized. Currently the layer-by-layer procedure is conducted by hand, requiring at least a weak for sorbents with a shell of 55 layers. In future the procedure should be automated and simplified if possible. If such an automatization and scale-up of shell-core MOF sorbent production is successful, there are good reasons to assume that due to their shown advantages they will become a serious alternative for today's sorbents used in analytical HPLC.